OPTICALLY MODULATED FLUORESCENT PROTEINS

A Thesis
Presented to
The Academic Faculty

by

Amy E. Jablonski

In Partial Fulfillment
of the Requirements for the Degree
Doctor of Philosophy in the
School of Chemistry and Biochemistry

Georgia Institute of Technology
August 2014

OPTICALLY MODULATED FLUORESCENT PROTEINS

Approved by:

Dr. Robert M. Dickson, Advisor
School of Chemistry and Biochemistry
Georgia Institute of Technology

Dr. Mostafa El-Sayed
School of Chemistry and Biochemistry
Georgia Institute of Technology

Dr. Laren M. Tolbert
School of Chemistry and Biochemistry
Georgia Institute of Technology

Dr. Melissa Kemp
School of Biomolecular Engineering
Georgia Institute of Technology

Dr. Christoph Fahrni
School of Chemistry and Biochemistry
Georgia Institute of Technology

Date Approved: June 17, 2014

ACKNOWLEDGEMENTS

I wish to thank the many individuals who I have worked with and learned from over the course of my Ph.D. First and foremost, I would like to thank my advisor, Dr. Robert Dickson for giving me the opportunity to pursue this interesting research and guiding me through this process. I am also grateful to the many group members that have been vital to my success and understanding of this project. I thank past member Nathan Hull for his guidance when I first arrived and Dr. Saugata Sarkar and Dr. Chaoyang Fan for their encouragement and words of wisdom. Additionally, I would like to thank all present members of the group, Blake Fleischer, Tzu-Hsueh Huang, Dan Mahoney, Soonkyo Jung, Aida Demissie, and Joe Richardson, for their support, especially Jung-Cheng Hsiang and Yen-Cheng Chen whom have spent a lot of time helping we work through the intricate details of my project.

I also wish to thank the many collaborators that I have had the opportunity to work with over the years. Thanks to Dr. Christoph Fahrni for his insight on all things biology as well as his members Dr. Pritha Bagchi and Dr. Irina Issaeva for providing the technical expertise for protein purification and transfection and deep knowledge of mammalian systems. Additionally, I would like to thank Dr. Laren Tolbert and his members Dr. Kyril Solntsev and Dr. Russell Vegh for their support and wealth of knowledge of fluorescent proteins; I have learned so much through our discussions. Also, thanks to Dr. Andreas Bommarius and Dr. Bettina Bommarius for their speedy and outstanding assistance with blue fluorescent protein project. Without these fun and hard-working people, this project would not have been possible.

I wish to thank my whole the committee, Dr. Christoph Fahrni, Dr. Laren Tolbert, Dr. Mostafa El-Sayed, and Dr. Melissa Kemp for their unwavering support and the enlightened discussions over the years. Additionally, I thank all Georgia Institute of Technology professors and staff that have supported me and help me nagivate this Ph.D. process.

Lastly, I would like to thank all my friends and family for their patience, understanding, and encouragement. Trust me when I say, this was possible because of you guys.

TABLE OF CONTENTS

LIST OF TABLES

LIST OF FIGURES

LIST OF SYMBOLS AND ABBREVIATIONS

ε	Extinction coefficient
Φ	Quantum yield
σ	Absorption cross section
τ_c	Characteristic time
τ_{on}	On time
τ_{off}	Off time
ν_c	Characteristic frequency
ν_0	Fundamental zero frequency
ν_{mod}	Modulation frequency
I_F	Fluorescence intensity
k_{exc}	Excitation rate
k_{fl}	Fluorescence rate
k_{on}	On rate
k_{off}	Off rate
D	Dark state
S_0	Ground state
S_1	Excited State
T_1	First triplet state
n	Refractive index
T_m	Melting temperature

AcGFP	*Aequorea coerulescens* green fluorescent protein
APD	Avalanche photo diode
APS	Ammonium persulfate
BFP	Blue fluorescent protein
BODIPY	4,4-difluoro-4-bora-3a,4a-diaza-*s*-indacene
CCD	Charge coupled device
CFP	Cyan fluorescent protein
CW	Continuous wave
DNA	Deoxyribonucleic acid
DPBS	Deuterated phosphate buffered saline
EOM	Electro-optical modulator
ESPT	Excited state proton transfer
FAD	Flavin adenine dinucleotide
FCS	Fluorescence correlation spectroscopy
FCCS	Fluorescence cross-correlation spectroscopy
FP	Fluorescent protein
FRET	Förster resonance energy transfer
FWHM	Full width at half maximum
GFP	Green fluorescent protein
HPLC	High performance liquid chromatography
IR	Infrared
ISC	Intersystem crossing
kDa	Kilodalton

LUT	Lookup table
MWCO	Molecular weight cut-off
NADH	Nicotinamide adenine dinucleotide hydride
NMR	Nuclear magnetic resonance
OD	Optical density
OLID	Optical lock-in detection
PAA	Polyacrylamide
PBS	Phosphate buffered saline
PDB	Protein data bank
PVA	Polyvinyl alcohol
QD	Quantum dot
rcf	Relatice centrifugal force
RFP	Red fluorescent protein
TCSPC	Time-correlated single photon counting
TEMED	N,N,N',N'-Tetramethylethylenediamine
WT-GFP	Wild type green fluorescent protein
YFP	Yellow fluorescent protein

SUMMARY

Optical modulation has shown the selective and sensitive signal improvement in high background systems that are often limiting factors in cell imaging. However, cell applications are still limited due to biocompatibility and delivery issues. Extensively used in cellular imaging applications, fluorescent proteins have a variety of optically accessible states that make them ideal candidates for investigation of modulatability. Combining the optical modulation technique with the biocompatibility of fluorescent proteins is a major advance. This work focuses on evaluation fluorescent proteins and their optical states for modulation, as well demonstrations of cellular imaging.

Herein, we evaluate a variety of fluorescent proteins with interesting photophysical properties. Though hard to predict the long-wavelength absorption of a dark state, these proteins have optically accessible states that may be favorable for optical modulation. One particular green fluorescent protein is found positive for long-wavelength optical modulation. This provides a base for further investigation of the photophysical state and timescale dictating modulation and reveals the presence of a slow component on the order of milliseconds. This millisecond component suggested a cis/trans isomerization and to better understand the mechanism responsible modulation, blue fluorescent proteins are created to modify the chromophore environment to probe this effect. With mutation to amino acids with contact to both isomers, the extraction of photophysics confirm the alteration timescales of the modulated state based on these key mutations.

The continued investigation of other fluorescent proteins identifies modulatable proteins across the visible wavelength region creating a wide palette of modulatable fluorescent proteins. Many of the fluorescent proteins exhibit a dark state absorption into

the near infrared suggesting a complex mechanism of modulation. In addition to the structural dependence of modulation, additional environmental factors display a fluorescence enhancement and timescale dependence. This information brings to attention that suggest mechanism of cis/trans isomerization coupled with a proton transfer. With this knowledge of the properties dictating optical modulation, this allows for the engineering of improved modulatable proteins to study cellular dynamics.

Motivated by the ability to improve imaging and decode hidden dynamics, demodulation of these proteins demonstrates the selective recovery of signal in the presence of high cellular background. A blue fluorescent protein optimized for long-wavelength modulation demonstrates the removal of high autofluorescent background which is usually the limiting factor in blue fluorescent protein use. Additionally, a modulatable green fluorescent protein shows up to 20-fold signal improvement over high background of similarly emitting, unmodulatable fluorophores. This paves the way for combining better engineered fluorescent proteins with cellular imaging for high sensitivity imaging.

CHAPTER 1

INTRODUCTION

1.1 Motivation

At the forefront of the discussion, fluorescence microscopy has been become an essential tool in understanding the subcellular localization and dynamics of cellular processes.[1-10] Continued development of improved fluorescent probes and techniques is important to answer biological questions.[1,2,5,6,10-12] Current research is focused on both fluorophore improvement[13] for biocompatibility, brightness, labeling efficiency, and photostability and technique development.[14-19] Sensitivity improvements that directly distinguish weak signals with high background are crucial to improved cellular imaging.

Fluorescent proteins have become almost synonymous with fluorescent biological imaging. Mutagenesis of the protein's chromophore and surrounding amino acids has resulted in wide spectral range of emitters.[20] Addressing many of the pitfalls of other exogenous fluorophores, fluorescent proteins have been used extensively in fluorescent imaging[7,10,21-24], sensing[11,25,26], and protein interactions[27-29] applications, but have cellular imaging limitations such as signal discrimination in high heterogeneous background, spectral deconvolution, and detection of low concentrations. A common approach to autofluorescence is the use of red spectral fluorescent proteins.[24,30-33] However, limiting imaging to the use of only red fluorescing proteins narrows the useable proteins in multilabel/multicolor imaging.

An approach to improving signal to background in high background samples is optical modulation. Contrary to that in dual, high-energy laser photoswitching

schemes[16,17,34-36], fluorescence is encoded with the externally applied modulation waveform of a lower energy laser than fluorescence, enabling direct decoupling from unmodulated background upon demodulation. Fluorescence is specifically recovered from background through Fourier transformation of the encoded fluorescence signal to yield the amplitude at the modulation frequency. Synchronously amplified fluorescence image recovery (SAFIRe) enables selective detection at the external modulation frequency to greatly reduce background and noise while amplifying only the signal of interest.[19,37] Cellular imaging with this technique was shown with fluorescent, modulatable silver clusters attached to the cell surface even in the presence of high background.[37] The SAFIRe technique is capable of > 100-fold improvement of signal visibility[19]; however, to date, has been limited in live cellular applications. Combining the SAFIRe technique with the biocompatibility of fluorescent proteins would be a major advance in high background biological imaging and detection.

Expanding optical modulation to fluorescent proteins offers both greatly improved sensitivity by removing the spatially heterogeneous background typically encountered in biological imaging and the opportunity to further distinguish signals from multiple proteins with strongly overlapping spectra. This work focuses on the discovery and use of fluorescent proteins in optical modulation schemes for high sensitivity in fluorescent cellular imaging. Additionally, this work studies the optical states involved in modulation for fluorescent proteins for the determination of a possible mechanism and optimization pathway. This work will demonstrate the modulation of a number of native and modified fluorescent proteins across the visible wavelength spectral window and the usefulness across different cellular imaging conditions. In addition, the extraction of photophysical

parameters of modulatable fluorescent proteins provides information of optically accessible dark states in fluorescent proteins. This information is important in moving modulatable fluorescent protein development forward as it provides a mechanistic hypothesis for better fluorophore creation. Ultimately, the advancement of optically modulated fluorescent proteins will expand the range of addressable biological questions.

1.2 Fluorescence Microscopy in Biology

The field of cellular biology is intimately linked with the optical microscope. Using a very simple optical microscope, Robert Hooke was the first to visualize the cell, and Anthony van Leeuwenhoek discovered bacteria.[38,39] In the 1800s and 1900s, the optical microscope was used in many studies of anatomy and histology.[40,41] Thus, with the development of histological dyes the first visualization of cellular structures was made. With the discovery of fluorescence, new advantages of using fluorescence in combination with optical microscopy were realized. While Ellinger and Hirt in collaboration of Carl Zeiss is credited with the first fluorescence microscope, the technique has provided unparalleled insights into cellular structure and dynamics.[42]

1.2.1 Fluorescence Principles

Despite the observation of fluorescence in quinine and chlorophyll solutions in 1838, it was George Stokes that coined the term in 1852.[41-43] Fluorescence arises from the interaction of light with molecules and is often represented using a Jablonski diagram (Figure 1.1).[43] Unique to each molecule, the potential energy landscape is schematized as light connecting reduced dimensionality lower (ground state) and higher energy level (an excited state). Upon illumination, the absorption of a photon can temporarily excite an electron from the ground state to an excited state. Once in the excited state, the electron

can return to the ground state with emission of a photon of light. The difference in energy between ground state and excited state is dependent on the structure of a molecule. However, the wavelength of light emitted is shifted from the original absorption photon. When this shift is to lower energy it is known as the Stokes shift, and can be due to interactions with the environment while in an excited state. The Stokes shift causes the emission wavelength to be longer than the excitation wavelength, and this difference is crucial to utility and specificity of fluorescence techniques. The excited state electron can also relax through different paths. Part of the energy of an absorbed photon can be non-radiatively lost as heat or through chemical reactions as the excited molecule collides with molecules in its environment. Additionally, electrons can undergo intersystem crossing to the first triplet state T_1 in which it can non-radiatively decay to the ground state or emit a photon as phosphorescence. This emission is generally shifted to longer wavelengths and smaller rate constants than fluorescence.

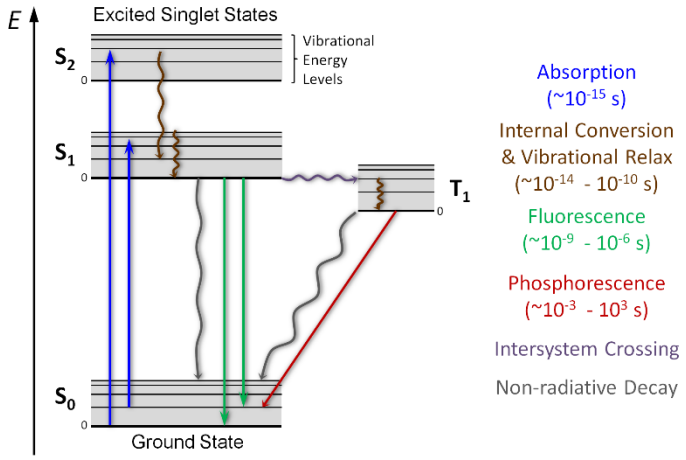

Figure 1.1 Basic Jablonski diagram for light absorption and emission.[43]

1.2.2 Fluorescence Microscope

At their core, fluorescent microscopes have the same optics as optical microscopes with the addition of special filters to filter the excitation and emission light used or collected. However, the use of fluorescence through a microscope has a number of advantages including specificity, sensitivity, and high temporal and spatial resolution not achieved in basic light microscopy.[44] Fluorescence microscopy uses the acquisition of spatial information (and in living specimens, temporal alterations in this spatial information) of objects that are either intrinsically fluorescent or which have been coupled to extrinsic fluorescent molecules too small to be seen with the naked eye.[43,45]

First developed in the 1960s, epi-fluorescence (or epi-illumination) microscopes are configured with the objective both focusing the excitation light and collecting light returning to the detector.[42] The resulting sample fluorescence is separated from excitation light by a dichroic mirror and appropriate filters so excitation light is reflected back into the objective and desired fluorescence is transmitted. In biological systems, epi-fluorescence is used in a wide-field configuration in which the entire sample is illuminated with a uniform beam of light. This allows for imaging of the entire sample at once; however, fluorescence from out-of-focus light interferes with the in-focus image decreasing the resolution, sensitivity, and imaging depth.

Recent advancements have worked to develop more specialized techniques to eliminate the out-of-focus light outside the imaging focal plane.[45] Confocal microscopy illuminates the sample with a light beam that is tightly focused, detecting signal only from the same tightly focused region where the sample is illuminated.[46] Multiphoton microscopy provides 3D imaging resolution and optical sectioning based on the excitation

point spread function, as opposed to confocal microscopy, which is governed by an illumination and collection pinhole.[47] The long wavelength and nonlinear nature of multiphoton imaging give it the advantage of better penetration depth for deep tissue imaging.[46,47]

1.2.3 Select Fluorescence Microscopy Techniques

Increasingly elaborate fluorescence techniques have been developed to get a deeper understanding of complexities and motions of cells and have shown great potential for qualitative and quantitative studies of the function and structure. The specialized techniques are numerous; however, a few representative techniques and their role in biological studies are described below.

1.2.3.1 Fluorescence Correlation Spectroscopy

Rather than use the fluorescence itself, fluorescence correlation spectroscopy (FCS) takes advantage of the fluctuations in the fluorescence intensity to gain insights into the light-induced photophysics as well as diffusion behaviour and absolute concentrations of detected particles.[48] The key to FCS is making the number of fluorophores small enough so that each substantially contributes to the signal. The small focal volume achieved in confocal microscope allows for the reduced concentration of studied molecules. In practice, fluctuations in the fluorescence signal are analyzed by temporally auto-correlating the recorded intensity signals. These fluctuations could be due to diffusion, concentration, or photophysical characteristics of the fluorophore.[49] With appropriate fitting functions, the characteristic time constants responsible for the fluctuations can be extracted. This has become an important tool in the investigation of fluorophore dynamics[50-53] and, more recently, the measurement biochemical parameters of protein-protein interactions.[27,54]

1.2.3.2 Förster Resonance Energy Transfer

Normally used in the investigation of intracellular proteins and protein conformational changes, Förster resonance energy transfer (or fluorescence resonance energy transfer) is able to report on the dynamic distance between two fluorescent molecules.[3,10,36,42,43,55,56] In FRET systems, two molecules having overlapping emission and excitation energy are used as "donor" and "acceptor", respectively. When donor molecules are excited with an appropriate wavelength to induce fluorescence, the emission energy is transferred to the excitation of a nearby acceptor.[42,56] Optimal transfer is reliant on a number of parameters including the overlap of the donor emission and acceptor excitation. However, the most important parameter is the distance between the two molecules. As the efficiency of transfer is extremely sensitive to the separation distance between fluorophores (1-100 Å), FRET can report on spatial distances within a fluorescence image to below 10 nm.[42,56] As a result, FRET has become a molecular ruler for biological processes that cannot be imaged alone.

1.2.3.3 Total Internal Reflection Microscopy

As an improvement to confocal microscopy, total internal reflection fluorescence (TIRF) microscopy restricts the excitation volume of a sample to a small section immediately adjacent to a glass-water (or glass-buffer) interface.[40,43,57,58] By aligning the excitation beam at a high incident angle (critical angle) through the glass coverslip, the beam of light is totally reflected from the glass/water interface, rather than passing through and refracting in accordance with Snell's Law.[46,57,58] The reflection generates a very thin evanescent wave (usually less than 200 nm) in the aqueous medium that undergoes exponential intensity decay with increasing distance from the surface.[57,58] Fluorophores

residing near the glass-liquid surface can be excited by the evanescent wave; however, because of the exponential intensity decay, fluorophores not in the focal plane avoid being excited. Due to the narrow excitation plane, TIRF rejects fluorophore signals outside the focal depth, and produces high-contrast images of surface events with a significant increase in signal-to-background ratio over classical widefield techniques.[46] As the evanescent wave restricts illumination to ~200 nm beyond the surface, TIRF is ideally used to visualize membrane interactions or internalization at the membrane.[59,60]

1.2.3.4 Optical Lock-in Detection

In contrast to super-resolution techniques[14,16,18,23,35,61,62], optical lock-in detection (OLID) aims to improve imaging contrast to be able to visualize the signal of interest over high background.[17,63] Developed by the Marriott group, OLID involves modulating the fluorescence emission of the fluorophore through optical control of its fluorescent and nonfluorescent states, and subsequently applies a lock-in detection method to isolate the modulated signal of interest from nonmodulated background signals.[17] Reconstructed images are based on the correlation of each image pixel to a reference fluorophore with the ideal waveform of the signal of interest. As a result, the signal of interest is amplified over background as background will not have the exact waveform and thus is only weakly correlated with the OLID signal. This approach has up to 20-fold improvement of one dye over high autofluorescent tissue background, when an exogenous reference dye can be used as a reference signal.[17]

1.3 Fluorescent Labels

The essence of fluorescence microscopy is the identification of a target based on its own fluorescence or that of a fluorescent tag. This requires that its fluorescence must be

unique in some way, and ideally have negligible background signal. An ideal fluorescent label should meet some or all of the following requirements[42]:

i) Convenient and selective excitation and detection.

ii) High brightness.

iii) Good chemical and photochemical stability.

iv) Easy and fast deliverability to the target.

v) High affinity and high specificity for the target.

vi) Insensitivity to the chemical environment of the target.

vii) Absence of biochemical and structural perturbation of the system under study.

A number of fluorescent labels exist each with their own advantages and disadvantages. In addition to these ideal conditions, fluorescent labels must be selected based on the application.

1.3.1 Intrinsic Fluorophores

There is a small portion of natural fluorophores that absorb in the ultraviolet, visible, and near-infrared spectrum and are fluorescent. These natural emitters are usually organic molecules with extended π-conjugation. Examples of intrinsic fluorophores include amino acids, coenzymes and vitamins, nucleic acids, alkaloids, oxygen ring compounds (like coumarins), and dyes and pigments (like the chlorophylls).[41,42] Amino acids are of particular interest to cellular imaging due to their ubiquity, and of these only phenylalanine, tyrosine, and tryptophan are aromatic and fluorescent. They are mainly responsible for protein fluorescence under UV excitation. Of the three, tryptophan dominates when present because of its moderate fluorescent quantum yield, absorption coefficient, and the long emission wavelength (310-340 nm) compared to the other two

fluorescent amino acids.[64] Other natural visible fluorophores include the coenzymes, nicotinamide adenine dinucleotide hydride (NADH) and flavin adenine dinucleotide (FAD).[65,66]

1.3.2 Organic Dyes

The most established biological labels are organic dyes. In general, these organic dyes are based on the same extended π-conjugation found in natural fluorophores. However, these dyes have been engineered with larger π systems and increased rigidity to have much higher fluorescent quantum yields and/or extinction coefficients.[42] Available organic dyes range in emission colors across the UV/Visible spectrum and into the near-IR. The most common, brightest organic fluoroscent labels belong to the xanthene, BODIPY (4,4-difluoro-4-bora-3a,4a-diaza-*s*-indacene), and cyanine families.[67] Additionally, the relatively small size compared to their target protein make organic dyes highly favored in applications for minimum perturbation to the investigated system. Protein labeling *in vitro* is well-established, and usually involves the formation of a covalent bond between the target and the fluorescent label. However, *in vivo* labeling requires exceptional selectivity in techniques to deliver the dye across cellular membranes.

1.3.3 Nanoparticles

An alternative to small organic organic fluorophores, intrinsic or extrinsic, is the use of quantum dots (QDs) and other luminescent nanoparticles.[68-70] A recent advancement driven by the need for brighter fluorophores for single molecule studies and use in high background biological samples, quantum dots have the advantage of better photostability, high luminescence, narrow emission bands, and high two-photon absorption cross sections. In general, quantum dots contain a semiconductor core surrounded by a stabilizing alloy

shell. The wavelength of the quantum dot is tuned by the size of the core. To increase the usefulness in biological applications, the ligands used in synthesis are exchanged with more biocompatible ligands such as polyethylene glycol.[70] However, when functionalized and optimized for cellular studies with targeting ligands quantum dot size can reach 20-30 nm in diameter.[69] This makes delivery and release to the cytoplasm difficult limiting the application usefulness of QDs. Additionally, a few studies have suggested that the alloy metals have an increased toxicity compared to organics.[71,72]

Additionally, other luminescent nanoparticles have been developed to overcome some of the disadvantages of QDs. The emergence of fluorescent silver clusters that possess advantages of both small size and good brightness opens a complementary path toward biologic labeling.[73] Specifically in our lab, we have developed spectrally pure silver nanoparticles encapsulated in single stranded DNA (ssDNA).[74] Taking advantage of the affinity of DNA to silver, silver clusters have been created ranging in size of 5 to 11 atoms of silver and exhibiting optical properties ranging from blue to near-IR emission and up to 40% fluorescence quantum yields.[74,75] While the optical properties are mostly dependent on the cluster size, sequence dependence is also important allowing for fine-tuning for specific applications.[76] Our lab has demonstrated the use of silver nanoparticles in cellular labeling and the extraction of signal in high background.[37]

1.3.4 Fluorescent Proteins

Used extensively from cell biology to physiology, fluorescent proteins are used to localize and elucidate the dynamics of proteins, organelles, and other cellular compartments.[1,2,5,21,22,36] In general, fluorescent proteins are proteins with chromophores embedded in a β-barrel structure.[77] The main advantage fluorescent proteins have over

exogenous fluorophores such as organic dyes and nanoparticles is the high biocompatibility. There exist established protocols for the expression of the target protein as a chimera with the choice fluorescent protein to allow for the labeling of almost any protein of interest in the cell.[36,78] The disadvantage to organic dye counterparts is that maturation of the protein can take 30 minutes to a few hours, making the ability to label a longer process. A further detail discussion of fluorescent proteins and their use in biology is presented in 1.4.

1.4 Fluorescent Protein Background

Within the last 20 years, fluorescent proteins have become an essential part of biological fluorescence microscopy. Origins of fluorescent proteins stem back to the investigation of the jellyfish *Aequorea victoria* and its green emission from certain organs. Through isolation of fluorescent extracts, the aequorin chemiluminescent protein was discovered, though the aequorin emitted blue light instead of the expected green emission.[79] The companion protein to the aequorin was the green fluorescent protein (GFP). It was determined the aequorin complex undergoes energy transfer to GFP to give off the green fluorescence observed *in vivo*.[80,81] Surprisingly, GFP is present in a variety of organisms which have the same chromophore.[82,83] It was not until the advent of cloning techniques that GFPs made their way into cellular imaging. In 1992, Douglas Prasher cloned the complete GFP gene for the first time which led the way to expression of the gene in organisms.[84] The usefulness of fluorescent proteins was gaining traction and researchers were getting interested in events inside living cells.[85] However, alone the optical properties of wild-type GFP (WT-GFP) were not optimal for fluorescent imaging. In 1994, Roger Tsien and his group established a single point mutant (S65T) of GFP with

a much better intensity and photostability than the WT-GFP.[86] In 2008, Osamu Shimomura, Martin Chalfie, and Roger Tsien won the Nobel Prize in chemistry for their pioneering work with the green fluorescent protein.[87]

1.4.1 Protein Structure

Two independent reports of the x-ray crystal structure of *Aequorea* green fluorescent protein (PDB IDs 1EMA[88] and 1GFL[89]) revealed that the GFP has a unique overall secondary structure comprised of an 11-stranded β-sheet wrapped into a cylindrical β-barrel protein[88-91] (Figure 1.2 A). Attached to a helical segment of the protein, a chromophore is located near the center of the protein protected by the barrel. Numerous subsequent structures of fluorescent protein homologues from other organisms have revealed that all fluorescent proteins share the β-barrel fold.[77,78,92] Overall stability is maintained by the β-barrel, helping to resist unfolding due to heat or other denaturants.[77,91] The chromophore of GFP is a tripeptide consisting of the residues serine, tyrosine, and glycine at positions 65-67 in the sequence. The chromophore (Figure 1.2 B) forms after translation through a self-catalyzed intramolecular rearrangement of the tripeptide sequence, without the requirement for cofactors or external enzyme components (other than molecular oxygen).[86,91,93] The fluorescent species is a result of highly conjugated π-electron resonance system that largely accounts for the spectroscopic properties of the protein.[94] Extensive mutagenesis studies suggest that the G67 is critical in formation of the chromophore.

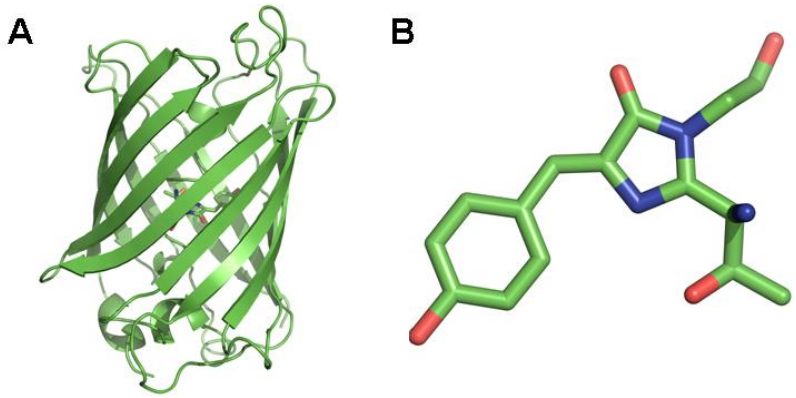

Figure 1.2 Model fluorescent protein and chromophore. (A) Cartoon rendering of green fluorescent protein (PDB: 1EMA)[88] and (B) the autocatalytically modified chromophore. Drawn using PyMOL Molecular Graphics System, Schrödinger, LLC.

1.4.2 Color Palette

Mutagenesis efforts in the original *Aequorea victoria* jellyfish green fluorescent protein have resulted in new fluorescent labels that span almost the entire visible spectrum. The secondary structure of the protein has a high degree of stability making it resistant to temperature and environment, and slight modifications to the amino acid sequence rarely destroys fluorescence.[77] While many spectral variants have been developed by engineering specific mutations to the WT-GFP, other redder variants have been discovered from reef corals. Those from the WT-GFP include the blue[95-99], cyan[100-103], green[78,88,100,104,105], and yellow emitters[106-112]. One example of non-bioluminescent reef corals is the dsRed derived from the *Discosoma* species.[92,113-117] Site-directed and random mutagenesis investigations have revealed that fluorescence is very dependent on the three-dimensional structure of amino acid residues surrounding the chromophore.[91,100] Not only do these mutations alter spectral characteristics of fluorescent proteins, single point mutations of fluorescent proteins have demonstrated the change in photophysical lifetimes.[50,118]

Additionally, proteins that undergo photoswitching between a fluorescent, bright state and non-fluorescent dark state have been developed.[118-121] This photoswitching occurs in part by interconversion between the deprotonated (on state; bright) and protonated (off state; dark) forms and from *cis-trans* isomerization of the chromophore moiety.[122-127]

1.4.3 Photophysics

The tyrosine-based chromophore in wild-type GFP exhibits two main absorption peaks with maxima at 398 nm (band A) and 478 nm (band B), associated with the chromophore and its conjugate base, respectively.[128-137] Excitation of band A simultaneously yields weak 460 nm and strong 508 nm emissions. The dual absorption and emission, together with a large kinetic isotope effect and extensive photophysical studies, have led to the conclusion that an excited state proton transfer (ESPT) reaction[138] (Figure 1.3), followed by additional structural changes, dominate much of the fluorescent protein photophysics. Non-covalent coupling of the chromophore to the protein backbone is facilitated via an extended hydrogen-bonded network[139], within the protective β-barrel.[77,89]

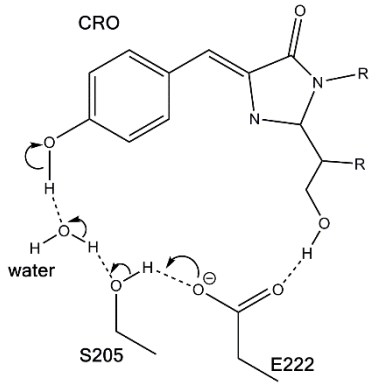

Figure 1.3 Excited state proton transfer in WT-GFP as reported by Chattoraj et al.[138]

While modification of ESPT rates leads to emission wavelength control, photoinduced isomerization ("trans/cis") is a parallel but generally low quantum yield process. When coupled to the proton transfer process, the combined long-lived (isomerization) and wavelength-shifting (proton transfer) processes have yielded several photoactivatable (or "kindling") proteins, as well as switching proteins. Although published crystal structures of the fluorescent proteins all indicate a ground-state in the cis conformation, the trans conformation, coupled with proton transfer to yield the neutral chromophore leads to the presence of dark states from which anionic fluorescence is recoverable upon re-irradiation at 405 nm.[140] Several recent crystal structures of both stereoisomers have been obtained in photoswitchable proteins[118,120,122-125,127,141,142], providing further evidence that the so-called dark state[143] of GFP and some of its derivatives is the trans isomer.[144] There is a considerable amount of information about the role of isomerizations in blinking, which has largely been attributed to intersystem crossing.[140]

1.5 Fluorescent Proteins in Biological Applications

The high biocompatibility of fluorescent proteins has made them useful in a variety of biological applications. With the copious numbers of fluorescent protein fusion tags in a rainbow of colors, the complexity of biological applications has increased. The development of proteins yielding various emission colors has extended multi-color imaging.[3,95,119] Proteins with increased two-photon absorption cross-sections make it possible to image at greater tissue depths.[145,146] Additionally, the information extracted from specialized techniques using fluorescent proteins has expanded the knowledge of

cellular dynamics and interactions. The following discussion is not meant to showcase every use but rather the breadth of uses that benefit from fluorescent proteins.

1.5.1 Imaging

Fluorescent proteins are probably most utilized in biological imaging. Fluorescent proteins are easily expressed in cells to make them fluorescent.[85] However, as subcellular localization of a protein is often tied to its function, it is extremely useful to determine where a protein of interest resides. While there are many methods for determining subcellular localization including electron microscopy[147], fluorescence microscopy combined with fluorescent proteins provides a convienient way for live cell studies.[4,22,36,148] Molecular cloning and extensive libraries of fluorescent protein fusions allows for the labeling of almost every protein of interest. Additionally, procedures are available to label multiple target proteins, and then visualize the location of these target proteins at once with appropriate filter sets. This has been taken a step further with super-resolution techniques and photoswitchable proteins to overcome the diffraction limit and have finer resolution of cellular structures.[14-16,23,61,149]

1.5.2 Sensing

Fluorescent proteins can be engineered to sense physicochemical parameters such as pH, ions, or metabolites.[6,11] Fluorescent protein sensors can be divided into three classes: intrinsic, fluorescent proteins with an additional domain added, and FRET-enabled. The simplest is the sensor that uses the intrinsic properties of fluorescent proteins to affect the fluorescent protein. As discussed in Section 1.4, environmental factors can affect the fluorescent protein chromophore and thus fluorescent output. For example, the steady-state fluorescence of wild-type GFP is pH-dependent because of protonation-

deprotonation of the chromophore.[91,106,147,150] Additionally, many yellow fluorescent proteins are intrinsically sensitive to halides via a mechanism involving halide-dependent shifts in pK_a.[25,111] To extend the sensing capability of single fluorescent proteins, extra domains are grafted such that changes in analyte concentration indirectly produce a change in fluorescence, i.e. conformational change. Examples include calcium ion[151-153] and voltage sensors[154,155]. Finally, the most diverse group, using FRET between spectrally distinct fluorescent proteins, has been used as a reporter of analytes. The engineered linkers between the fluorescent proteins are designed to alter the distance in the response to the desired analyte. FRET can either be disrupted as in the case of protease-cleavable linkers upon protease activity[156-158] or enhanced as in the case of calcium binding to calmodulin[159,160]. Compared to classical chemical probes, fluorescent proteins and constructs have the advantage of being useful in vivo, with quantitative labeling, and in some cases real-time without increased cytotoxity.

1.5.3 Protein-Protein Interactions

Fluorescent proteins can be used in at least three principal ways to investigate the dynamic or stable interactions of proteins of interest: FRET, fluorescence cross-correlation spectroscopy (FCCS), and split fluorescent proteins. In FRET, two proteins of interest are fused correspondingly to donor and acceptor fluorescent proteins.[56] If the protein interaction of interest brings the fluorescent proteins into close proximity, energy transfer may take place (see Section 1.3). An alternative method is based on FCS as discussed in Section 1.3. In dual-color FCCS, the fluctuation of signals is recorded simultaneously for two different fluorophores.[27] The cross-correlation is a degree to which the two signals fluctuate together, which allows one to estimate the interdependence of diffusion rates of

two types of molecules due to their interaction in living cells.[29,161,162] Unlike FRET, there is no distance dependence of the interaction of interest. Recent work has been on developing split-fluorescent proteins in which fluorescent protein halves are fused to the two proteins of interest.[163] If the target proteins interact, they bring the halves into contact, resulting in reconstitution of fluorescent protein and fluorescence appearance. Split proteins are considered to have greater sensitivity than FRET, but as the assembly of the fluorescent protein halves is irreversible, a trapped complex may affect the cellular function of the complex.

1.5.4 Limitations

Fluorescent protein based technologies for *in vivo* imaging continuously push the envelope of experimental biology. On the scale of whole organisms, fluorescent proteins make it possible to visualize cells, tissues, organs and even monitor division and migration of cells in development.[2] However, despite continuing development of these techniques, the adoption of fluorescent proteins in certain applications is still limited. Most fluorescent proteins have a fluorescent brightness that is weaker than many organic dyes and fluorescent nanoparticles[43,67] and are especially problematic for low target protein concentration. Copious amounts of work have been performed to improve the brightness.[36] However, the inherent nature of cellular imaging confounds the issue. One such issue is autofluorescence from intrinsic fluorophores found within the cell.[41,42] These fluorophores induce a heterogeneous background in imaging while using UV excitation commonly used for blue fluorescent proteins and photoswitchable proteins. Solutions include changing to red-emitting fluorescent proteins or "filtering" techniques to suppress unwanted signal and magnify the desired one. However, the consequence is the limitation of multi-labeling

schemes in which blue fluorescent proteins can be advantageous. Additionally, most common techniques are based on detecting within a desired spectral window with fluorophores as spectrally separate as possible to avoid cross-talk within other emission windows. This limits the number of fluorophores used within a single experiment and ultimately results in a reduction in the dimensionality of imaging.

1.6 Optical Modulation

Recent techniques have been developed for dealing with complex, high background in biological samples. As discussed in 1.2.3.4, OLID shows improved image contrast by controlling the conversion of fluorescent and dark states in photoswitchable proteins to regenerate fluorescent populations and correlating with the internal reference to amplify the signal of interest.[17] However, OLID has disadvantages in cellular imaging. The first is the addition of an exogenous, background-free reference fluorophore from which the reference waveform is taken. Secondly, as the fluorophores commonly used in OLID are photoswitchable dyes that need the use of two high-energy lasers relative to fluorescence, the addition of background can reduce the contrast achieved.

As seen with the basic Jablonski diagram (Figure 1.1), intersystem crossing to a non-fluorescent dark state saps electrons from the fluorescent manifold decreasing the fluorescent quantum yield of the molecule. As discussed in 1.2.1, excitation results in electrons filling the higher electronic levels. Once there, they can either radiatively decay to the ground state via fluorescence or non-radiatively decay into a dark state. The rate of decay into the dark state, k_{on}, is a product of the excitation rate constant, k_{exc}, and dark state quantum yield, Φ_D. Once in this state electrons are "trapped" until they naturally decay

back to the ground state, with a rate constant k_{off}. A depopulation of this dark state would increase the number of molecules in the fluorescent manifold.

In contrast to photoswitched-based OLID, our lab recently developed SAFIRe (Synchronously Amplified Fluorescence Image Recovery)[19], a detection scheme that recovers transient dark states of a fluorophore by secondary excitation at wavelengths longer than those of the collected fluorescence (Figure 1.4). Similar to photoswitches, the secondary laser excitation alters the relative population between the emissive and dark states, and thus the magnitude of the fluorescence intensity increase is directly dependent on the rates in and out of the dark state manifold.

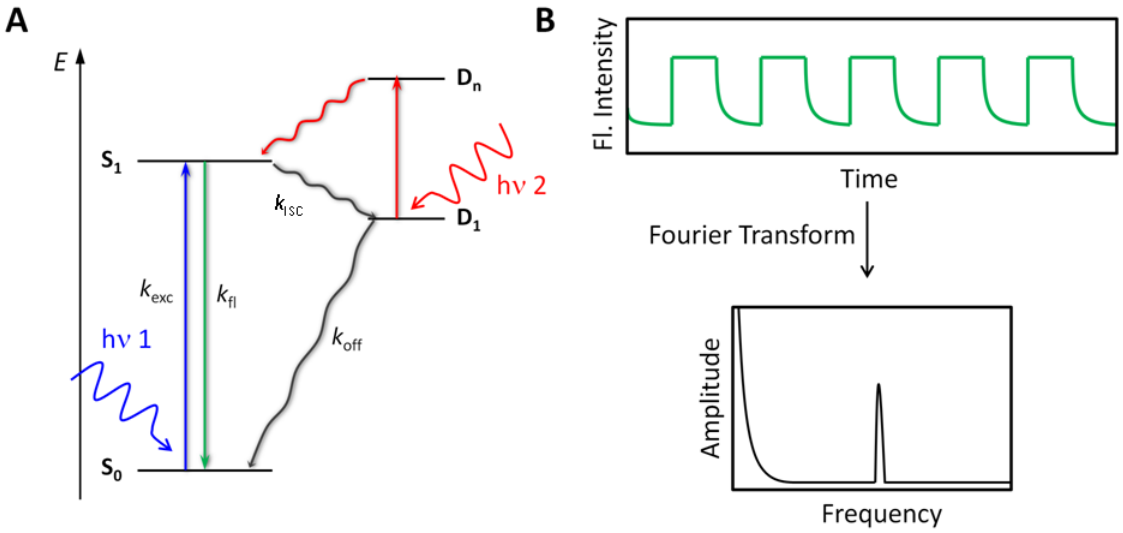

Figure 1.4 Basic overview of two laser optical modulation. (A) Simplified Jablonski diagram showing the processes upon primary laser illumination (hν 1) and depopulation with the secondary laser (hν 2). (B) The extraction of modulation frequency from fluorescence intensity data to selectively recover signal.

This method improves upon some of the drawbacks of OLID. First, replacing second high-energy laser with a low-energy laser compared to emission circumvents additional

background imposed by a second switching laser. Secondly, the Fourier transformation or lock-in detection at the modulation frequency of the secondary laser eliminates the need for an internal reference dye.

Optical modulation is experimentally performed by illumination with a primary laser to excite the molecule and generate the dark state, dictated by $k_{on} = k_{exc}*\Phi_{isc}$. Instead waiting for the dark state lifetime (k_{off}^{-1}) to return to the ground state, the secondary long-wavelength laser is applied to the system (Figure 1.4 A). Dual-laser excitation more rapidly depopulates the dark state, thereby more quickly regenerating the fluorescent manifold and giving a higher probability of emission than with single-laser excitation alone. Modulating the second laser with a specific waveform, encodes this waveform on the dual-laser-excited fluorescence by optically depopulating the dark state at regular intervals. The resulting fluorescence time trace can be Fourier transformed to selectively recover the signal of interest (Figure 1.4 B) which can eventually be used in image reconstruction.

1.7 Organization of Thesis

Optical modulation has only been demonstrated with organic dyes and silver nanoclusters. However, the known photophysical states of fluorescent proteins suggest that they could form nearly ideal optically modulatable fluorophores for intracellular and in vivo imaging. This work investigates select fluorescent proteins for the capability of optical modulation. Additionally, those discovered to be optically modulated are investigated for photophysical timescales responsible for modulation and the possible states involved. An understanding of the optical states involved allows for engineering of fluorescent proteins for specific applications.

Chapter 3 focuses on work on a modified blue fluorescent protein conducted in collaboration with members of the Tolbert and Bommarius groups of Georgia Institute of Technology. Unlike WT-GFP, this tyrosine-based fluorescent protein is not capable of cis-form excited state proton transfer (EPST) and serves a simplified system to investigate modulation and the role of cis/trans isomerization as a possible modulation mechanism. Thus, this chapter investigates an engineered protein blue fluorescent protein, modBFP, and variants, for long-wavelength modulation and photophysical properties characteristic of the modulation. Additionally, the selective recovery of one variant, modBFP/H148K, from high autofluorescent background is demonstrated and points to the renewed utility of blue fluorescent proteins.

Chapter 4 highlights work examining a green fluorescent variant, *Aequorea coerulescens* green fluorescent protein (AcGFP) in collaboration with members of Fahrni group at the Georgia Institute of Technology. In contrast to Chapter 3, the anionic chromophore of the green fluorescent protein is investigated. With the emission shifted from a spectral region of high background such as with BFPs and copious amounts of characterization, green fluorescent proteins have become a staple in biological imaging. The optical modulation and photophysical parameters of modulatable states are discussed. Additionally, the utility of modulatable GFPs in inhomogeneous background environments was demonstrated in cells.

Chapter 5 expands upon the work in the previous chapters to further understand the mechanism of modulation in fluorescent proteins. This chapter demonstrates the modulation of varying colors of fluorescent proteins as well as conditions such as structure, pH, and deuterated solvent that lead to alterations in enhancement and photophysical off

times of the modulatable state yielding a possible mechanism by which modulation occurs in the complex network of fluorescent proteins. This work serves two roles: the expansion of fluorescent probes for better sensitivity in cellular imaging and the understanding of hidden protein dynamics for the engineering better proteins whether for optical modulation or reduction of dark-forming states.

Chapter 6 discusses an alternative to single modulation technique, known as dual modulation. The major difference between the two techniques is that in dual modulation the primary and secondary laser are modulated, usually at different frequencies. While dual modulation can be used with many optically modulated fluorescent proteins, this chapter focuses on the demonstration with photoswitchable proteins. The characteristic frequencies of these proteins are investigated as well as their intensity dependence. Additionally, the sensitivity gains in cellular imaging are explored and compared to other techniques.

Appendix A focuses on work done with cyan fluorescent proteins. This work, while still involving the investigation of fluorescent proteins, has been placed in an appendix as the chromophore in cyan fluorescent proteins is tryptophan-based unlike the tyrosine-based chromophores discussed in the previous chapters. Thus, the mechanism of modulation in these proteins may be different than those already discussed. Reported in this section are the modulation results of enhanced cyan fluorescent protein (ECFP) and monomerized Cerulean (mCerulean) and the efforts to characterize these proteins as done in previous chapters.

CHAPTER 2

EXPERIMENTAL SECTION

2.1 Protein Preparation

Fluorescent experiments can be carried out on fluorescent proteins in a number of environments, including purified protein in buffer, fixed or in live cells, or purified protein immobilized on a gel matrix. For the purpose of photophysical characterization, the easiest way to perform most experiments is with purified fluorescent proteins. All proteins presented in the following chapters were purified or transfected by collaborators (Tolbert and Fahrni groups) at Georgia Institute of Technology. While appropriate protocols for each protein can be found in publications, purification in general is performed through transformation of *E. coli* DH5αPRO cell and induction for protein expression. Cells were then lysed and purified with immobilized metal affinity chromatography. Purified protein is then stored in phosphate buffered saline (PBS) at pH 7.4 in the 4°C refrigerator.

While most purified proteins are directly usable, some mutants require further attention and cleaning. Protein solutions appearing cloudy or having precipitates can result in fluorescence spikes while recording data that produce errant results, dominate signals, and/or damage photon sensitive equipment. In this case, a small portion of protein solution is taken (~500 μL) and centrifuged in a 1 mL centrifuge tube at 8000 rcf for 3 minutes. This removes most of the precipitate in the solution. A Nanosep filter centrifuge tube with a molecular weight cut-off (MWCO) 100 kDa is prepared by adding ~50-100 μL of PBS pH 7.4 to the filter and running at 5000 rcf until almost dry (~30 seconds). A 100 kDa filter was chosen for adequate retention (> 90%) of the ~25-30 kDa proteins. This is

important as some experiments require the dilution of the protein in various other buffers which require a ~1 mM stock concentration, thus adequate retention ensures plenty of working protein solution. Using a 30 kDa MWCO for a reported 27 kDa protein results in about only 60% retention of the desired protein. Thus, if concentration is not a concern, a 30 kDa MWCO filter can also be used. The pre-rinse PBS flow-through is removed from the bottom tube as this PBS contains filter preservative (azide). The supernatant of the centrifuged protein solution is removed and placed on the filter of the prepared Nanosep tube. With appropriate counterweight, the Nanosep filter tube is run at 10000 rcf until most of the solution is collected (~5 minutes). What remains on the filter are undesired particulates or aggregates that are greater than 100 kDa. A UV-Vis and emission spectrum of the collected protein is collected afterwards to ensure the fraction collected is correct and appropriate for the particular protein.

2.2 Protein Sample Preparations

Depending on the experiment, the working protein sample is diluted from pre-filtered stock solutions for the particular experiment. For many experiments, a dilution of the protein to desired emission intensity is all that is needed. However, there are a number of different environments the protein is exposed to that can give information about the photophysical properties and possible mechanism of modulation. As discussed 1.4, environmental changes can affect many fluorescent protein properties including emission color, fluorescence lifetimes, and triplet states. It is this interplay between protein chromophore and environment that is of great interest to this research.

2.2.1 Bulk Solution Measurement

Many experiments discussed in subsequent chapters are based on the bulk protein solution. Bulk fluorescence measurements were performed with a Photon Technology International (PTI) Quanta Maser 40 which is equipped with a xenon arc lamp as an excitation source and a photomultiplier tube sensitive out to 900 nm as a detector. Concurrent absorption measurements were taken with a Shimadzu UV-2401 PC spectrophotometer. Data was collected from samples in either a glass (Starna Cells) or quartz (Hellma Analytics) cuvette with a 1 cm path length. The protein solution used for bulk experiments is prepared by diluting the stock protein into room-temperature (23°C) PBS at pH 7.4. The final working concentration can range between ~ 50 nM to ~3 μM depending on the absorption at a particular excitation wavelength. An estimate of concentration is made by recording the absorption spectra and taking the absorption maximum and dividing by the extinction coefficient of the protein. If the extinction coefficient of a protein is unknown, 50,000 $M^{-1}cm^{-1}$ is used as an estimate. Most working concentrations will result in emission intensities between 25 killicounts/sec and 100 killicounts/sec on the avalanche photodiode (APD).

2.2.2 Bulk Immobilized Measurements

While bulk solution preparations are adequate for most experiments described, there are experiments in which protein diffusion in the focal volume is unwanted. In these cases, the protein must be immobilized. There are a number of ways to do this, including, but not limited to: polyacrylamide or agarose polymer matrix, polyvinyl alcohol (PVA) spin coating, and bioconjugation to a coverslip. PVA and bioconjugation were not used in this project but have their advantages and disadvantages. For example, dilution of the

protein in PVA followed by spincoating is relatively fast and creates an optically thin sample to work with. However, this also removes most, if not all, water from the sample. As possible stability and networks rely on water surrounding the protein this method is disfavored. Though PVA spincoating and bioconjugation to a coverslip are not discussed, it is important to note other methods that may be used.

The preferred and predominately used method is creation of a polyacrylamide (PAA) matrix. This polymer has been used extensively with fluorescent proteins in the literature, and has the advantage of controllable pore sizes, water retention, and free rotational diffusion within the pore.[164,165] With a ~10% PAA matrix, the pore size is appropriate for proteins in the 20-80 kDa range which is close to the size of a fluorescent protein.[164] To create this matrix, 50 μL of acrylamide solution (40% w/v solution with 3.3% bis-acrylamide) and ~150 μL of PBS at pH 7.4 is mixed with ~5 μL of protein (or the appropriate amount for a final concentration of ~100 to 500 nM). A fresh 10% ammonium persulfate (APS) stock is made with nanopure water. After the acrylamide solution, PBS, and protein are mixed, 5 μL of 10% APS is added to the solution followed by 1 μL of N,N,N',N'-tetramethylethylenediamine (TEMED). The APS is a strong oxidizing agent that creates free radicals in which the TEMED stabilizes so that the reaction of crosslinking between the polyacrylamide and bis-acrylamide can take place. This reaction is fast and 2-3 μL of solution must be extracted and sandwiched between two glass coverslips before polymerization is complete. Before adding TEMED, the coverslips are laid out and ready. The sandwiched coverslips are left for a few minutes in the dark, and then are ready for use. The polymerization reaction can be tested by turning the remaining solution upside down and tapping the tip. If the sample remains in the tip, the

polymerization was successful. Of particular note, the APS is very important in the reaction and too much can result in destruction of the fluorescent protein. Solid APS that has been exposed to too much water (atmospheric or other) appears swollen and fluffy. Using this APS results in the wrong concentration of APS solution and a slow reaction. Adding more can speed up the reaction, but too much creates an excess of free radicals that affect the protein stability.

In the case that PAA cannot be used, low melting agarose is also a possible matrix material to immobilize fluorescent proteins. Most fluorescent proteins are thermally stable up to high temperatures of about 70°C. Low-melting agarose has a melting temperature of ≤ 65°C[166] making it a viable alternative for most fluorescent proteins. A 1% agarose solution is made with the desired buffer and placed in a water bath set to 65°C. The agarose melts which is noted with the visible change from cloudy to clear solution in the Eppendorf tube. Once melted, stock fluorescent protein is added at the final desired concentration for the experiment and pipetted a few times. A small portion is then added to a pseudo-flow channel created from two coverslips and double-sided tape. The polymerization is gauged the same way as the PAA was and once polymerization is completed the experiment can be run. Though, not all fluorescent proteins are thermally stable enough to withstand 65°C and results in no fluorescence being detected during the experiment. A possible remedy to this is to decrease the water bath temperature and to add the protein even if the solution is not fully melted. This has not been tested, but may be a solution if thermal stability is a problem and PAA cannot be used.

2.2.3 Buffer Exchange

As all proteins are stored in PBS at pH 7.4, the pH of the solution must be exchanged to investigate pH effects. Buffers are made using normal procedures at 10 mM buffering salt at pHs between pH 4 through 10.5 based on the properties listed in Table 2.1.

Table 2.1 Buffer Solutions for Varying pH Ranges

Buffer	Conjugate Acid/Base	pKa	Useful pH range
Acetate	Acetic acid/sodium acetate	4.76	3.6 – 5.6
Phosphate	Monobasic phosphate/Dibasic Phosphate	7.20	5.8 – 8.0
Tris	Tris/HCl	8.06	7.0 – 9.0
Carbonate	Sodium bicarbonate/sodium carbonate	10.2	9.2 – 10.8

pH measurements are made with Ag/AgCl pH electrode (VWR) and ThermoScientific Orion Star module. The electrode is calibrated at 23°C with standard buffers for pH 4, 7, and 10 creating a linear calibration curve in the module which is then used for pH measurements. Sodium chloride is added to reach a final concentration of 140 mM. Once the buffers are made, the pH is adjusted with concentrated sodium hydroxide or hydrochloric acid. In order to make the exchange from the storage PBS pH 7.4 to the desired pH, the concentrated stock protein is diluted in the target pH buffer to the desired concentration for the experiment. Depending on excitation wavelength and emission collection window, the final protein concentration is between 100 nM and 3 μM. This depends on the absorption cross section of the protein for the particular laser used. Higher concentrations are normally used for the blue and cyan fluorescent proteins in which 405 nm excitation was not very efficient as the excitation peak maxima were 10-20 nm away from the excitation. The final working solutions at various pHs are then mixed and left in the dark for 30 minutes.

2.2.4 Deuterium Oxide Exchange

2.2.4.1 Deuterium Oxide Purity Validation

Excited and ground state proton transfers are crucial in understanding fluorescent protein photophysics. For deuterium isotope effects to be observed, a deuterated buffer must be created and exchanged with the hydrogen-rich PBS in which the fluorescent protein is stored. For the H-D exchange to be efficient and extensive enough to reach the interior of the β-barrel, deuterium oxide (D_2O) of > 95% purity must be used. With the assistance of the Dr. Thomas Morgan of the Fahrni lab at Georgia Institute of Technology, NMR was performed on the deuterium oxide to be used. In a NMR tube, 700 μL of D_2O was added with a 1mL syringe equipped with a 25G needle. Making sure to not lose any to the side of the tube, 10 μL HPLC grade acetonitrile (CH_3N) is added to the D_2O for a final concentration of 0.27 M. A proton NMR spectrum was taken and the resulting integrations were recorded (Table 2.2).

Table 2.2 NMR Results of Deuterium Oxide in Acetonitrile

Compound	**Theoretical Chemical Shift (ppm)**	**Experimental Chemical Shift (ppm)**	**Integration of Peak**
Acetonitrile	1.9	1.899	3.5
Deuterium Oxide	4.6	4.647	5.10

Based on the Equation 2.1 using the above integration peaks, the concentration of water in the working deuterium oxide can be determined from the known concentration of acetonitrile.

$$[H_2O] = [CH_3N] \times \frac{\mathrm{Int}(H_2O)/2}{\mathrm{Int}(CH_3N)/3} \qquad \text{Equation 2.1}$$

As pure H_2O has a concentration of 55.6M, then D_2O of 99% purity has 0.55 M H_2O. Thus, based on the integrations obtained from the deuterium oxide used for the experiment, the reported 99% D_2O has 0.64M H_2O. To ensure a high level of purity, the stock bottle of deuterium oxide is opened under an inert gas and the mouth of the bottle is purged before storage.

2.2.4.2 Deuterated Buffer Preparation

There are two ways to prepare deuterated phosphate buffered saline (DPBS). The preparation of large amounts (> 5-10 mL) of DPBS is best effected by drying the deuterated salts in a vacuum oven. DPBS is good for about a month at pD 7.4, so normally large batches are not created. The method described herein is a modification of the SpeedVac method described in Shaw, et al.[167] As this modified method creates smaller amounts of DPBS, it is used more regularly for the experiments preformed in this project.

To begin, a buffer is chosen with a pH ~ 0.4 units lower than the final desired pD. In a 1 mL Eppendorf tube appropriate for vacuum centrifuge, 250 μL of the buffer is added and placed in the Savant SpeedVac at high drying for approximately 3 hours depending on the pressure created in the vacuum system. The first round of drying results in elimination of the water in the buffer; however, the dried salts still have hydrogen that needs to be exchanged with deuterium. In the second round of drying, the salts are resuspended with D_2O, mixed, left for 20 minutes, and then placed in the SpeedVac again. Here, the deuterium exchanges with most of the hydrogen of the salts within the first 5 minutes, with additional minutes of waiting for added probability of reaction. The salts obtained are

mostly exchanged with deuterium, though the process is repeated a total of 3 times with resuspension and drying of D_2O to minimize water contamination from atmospheric exposure. After the last exchange cycle, the solution is measured for pD taking into account the correction factor for glass electrode pH meters (Equation 2.2).[168,169] The pH electrode is calibrated with standard buffers (pH 4, 7, and 10) at 23°C.

$$pD = pH_{meter} + 0.4 \qquad \text{Equation 2.2}$$

2.2.4.3 Deuterated Buffer Exchange

Stock protein of high concentrations (≥50 μM) is advantageous for exchange as only a small amount is used, introducing water into the buffer. The protein is added to 200-250 μL DPBS at a concentration ~10 times the final desired concentration for experiments. This ensures that any loss of protein later will not affect experiments. After 10 to 20 minutes, the mixture is placed on a prepared 3 kDa Nanosep filter to concentrate. This step allows the PBS/DPBS mixture to flow through while the protein remains on the filter to be resuspended with more DPBS. Repeating the cycle 3 times ensures that most of the water of the original stock buffer is removed and the major contacts with the protein are the DPBS. While this is the preferred method of exchange, effects can also be seen with just dilution of the stock protein in DPBS, though results are less consistent.

2.3 Bulk Characterization

For many of the florescent proteins investigated, the photophysical parameters of fluorescent proteins have already been determined. However, in the case of the blue fluorescent proteins modified and mutated as discussed in Section 3.3, the photophysical properties are unknown. Understanding these parameters gives insight to the possible

mechanism and reasons for enhancement changes. Normal bulk characterization methods are discussed below.

2.3.1 Fluorescence Quantum Yield

The fluorescence quantum yield (Φ_F) is the ratio of photons absorbed to photons emitted through fluorescence.[43] In other words the quantum yield gives the probability of the excited state being deactivated by fluorescence rather than by another, non-radiative mechanism. The most reliable method for recording Φ_F is the comparative method of Williams et al.,[170] which involves the use of well-characterized standard samples with known Φ_F values. The quantum yield is calculated using the slope of the line determined from the plot of the absorbance against the integrated fluorescence intensities (Equation 2.3).

$$\Phi = \Phi_R \left(\frac{m}{m_R}\right)\left(\frac{n^2}{n_R^2}\right) \qquad \text{Equation 2.3}$$

In which *m* is the slope of the line obtained from the plot of the integrated fluorescence intensity vs. absorbance, *n* is the refractive index of solvent and the subscript R refers to the reference fluorophore of known quantum yield.

The protein of interest and reference protein, mKalama1, are diluted so that the OD at the excitation wavelength ranges between 0.01 and 0.05. The emission spectra of these samples as well as the solvent are taken. The correct excitation wavelength is located so that upon correction of the spectra with the solvent spectrum there is not a negative dip in the resulting spectrum. The integrated intensity is calculated for each corrected spectrum and plotted against OD. As the solvent is the same for the two proteins, the refractive index

ratio is 1 and the slopes and reference quantum yield is used to determine the quantum yield of the protein of interest.

2.3.2 Extinction Coefficient

Extinction coefficient is a measure of the rate of diminution of transmitted light via scattering and absorption for a fluorophore. Defined by the Beer-Lambert law, the extinction coefficient (units: $M^{-1}cm^{-1}$), ε, is the capacity to absorb transmitted light. Also important is the fluorescence output per fluorophore ("brightness"), which is proportional to the product of the extinction coefficient (at the relevant excitation wavelength) and the fluorescence quantum yield.

In order to experimentally determine a fluorescent protein extinction coefficient, the protein is diluted over at least an order of magnitude at the 280 nm peak, as this is the common absorbance for all proteins. As the exact concentration of the protein is unknown, the sequence obtained from the Tolbert group was input into the ExPASy ProtParam program to determine the coefficient of the protein.[171] The protein coefficient determined by ExPASy is based on the individual coefficients at 280 nm of each absorbing amino acid in the sequence (Equation 2.4) where for proteins measured in water: ε_Y is 1490, ε_W is 5500, and ε_C is 125.[64]

$$\varepsilon_{protein} = (\#Y * \varepsilon_Y) + (\#W * \varepsilon_W) + (\#C * \varepsilon_C) \qquad \text{Equation 2.4}$$

Y refers to tyrosine and W refers to tryptophan. "C" here is for cystine that is the amino acid formed by the oxidation of two cysteine (cysteine itself does not contribute to extinction coefficient at 280 nm) molecules that covalently link via a disulfide bond. Once the extinction coefficient of the protein is calculated, the Beer-Lambert equation can be

used to get the protein concentration. With this and the absorbance at 390 nm of each dilution, the extinction coefficient of the fluorophore can be determined.

2.3.3 Apparent pK_a Measurements

To compare with known blue fluorescent proteins, apparent pK_a measurements are based off the procedures described in Ai et al. in which proteins were dialysised into 5 mM buffer and then diluted into a series of 200 mM buffers.[95] After dilution, the fluorescence intensity of each dilution is measured using a fluorescence plate reader. In the absence of a plate reader, 300 mL fluorescent protein solutions in buffers pH 4 through 10.5 and the emission spectra were taken. The resulting plot of fluorescence intensity versus pH appeared linear leading to difficulties determining a pK_a. As fluorescence intensity measurements were inconclusive, the alternative was measuring the enhancement as a function of pH. The fluorescent proteins were diluted in buffers for 30 minutes and the enhancement was recorded with 372 nm pulsed excitation and 514 nm secondary excitation over three separate trials.

In titration curves, there is a point that occurs halfway through a buffered region where the pH barely changes for base added, the half-equivalence point. The half-equivalence point is when just enough base is added for half of the acid to be converted to the conjugate base. When this happens, the concentration of H^+ ions equals the K_a value of the acid, thus $pH = pK_a$. Thus, from the enhancement versus pH graph the buffering region can be identified and the midway point of the region is the pK_a of the protein.

2.4 Fluorescence Correlation Spectroscopy

Fluorescence correlation spectroscopy (FCS) records temporal changes in the fluorescence emission intensity caused by single fluorophores passing through the focal

volume of an excitation source.[48,49] These intensity changes can be quantified in their strength and duration through a temporal autocorrelation of recorded intensity signal. The average number of fluorescent particles in the detection volume and their average diffusion time through the volume can be extracted from the auto-correlation. Additionally, fluorescent proteins have been known to blink and this "flickering" in the fluorescence intensity is treated as the result of transitions between an excited dark state and an emissive fluorescent state. During these intervals, the fluorescent protein cannot emit any photons and appears dark. If the dark state has a lifetime longer than 1 ms, then this dark state can also be detected though it is likely convolved with diffusion of the protein.

Previous studies had studied the excited dark state of other fluorescent proteins such as EGFP through FCS[50], and thus FCS was also performed on fluorescent proteins in this work. Of interest is the effect of the secondary laser on the apparent on and off times of the fluorescent protein. Fluorescent protein samples are prepared as discussed in Section 2.2.1 to a concentration 10 nM to 50 nM depending on protein. The optical setup is the same as the optical modulation setup in Section 2.6. However, the modulator in this case is a shutter or beam block, as no repetitive modulation of the secondary laser is needed. Once approximately one million or more photons are collected with the detector, the resulting data is autocorrelated and fit via BIFL Data Analyzer software.

BIFL Data Analyzer is a software program that allows for the import of time correlated single photon counting (TCSPC) data and has the subsequent analysis models for fluorescence decays, anisotrophy, and autocorrelation. The autocorrelation analysis is used for the fit of the correlation curve of the data collected. In the case of the autocorrelation function of molecules in solution (FCS), BIFL uses a function that extracts

F and *t* (triplet-state faction and lifetime, respectively, while accounting for diffusion components. In the FCS experiment, a proper dilution of the fluorescent protein solution will have an average of 1 to 3 molecules in the focal volume. The triplet-state fraction and lifetime are used to calculate the on and off times of the dark state (Equation 2.5 and Equation 2.6) where *F* and *t* are the triplet-state fraction and lifetime solved from the fit.

$$\frac{1}{t} = \frac{1}{\tau_{on}} + \frac{1}{\tau_{off}} \qquad \text{Equation 2.5}$$

$$\frac{\tau_{on}}{\tau_{off}} = \frac{1 - F}{F} \qquad \text{Equation 2.6}$$

2.5 Single Molecule Measurements

Ensemble averages of molecular properties, as measured in bulk biochemistry studies, tend to mask the underlying molecular dynamics because the measured signals are the unsynchronized average of the contributions of every molecule in the sample. As a result, individual processes can be obscured by other, more dominating processes with which signals are convolved, often resulting in fit analysis giving misleading or inconclusive pictures of the true dynamics. At the single-molecule level, signals display each random and stochastic dynamic process that could otherwise be lost at ensemble level. Thus, while much has been learned using traditional bulk biochemical approaches, there are important reasons to obtain single-molecule trajectories to describe certain processes. In the case of fluorescent proteins, previous studies had suggested the presence of a longer, millisecond-lived dark state could be convolved with other physical processes detected by FCS such as diffusion. Thus, to obtain a true picture of the photophysics in the absence of diffusion, single-molecule experiments are advantageous.

Single molecule samples are prepared as discussed in Section 2.2.2 at a final concentration of about 50 nM. Samples can be checked on the microscope, illuminating with a defocusing lens to visualize the fluorescent proteins immobilized in the PAA. At the appropriate concentration, individual proteins will be seen and in some cases blinking will be observed. To perform the experiment, the optical setup is the same as discussed in Section 2.6. The camera and defocusing lens are used to identify the individual fluorescent proteins, then the defocusing lens is removed to illuminate with the full focused intensity of the laser to collect individual fluorescence trajectories. Experiments are separately performed with primary-only and with dual-laser excitation. Each time trace for the fluorescent protein is collected until photobleaching occurs. For each time trace, an autocorrelation is performed and then fit with multiple dark state model function for immobilized molecules where c_j are pre-exponential factors, τ are triplet-state lifetimes, K is number of exponents.

$$G(t) = 1 + \sum_{j=1}^{K} c_j e^{t/\tau} \qquad \text{Equation 2.7}$$

The number of exponents the curve is fit to can be changed to yield a better fit. Again, the times and amplitude of the components can be used to calculate the on and off times similar to calculations done with FCS in Section 2.4.

2.6 Optical Modulation

The majority of the experiments done in this project are basic optical modulation experiments. The theory of optical modulation is discussed in Section 1.6. This section is the explanation of the practical optical setup and analysis of the experiments.

2.6.1 Basic Experimental Setup

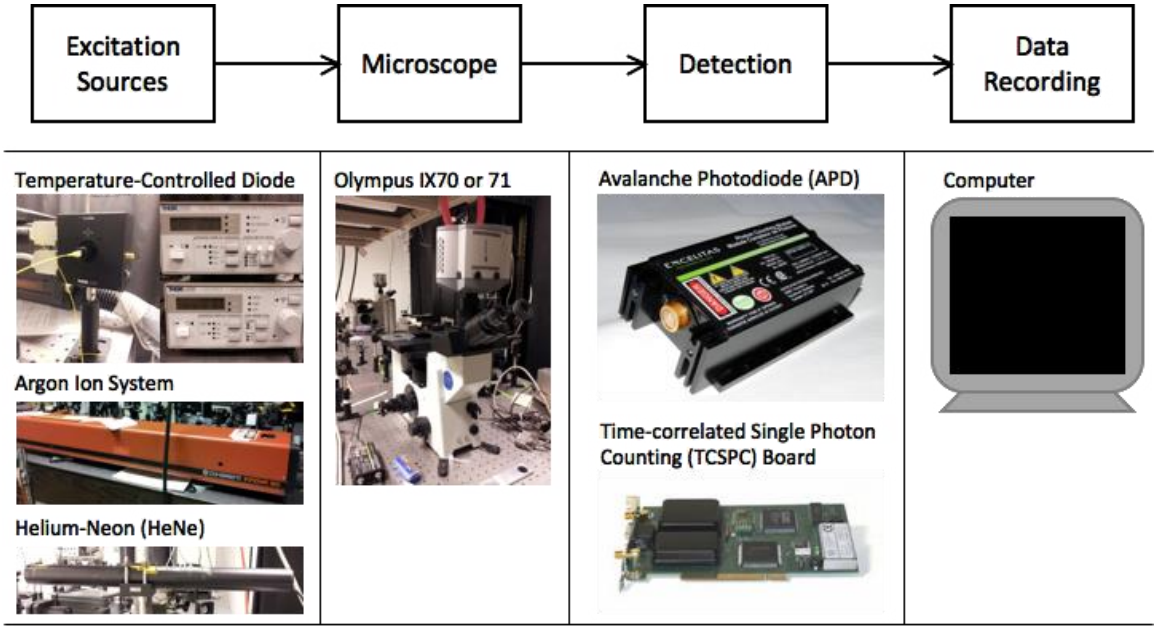

Figure 2.1 The basic optical components for experimental setup. In general, the excitation sources for the experiment are directed into a microscope. The resulting fluorescence from the sample is collected and detected and recorded. The shown devices are some of the most common devices used for each step and can be specialized for particular experiments.

Figure 2.1 represents the basic components of all optical experiments done in this project. The first considerations are the excitation sources being used and the available optics, such as dichroics and bandpass filters. The first laser (primary) is chosen so that it can adequately excite the molecule of interest. The second laser (secondary) should be longer wavelength than the emission window. Table 2.3 is a collection of the primary and secondary wavelengths and systems used for each protein class.

Table 2.3 Excitation Sources for Optical Modulation

Protein Emission	Primary Laser	Laser System	Secondary Laser	Laser System
Blue (~450 nm)	372 nm 405 nm	Picoquant Pulsed ThorLabs Diode Controller + 405 nm diode	488 nm 496 nm 514 nm	Coherent Ar^+ Water chilled systems
Cyan (~480 nm)	405 nm	ThorLabs Diode Controller + 405 nm diode	514 nm	Coherent Ar^+ Water chilled systems
Green (~510 mn)	476 nm	Coherent Ar^+ Water chilled systems	561 nm 594 nm 633 nm 700-950	Sapphire Solid State HeNe Tube HeNe Tube Mira System CW
Yellow (~530 nm)	476 nm	Coherent Ar^+ Water chilled systems	594 nm 633 nm 700-950	HeNe Tube HeNe Tube Mira System CW
Red (~600 nm)	543 nm 561 nm	HeNe Tube Sapphire Solid State Laser	700-950	Mira System CW

Once the excitation sources are chosen, the lasers are aligned into the back of the microscope (Figure 2.2). Normally, the secondary laser intensity will need to be dynamically changed at a specified frequency. To do this, a modulator is placed in the path of the secondary laser as it is aligned to the microscope. The modulator can be a shutter, chopper wheel, or electro-optical modulator (EOM) as shown in Figure 2.2. A function generator externally controls the modulator frequency and, in most cases in this work, is a square wave. When performing dual-laser experiments, the two excitation sources are overlapped before entering into the back of the microscope. In Figure 2.2, the optical path is laid out so that the primary is reflected off and the secondary is transmitted through the dichroic.

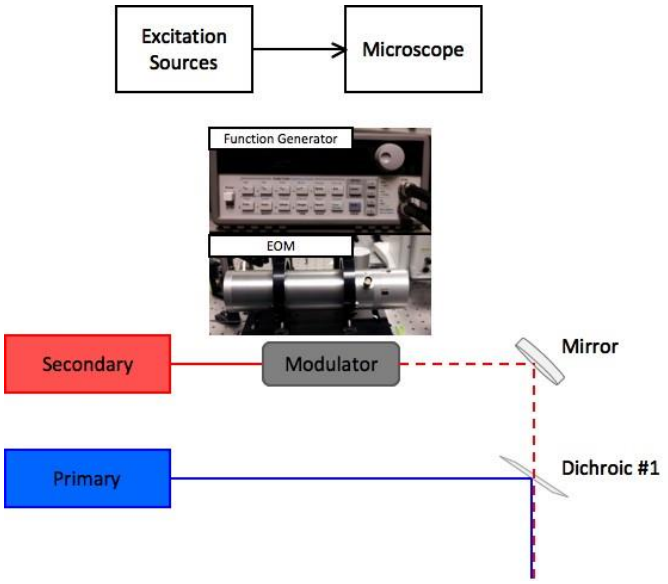

Figure 2.2 Typical optical excitation path for long-wavelength modulation.

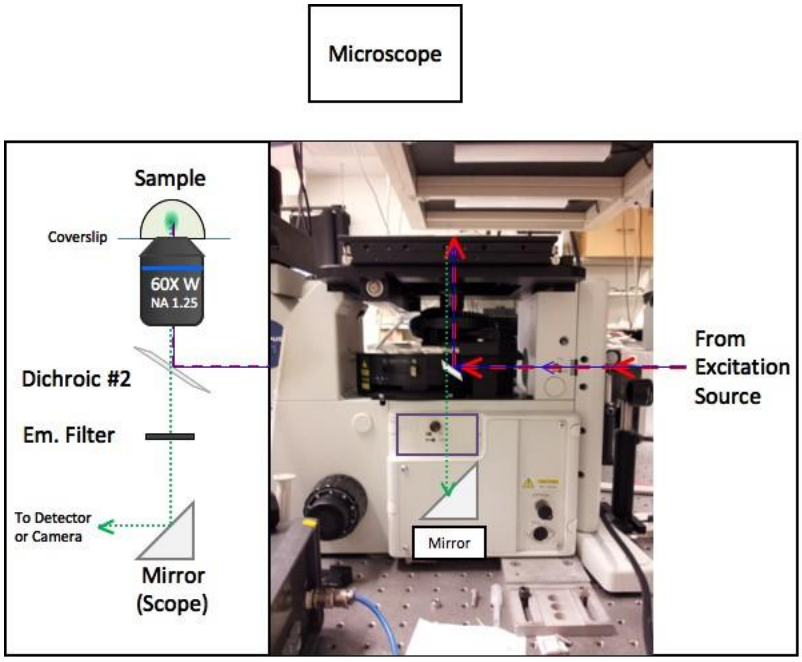

Figure 2.3 Optical path inside the inverted microscope. The green dotted line indicates fluorescence generated by the sample. The mirror is an internal component of the microscope.

Once the laser path is directed to the recombination dichroic (dichroic #1) both beams are diverted into the microscope. Inside the microscope, another dichroic (dichroic #2) directs the beams up and through the objective and sample (Figure 2.3). It is important to choose a dichroic that will reflect both lasers and transmit most of the desired emission. The emission is collected through the objective and passed through dichroic #2. After the internal dichroic, an emission filter is placed. The emission filter should pass the desired emission, but block any transmitted laser light. However, before fluorescence from the sample is collected the beams must be overlapped to follow the same path through the objective. For convienience, light reflected from a glass coverslip is used for initial alignment. Once reflected through the objective, the laser beam must be positioned to a spot in which the scatter transmitted from the coverslip is centered on the sideport adapter. The fluorescence will travel a similar path as the lasers, thus this will roughly align the sideport to collect fluorescence. It is easier to start with one beam and work on the position of that beam and move the other beam to the same position. This is especially crucial when near ultraviolet and infrared lasers are used, as the beams are difficult to see.

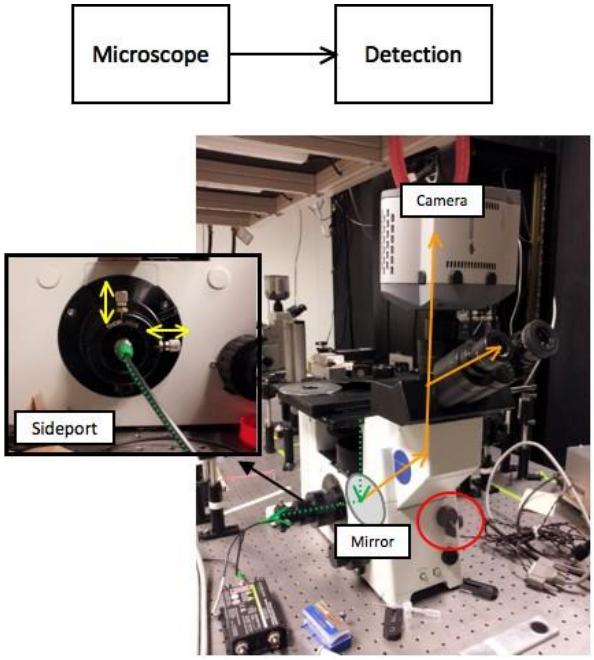

Figure 2.4 Optical path from the microscope to the detection device. The internal mirror direction is controlled by a knob on the microscope (red circle). This directs the light path up to the eyepiece with camera or to the sideport. Translational motion of the sideport is adjusted with adjustment knobs (inset).

With the use of the 2 mirrors before entering the microscope, the beam is centered in the sideport and then the beam shape is observed with the use of a camera. This shaping and positioning is repeated until the transmitted laser beam can pass through the sideport adaptor unobstructed (Figure 2.4). The position is marked on the camera and the second beam is then positioned and shaped to the mark. The sideport is connected to a detector, normally an avalanche photodiode (APD), with an angle cut multimode optical fiber (50 μm or 100 μm diameter core). The APD is synchronized with a time source and the output is directed to photon counting board (Time Harp 100 or SPC-360). Figure 2.5 displays the configuration and equipment used. A reference dye is used to fine-tune the sideport position and collect the maximum fluorescence. It is also important to check for laser bleed-through into the emission window by placing water on the coverslip. In order to

check the overlap of the 2 beams, the reference dye or known modulatable protein can be used to check for modulation.

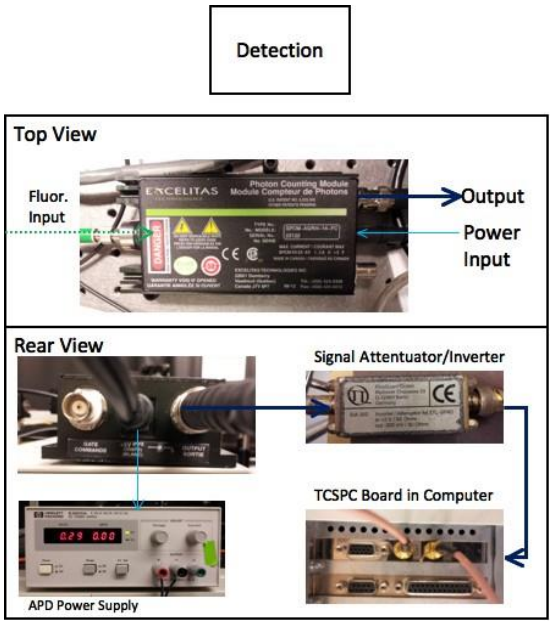

Figure 2.5 Detection configuration of collected fluorescence.

2.6.2 Analysis

2.6.2.1 Enhancement

The measure of modulation or modulation depth is fluorescence enhancement. This is defined in Equation 2.8 by the increase in fluorescence intensity due to the illumination with the secondary laser where I_F is the recorded fluorescence intensity recorded in photon counts per second and the subscript designation is whether the illumination is with the primary only (1 laser) or both lasers (2 laser). No enhancement is equal to 1. This method of calculating enhancement is good for real-time evaluation of intensity change.

$$\text{Enhancement} = \frac{I_F^{2laser} - I_F^{1laser}}{I_F^{1laser}} \qquad \text{Equation 2.8}$$

However, this calculation is somewhat subjective as concentration and total counts can yield somewhat varied results. An alternative method is to take a Fourier transform of the fluorescence time trace. Data is binned at least 2.5 times faster than the highest frequency, and from the resulting Fourier transform the amplitude at the modulation frequency (ν_{mod}) and zero frequency (ν_0) component which the amplitude of all fluorescence, the enhancement can be calculated (Equation 2.9). The resulting graph of Fourier transform displays the positive side where ν_{mod} is recorded, though there is a symmetrical peak on the negative side of zero frequency (ν_0) component that must be accounted for, thus the factor of two in Equation 2.9.

$$\text{Enhancement} = \frac{Amplitude\ \nu_{mod}}{Amplitude\ \nu_0} \times 2 \qquad \text{Equation 2.9}$$

2.6.2.2 Characteristic Frequency

As the secondary laser modulation is scanned from low to high frequency, a plot of the enhancement (Equation 2.9) versus the modulation frequency is created. Analogous to frequency domain lifetime, the buildup and decay of steady state population takes a finite time and results in decreased modulation depths at frequencies higher than the inverse time to establish these populations. The fluorescence enhancement as a function of secondary laser modulation frequency was fit to Equation 2.10 in which *m* is modulation depth or enhancement, ν_{mod} is the modulation frequency, and τ_c is the characteristic lifetime. For this project, the characteristic frequency is defined as the frequency at which the enhancement drops to 50% of its original value.

$$m = \frac{1}{\sqrt{(1 + (2\pi\nu_{mod}\tau_c))^2}}$$ Equation 2.10

2.7 Dual Modulation

Dual modulation is an extension of the optical modulation described in Section 2.6, in which both lasers are modulated. The major difference between the two experimental setups is that in dual modulation the primary and secondary laser are modulated, usually at different frequencies. Exclusively discussed in Chapter 6, dual modulation has been most productive with photoswitchable fluorescent proteins.

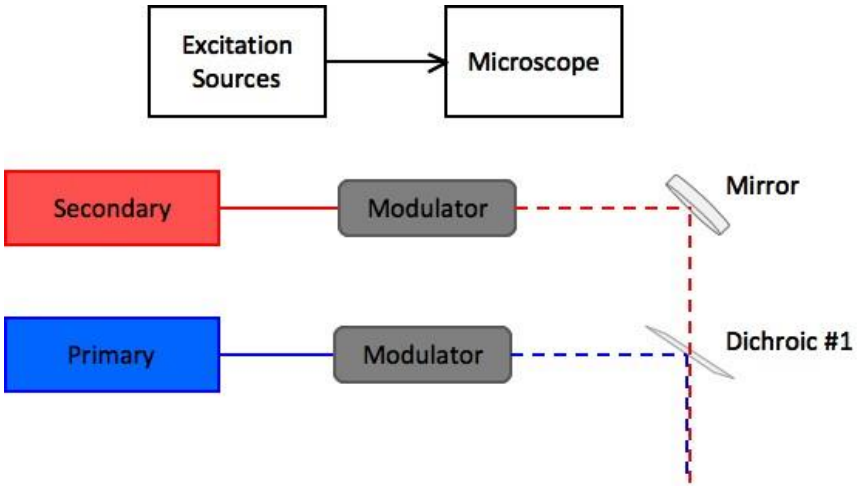

Figure 2.6 Optical path for dual modulation. In this case, primary refers to the laser that produces fluorescence and secondary is the switching laser.

The basic setup for a dual modulation experiment is very similar to the longer wavelength, secondary technique. However, the lasers used are ThorLabs 405 nm diode and Coherent Ar^+ laser tuned to 488 nm. The setup and alignment procedure is the same as the optical modulation case, but now both lasers are modulated (Figure 2.6). In principle, any laser

can be aligned through a modulator as the secondary laser is in basic modulation experiments. However, as the 405 nm laser used in the experiment is a diode in a diode head that can be externally controlled, the current running to the diode can be modulated with a function generator. Thus, the 405 nm laser and modulator are one unit in Figure 2.6. The resulting fluorescent time traces are binned at least 2.5 times faster than the highest expected sideband. The sidebands result from both sequential two photon absorption – both lasers give rise to the observed emission. The first laser generates fluorescence and prepares the dark state, the second depletes the dark state so the first laser can generate more fluorescence. Both lasers are necessary to produce the modulated fluorescence – essentially mixing in the fluorophore due to its optical response. As with the optical modulation, a Fourier transform is taken of the trace and the enhancement is calculated (Equation 2.11) where $Amp_{\nu(+)}$ is the amplitude of the sum frequency, $Amp_{\nu(-)}$ is the amplitude of the difference frequency, and $Amp_{\nu(488)}$ is the amplitude at the frequency of 488 nm. Instead of the modulation frequency of the secondary laser, the sum and difference sidebands of the 488 nm frequency are used to calculate the enhancement.

$$\text{Enhancement} = \frac{Amp_{\nu(+)} + Amp_{\nu(-)}}{Amp_{\nu(488)}} \qquad \text{Equation 2.11}$$

2.8 Imaging Configurations

As fluorescent proteins are easily encoded into the cells, many of the applications of optical modulation discussed in this thesis are related to cellular imaging. Below is a description of cell preparation and imaging modality for the various projects.

2.8.1 Cell Preparation

For all imaging projects, NIH 3T3 cells are used. The cells are cultured and prepared by the Fahrni lab for the GFPs and the Bommarius lab for the BFPs (Figure 2.7). For fixed cells, cells are prepared with formaldehyde fixation in two ways. The first way is the growth of cells in a 6-well plate in which the wells have a clean, glass coverslip in the bottom. Cells are then transfected with the desired plasmid and transfection agent and when ready, the cells are fixed with a solution of 4% formaldehyde in PBS. After fixation, the glass coverslips are removed from the well and placed on slides with a drop of mounting medium. The second method is to grow the cells in MatTek 35 mm glass bottom imaging plates that have a shallow 14 mm opening to image through. Transfection and fixation are the same; however, the fixation is done in the imaging plate and no mounting medium is used, just a 1 mL layer of PBS. For live cells studies, cells are grown and transfected in imaging dishes. At time of preparation, the cells are washed of the phenol red containing medium and provided PBS either alone or supplemented with 1-3% fetal bovine serum (FBS). In blue fluorescent proteins, the FBS caused extremely high fluorescent background, which is why unsupplemented PBS was used. Detailed protocols are available for the respective labs in which the cells are prepared.

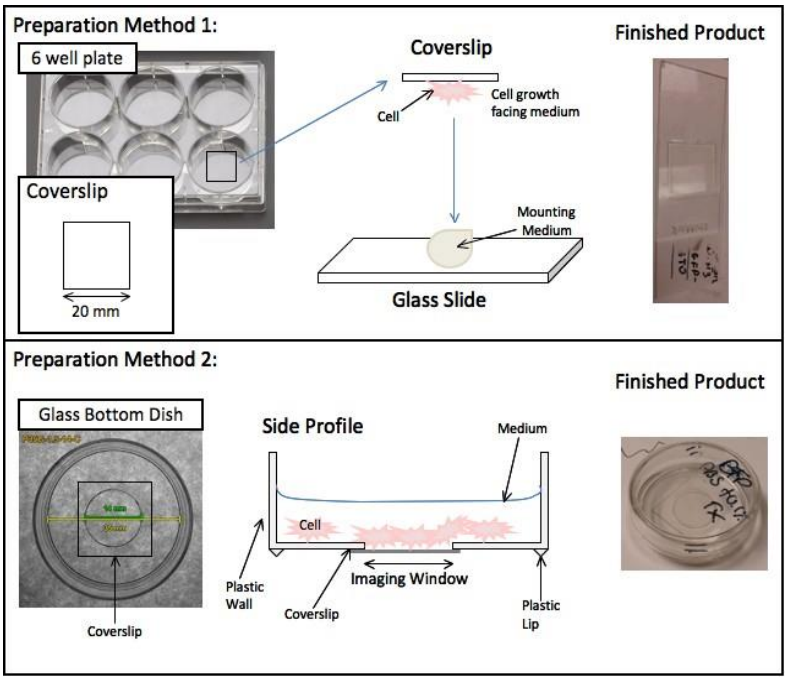

Figure 2.7 Preparation methods for cellular imaging. Cells are grown and prepared by collaborators in the Fahrni or Bommarius lab.

2.8.2 Point-by-Point Scanning

Primarily used when imaging cells transfected with GFP, this imaging modality collects information at a diffraction-limited spot and the image is reconstructed with information at each of those spots. This method is useful for cases where modulation depth is low, and thus, a need for high excitation intensities.

2.8.2.1 Experimental Setup

Overall, the setup is similar to the single laser experiment. The two laser combinations are the same as in Section 2.6.1. The secondary laser is still aligned through a modulator. However, both lasers are expanded to fill the back of the objective. The expansion of the beams are done in this case with a lens pair with appropriate focal lengths magnifying the beam by 2 to 3 times while maintaining collimation (Figure 2.8). The

purpose of this is to create a smaller focal volume and thus approach a diffraction-limited excitation spot. In turn, the z dimension sectioning is a bit better as well. The alignment from the recombination at the dichroic to through the objective is the same. Depending on the sample, an oil or water 60X objective is used.

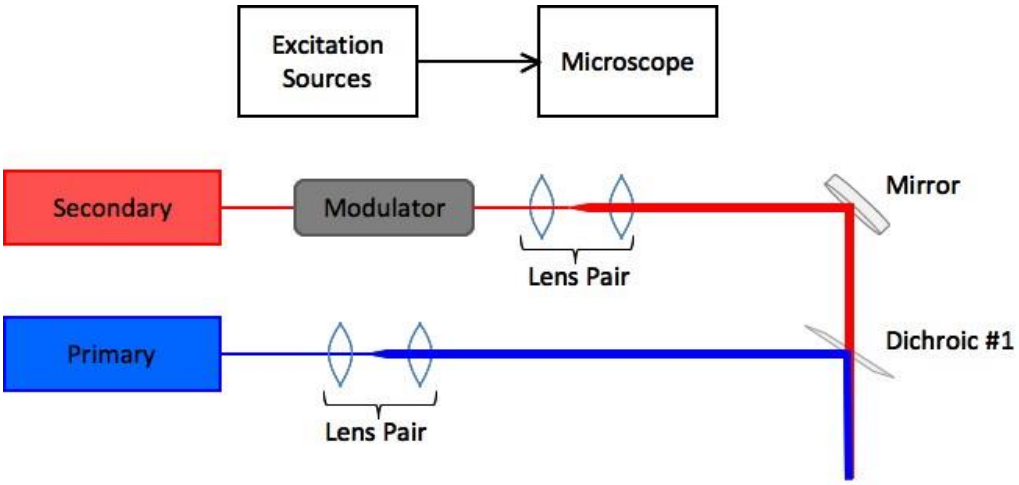

Figure 2.8 Optical path for laser beam expansion for point-by-point scanning experiments.

Both a 1.6X expansion lens in the microscope (Figure 2.9, purple box) and a motorized piezo stage (Figure 2.9 A) are used. The cell sample is held on piezo- stage (Mad City Labs) in either an attachment designed for slides or circular dishes (Figure 2.9B). Live cells must be held at 37°C. Thus, a heated stage is placed on the piezo- stage and secured to the moving part of the stage. The controller is set to 47°C because the transfer of heat from the stage to the liquid covering the cells is through the lip of plastic on the imaging dish (Figure 2.7). This results in a heterogeneous heating of the dish with a higher ~45°C temperature of solution/dish at the edge and ~37°C temperature in the 14 mm imaging area.

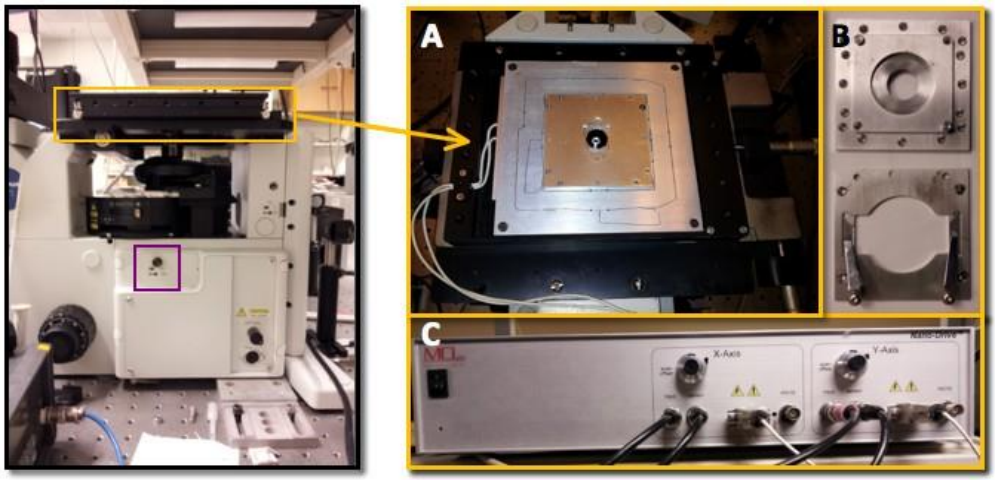

Figure 2.9 Additional parts to optical modulation for point-by-point scanning experiment. The purple box indicates the 1.6X magnification lens. The yellow box is the motorized stage used to move the sample for fluorescence collection of various spots. (A) Top view of stage. (B) Cellular sample holders for (top) 35 mm dishes and (bottom) glass slides. (C) Controller unit for the x and y dimension of the stage.

The fluorescence detection uses the same equipment used in other optical modulation techniques, though additional equipment is added and new connections are made in order to reconstruct an entire image. Figure 2.10 gives the general flowchart of the connections between equipment that are needed. The fluorescence is collected in two possible ways. Each utilizes the same equipment, but the connections are slightly different. The first way is to collect all the fluorescence with a 50 μm optical fiber connected to an APD. The output of the APD is then directed to a TTL splitter that splits the signal equally to one of two instruments. One is a digital lock-in amplifier (which is also synced with the function generator controlling the modulator), which detects and amplifies the modulation signal. The other is the photon counter board to detect the fluorescence intensity at each detection spot. The alternative is to use an optical splitter fiber that collects the fluorescence and then splits 50/50 to other fibers connected to two APDs that each output is directed to

the appropriate recording device and to the computer. The computer control is a program written in LabView that the lock-in amplitude and total photon count at each point. The position of the stage is recorded as well as the relevant parameters and then a signal is sent to the stage to more to the next spot. In-program directions exist, but briefly the step size and dwell time at each pixel is set before the experiment. The step size should be set no lower than 100 nm and the dwell time must be longer than time constant used for the lock-in amplifier. The program will then plot the values in split matrices, one being the lock-in value and the other the total photon counts.

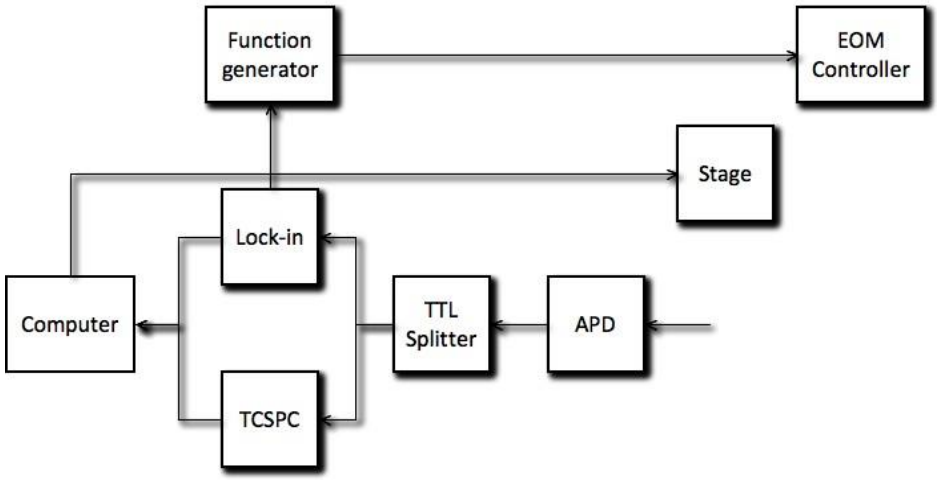

Figure 2.10 Flowchart of equipment connections necessary for point-by-point scanning.

2.8.2.2 Analysis

The resulting files are in matrix format which are a compilation of the lock-in amplitude or total photon counts at each x,y position. These files can be imported into a program such as MatLab and with the in-program software the image can be displayed. The resulting image will be flipped from how it was displayed in the LabView Program.

All analysis is done on the raw images, before any resizing or coloration. The analysis done for these experiments is to determine improvement of signal to background of demodulation compared to fluorescence imaging alone. In order to do this, in MatLab spots of desired protein with low intensity and high intensity of background are selected and the resulting photon counts and lock-in amplitude are recorded. Once ~10 spots are chosen at random, the protein signal is divided by the background signal to yield a ratio. Comparison of the total photon counts of protein fluorescence to background fluorescence yields a fluorescence ratio. Similarly, comparison of the same locations lock-in amplitude yields a demodulation ratio. The x-fold improvement is determined by comparing these two ratios.

2.8.2.3 Image Processing

In addition to analysis, MatLab can be used in image processing to easily normalize an image, subtract constant background, and/or reduce the size of the image. For samples collected using point-by-point scanning, images were made by averaging over 5 points to get the constant background (a spot where there is no cell). This constant is subtracted from all pixels within the image matrix and then normalized by the max pixel value. This normalization is necessary to divide the demodulation and fluorescence image as well as to the range linearly so each image is processed the same. The ratio image is the normalized demodulation image matrix divided by the normalized fluorescence image matrix. The resulting matrix and each individual matrix can be saved as a .txt file and transferred into ImageJ for further processing. To read into ImageJ software, the text file is imported as a "Text Image." The brightness/contrast to imported images can be altered by *Image* > *Adjust* >*Brightness/Contrast* command. Additionally, a lookup table (LUT) can be applied

by *Image* > *Lookup Tables* > *Royal*. The "royal" LUT displays the highest value as white and the lowest value as black with a rainbow colormap between the two.

2.8.3 Illumination via Defocused Laser

This imaging configuration is similar to wide-field imaging obtained with a lamp. A defocusing lens is used in setup to achieve a wide illumination of an area on the camera so that the whole image can be collected. Unlike point-by-point scanning, this method records all points at once, significantly decreasing imaging times and is used primarily with lower laser intensities and a higher modulation depth.

2.8.3.1 Experimental Setup

Unlike point-by-point scanning in which a small focal volume is desired, a wide area of illumination is required in this imaging modality. In order to achieve this wide (~10 to 50 μm) illumination, a lens is placed in the optical path usually before the back of the microscope to alter the focal point after the objective. Normally for imaging of NIH 3T3 cells, an illumination spot needs to be ~40 μm on the CCD camera to image an entire cell. The laser beams are aligned as described for typical optical modulation experiments. A lens is selected that has a focal length shorter than the distance from the lens to the back of the objective. A shorter length is crucial as focusing inside the objective may cause aberrations and, at high laser powers (~10 mW), objective damage. It is best to place the lens in a mount that has x,y translation capability to easily place the lens with the laser hitting the center. Once an appropriate lens is selected, the illumination area is viewed on the camera from laser scatter off a glass coverslip. Once rough adjustments are done with scatter to approximate the area and intensity of illumination, a sample of fluorescent beads can be used to evaluate the uniformity of illumination. Data is recorded with an Andor

iXon EMCCD. The frame rate is at least 3 times faster than the desired the modulation frequency to be recorded. The number of frames can vary based on modulation signal, modulation frequency, and/or photostability. The data is saved as an image stack.

2.8.3.2 Analysis

After the average image is achieved through demodulation (see 2.8.2.3), analysis of signal-to-background improvement is achieved similar to methods described in Section 2.8.2.2. All analysis is done on the raw images. Spots of desired protein with low intensity and high intensity of background are selected and the resulting average fluorescence intensity and Fourier transform amplitude are recorded. Approximately 5 cells with good background are chosen and the protein signal is divided by the background signal to yield a fluorescence or demodulated ratio.

2.8.3.3 Image Processing

The image stack is read into an imaging program by designed our lab lab (Jung-Cheng Hsiang). All frames can be merged to display an average fluorescence image. Once a desired frequency is inputted, a Fourier transform of each pixel is taken and a resulting demodulated image is reconstructed based on the amplitude of the input frequency. The resulting images can be saved as text files. Files can be imported into ImageJ software and processed as described in Section 2.8.2.3.

2.9 Protein Visualization Techniques

Swiss-PdbViewer is a program that provides a user-friendly interface to view and analyze proteins and DNA sequences. Proteins can be imported from the protein database (PDB) or created. Swiss-PdbViewer is tightly linked to Swiss-Model, an automated homology modeling server developed within the Swiss Institute of Bioinformatics (SIB) in

collaboration between GlaxoSmithKline R&D and the Structural Bioinformatics Group at the Biozentrum in Basel. Swiss PDB Viewer can perform a number of visualization and analysis functions to help understand the possible structural states the protein can conform to. The proteins can be superimposed in order to deduce structural alignments and compare their active sites or any other relevant parts. Also, the software has the ability to mutate amino acids, detect hydrogen bonds, angles and distances between atoms, and perform basic energy minimization with various modeling tools. A word of caution: this is a very basic modeling system and does not always give a clear picture of all interactions involved. In this work, it is used to hypothesize, but not prove, a possible mechanism of modulation in fluorescent proteins.

2.9.1 Protein Active Site Visualization

The first step to understanding the source of modulation in fluorescent proteins is to know the active chromophore site and the surrounding amino acids. While the proteins in this thesis all have a tyrosine-based chromophore, the protonation state and surrounding amino acids play a role in emission color and optical states (Section 1.4). This can be done in Swiss PDB Viewer by importing a PDB file into the program. Protein structures that have previously been crystallized and the X-ray crystallographic data solved are usually deposited in the online repository database. Proteins of interest can be searched and the .pdb file can be downloaded. Once the protein file is imported into the viewer, the protein viewing angle, protein chain, or select amino acids shown can be altered. For example, in order to only see the chromophore in the window, all the amino acids can be selected in the control panel window and hidden by pressing the (-) minus in the show category. Then, the 66th amino acid of the glycine-tyrosine-serine can be selected and the (+) plus pressed

displaying only the amino acid of interest. A script can be written to make this process faster, with additional commands to display the amino acids within 4 Å of that selection. For further information on viewing manipulation, consult the manual.

2.9.2 Amino Acid Mutation

The other features used extensively used in this work were the mutation tool, rotation tool, and energy minimization package. These are described in detail in the manual as well as in the program help page, thus only a brief description of how each was used is present here. The mutation tool is used to investigate the structural interactions the chromophore has in the presence of a particular amino acid. Used exclusively for the investigation of the blue fluorescent proteins, the mutate tool is engaged then the amino acid is selected and a list of amino acids that the position can be changed to is displayed. Once the new amino acid is selected, the most probable rotamer of the amino acid can be adjusted by evaluating the lowest side chain interactions and highest probability of the rotamer being present. After the mutation is made, all amino acids of the protein are selected and an energy minimization can be performed. The energy minimization is performed with partial implementation of the GROMOS96 force-field (see manual). Though, energy minimization is good to release local constraints, it will not pass through high energy barriers, stopping at local minima, thus it is important to start with an optimal rotamer.

2.9.3 C_α-C_β Bond Rotation

Rotation of the C_α-C_β bond is done much the same way, selecting the torison tool and clicking the two carbons in which the bond resides to rotate followed by energy minimization. Real time clashes and hydrogen bonding with other amino acids will be

displayed in pink and green (default) lines. With rotation, there maybe interactions with the chromophore after rotation and energy minimization will only slightly move an amino acid to remove those constraints, but that this does not take into account the total rearrangement of the backbone or if the rotation is more of a hula twist. This rotation is made easier by writing a script to identify the amino acid in which the bond will be rotated, rotate the bond, and perform the energy minimization afterwards.

CHAPTER 3

MODIFIED BLUE FLUORESCENT PROTEINS (modBFPs) AND VARIANTS

Blue fluorescent proteins (BFPs) are essential in multilabel/multicolor detection schemes.[3,95,99,172] Despite this usefulness in multispectral imaging, the high autofluorescence associated with the needed UV illumination cause blue fluorescent proteins to be underutilized in cellular imaging. The creation of blue fluorescent proteins served a two-fold purpose: multispectral imaging[95,172] and understanding of structural dependence of photophysical pathways of wild-type green fluorescent protein.[86,173] While different avenues have been taken to achieve blue emission, of interest to this chapter is the tyrosine-based chromophore blue fluorescent protein engineered to block excited state proton transfer while preserving the neutral form of the chromophore.[98,173-176] This chapter investigates an engineered protein blue fluorescent protein, modBFP, and variants, for long-wavelength modulation and photophysical properties characteristic of the modulation. Lastly, selective recovery of one variant, modBFP/H148K, from high autofluorescent background is demonstrated and points to the renewed utility of blue fluorescent proteins.

3.1 Introduction

Initial advances in the creation of blue fluorescent proteins (BFPs) for cellular imaging were achieved by enforcing neutrality of the chromophore by swapping the chromophore tyrosine for histidine.[36,86] The result was a variant with a fluorescence

emission wavelength substantially blue-shifted from that of the wild-type protein GFP.[86] However, the poor extinction coefficient and quantum yield necessitated further optimization. A bright and stable BFP for cellular imaging was created by double mutation of EGFP with Y66H/Y145F known as EBFP.[100,177] While used extensively in early multilabel schemes, the poor quantum yield and accelerated photobleaching lead to the creation of improved BFPs.[95,97] A parallel path to histidine-based EBFP optimization was the development of tyrosine-based BFPs by mutating residues in close proximity to the chromophore to better stabilize the neutral form in the ground state by blocking the wavelength-shifting excited-state proton transfer (ESPT).[95] The first tyrosine-based blue fluorescent protein optimized for brightness and cellular use, mKalama1, (extinction coefficient of 36,000 $M^{-1}cm^{-1}$ and quantum yield of 0.45) is 3.6-fold brighter and 25-fold more photostable than EBFP.[95] However, the significant autofluorescence generated under near-UV excitation still limits the utility of even the brightest available BFPs.

Almost simultaneous with the discovery of mKalama1 was the determination that the key amino acids in ESPT were the threonine at the 203 position (T203) and serine at the 205 position (S205). By using WT-GFP and systematically mutating these amino acids, Shu et al. produced a prominently blue emitting fluorescent protein.[98] The stable blue fluorescent protein is made upon mutation of T203 and S205 to valine (V) and characterized by a 390 nm absorbance peak, a lack of 500 nm absorbance, and a single 456 nm fluorescence emission.[98] In developing new applications, a wide variety of optically induced spectral shifts have been optimized through fluorescent protein mutation. BFPs make ideal candidates to optimize long-wavelength recovery of blue fluorescence through dark state engineering. Design of such a protein requires that the (fluorescent) state be

protonated in the ground state and the transient form be deprotonated to absorb the secondary light. Although there are no currently existing examples of such a protein, consideration of the theoretical and experimental structures suggest that this should be feasible and, moreover, achievable both by multiple site-directed mutagenesis through strategic placement of acidic residues and through random mutagenesis targeting the environment of tyrosine 66 (Y66) with additional selection strategies. Mutations designed to alter the chromophore protonation state in different chromophore configurations would likely also modify dark state lifetimes with spectrally shifted absorptions, thereby facilitating optical modulation. Mutation serves to improve modulation and also inform possible mechanisms for modulation.

3.2 modBFP Mutagenesis Rationale

The gene sequence containing the T203V/S205V as well as other mutations for improved maturation and expression was gifted to the Tolbert laboratory by S.J. Remington (Oregon). Dr. Russell Vegh of the Tolbert laboratory at the Georgia Institute of Technology did all the mutagenesis on the gene and purification of the proteins. The protein was referred to as modBFP in order to distinguish the parent mutant from the double mutant the gene came from. It is this particular protein that was used to begin the investigation of BFPs for optical modulation. Target amino acids for mutagenesis were selected by examining chromophore environment and identifying amino acids with possible interactions with the hydrogen of Y66. These amino acids in the vicinty of the chromophore would most likely be responsible for altering the photophysical states in the modBFP via protonation/deprotonation dynamics.

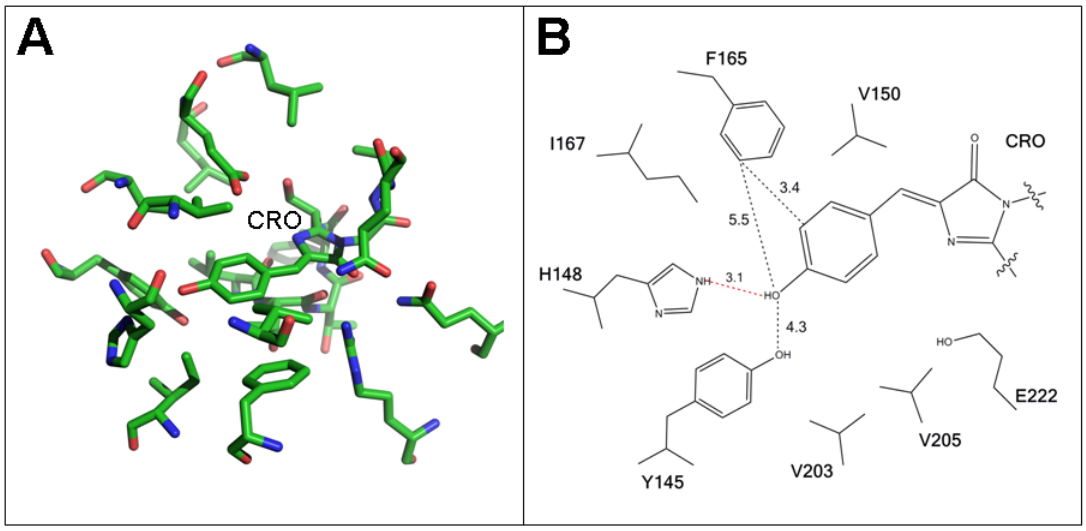

Figure 3.1 Chromophore environment of modBFP. (A) Amino acids within 4 Å of the Y66 of modBFP using 2QLE[98] as a reference. Drawn using PyMOL Molecular Graphics System, Schrödinger, LLC. (B) Simplified 2D rendering of studied amino acids with the cis-form chromophore. Bond (black) and hydrogen bond (red) lengths are shown in dashed lines, with lengths reported in Ångstroms (determined from Swiss PDB Viewer).

Using protein visualization software (such as Swiss PDB Viewer), the crystal structure of the GFP/205V (PDB: 2QLE)[98] can be used to as a starting place for modBFP as it > 95% homology in sequences. For better visualization of amino acids near the chromophore, the pocket can be limited to amino acids within 4 Å of the 66 position (Figure 3.1 A). As seen in the simplified version of Figure 3.1 B, the amino acid with the greatest interaction with Y66 in the ground state configuration is histidine at position 148 (H148). Assuming the possiblilty of cis/trans isomerization to also occur in photoinduced processes such as discussed in the Section 1.4.3, the amino acids that would be near the Y66 in the alternative, trans from were also investigated. Upon 180° rotation of the C_α-C_β of the chromophore, the interaction of F165 and V150 also becomes apparent though not identified while in the cis form. Of the target amino acids, the most interesting amino acid seems to be the H148 hydrogen bond interaction with the phenol of Y66 (Figure 3.1 B).

As the uncharged phenol form at Y66 is favored when another positively charged group with a higher pK_a is in the vicinity, the lysine (K) and arginine (R) variants of H148 were made. The phenolate form at Y66 is favored when a (negatively charged) carboxylate group with a higher pK_a is in the vicinity. Therefore, a single aspartate (D) or glutamate (E) variants were also created. In addition to charge, steric bulk was also considered in mutating to smaller amino acids. The mutations made to modBFP were: H148D, H148G, H148K, H148R, H148Y, V150A, F165H, and F165L which were all on the same β-strand. After selection of bacteria with blue emission, the proteins were purified and investigated.

3.3 modBFP Spectra and Photophysical Characterization

In order to characterize these proteins before modulation is performed, basic bulk experiments were carried out. Mutations around the chromophore can result in altered absorption and emission characteristics, thus, the presence of a blue emitter needed to be confirmed. Similar to the initial Remington protein (GFP-T203V/S205V),[98] modBFP has a dominant absorption maximum peak at 390 nm. Excitation at 390 nm results in maximum fluorescence at 456 nm (Figure 3.2 A).

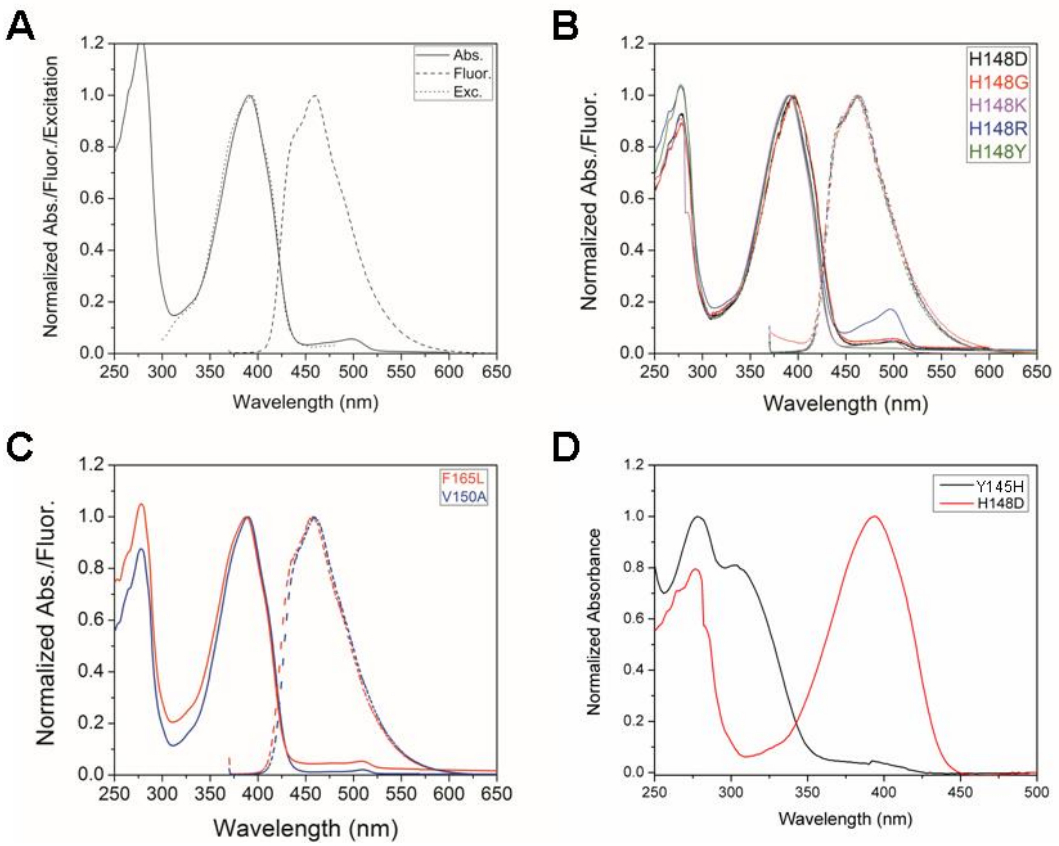

Figure 3.2 Absorption (solid) and fluorescence (dash) spectra of (A) modBFP, (B) H148 mutations, and (C) F165L and V150A mutations. (D) The absorption of F165H, as compared to H148D, shows little 390 nm absorption.

All mutations were measured with these same conditions. Of the blue emitters selected for modulation testing, most of the mutations have similar behavior of a maximum blue absorption peak at 390 nm and an emission peak ~450 nm (Figure 3.2 B and C). However, for some mutations, i.e. H148R, the weaker absorption peak at 500 nm is present, indicating a larger presence of the anionic phenolate in the ground state relative to modBFP (Figure 3.2 B). As seen in Figure 3.2 D, Y145H was one of the mutations that didn't show a strong absorption at 390 or anywhere in the near-UV spectrum and resulted in low 450 nm emission, thus was eliminated from modulation experiments.

For comparison to other known tyrosine-based BFPs, further analysis was done on modBFP and H148K (which later discussed in Section 3.4.2, showed the highest enhancement). The extinction coefficient, fluorescence quatum yield, and pK_a for modBFP and modBFP/H148K were recorded and were compared to the only other tyrosine-based BFP, mKalama1 (Table 3.1).[95] As few other mutations were made to the proteins from the original sequence obtained from Remington, the reduced photophysical properties in modBFP were not surprising. Additionally, the fluorescent quantum yield reported for GFP-T203V/S205V was 0.29[98] and this was also consistent with the measured results for modBFP. However, modBFP/H148K has a greater reduction of photophysical properties and an increased pK_a. This may point to the possible role of mutation in optically modulated states.

Table 3.1 Spectroscopic properties of select blue fluorescent proteins. [a]mKalama1 characteristics are reported in Ai et al.[95] Brightness is a product of the quantum yield and exctinction coefficient (in $mM^{-1}cm^{-1}$).

Fluorescent Protein	$\lambda_{abs}/\lambda_{em}$ (nm)	Quantum Yield (Φ_F)	Extinction Coefficient ($M^{-1}cm^{-1}$)	Brightness	Apparent pK_a
mKalama1	385/456	0.45[a]	36,000[a]	16[a]	5.5[a]
modBFP	390/455	0.33	27,000	8.9	5.5
H148K	390/455	0.17	25,000	4.3	5.7

3.4 Long-Wavelength Modulation: Continuous Wave Primary Excitation

The purified proteins kindly provided by the Tolbert group were diluted to a working concentration of approximately 1-2 μM. The absorption peak at 390 nm was excited with a continuous wave (CW) 405 nm diode and the fluorescence was collected from 430 to 474 nm. The secondary wavelength was chosen by finding a suitable spectral

line outside of the fluorescence window and an Ar^+ ion laser line at 514 nm was chosen. These were the conditions for determining optimal enhancement and modulation frequency for the tested proteins.

3.4.1 Intensity Dependence

As previously described of optical modulation, the rates into and out of the dark state are intensity dependent processes. Thus, appropriate excitation intensities for the primary and secondary laser were found for modBFP to 1) determine if modulation is possible and 2) use these intensities to compare all the proteins.

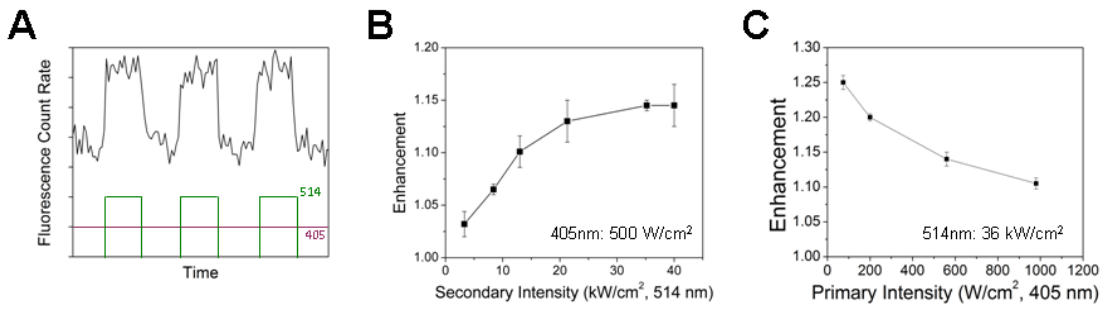

Figure 3.3 Intensity dependence of modBFP/H148K. (A) As the secondary laser is applied to the sample, the fluorescence intensity will increase and the difference between the 2 laser level and primary only level is used to calculate enhancement. The enhancement versus varying secondary (B) and primary (C) intensities informs optimal conditions to use for modulation.

Illuminating with the primary only establishes a steady-state fluorescence intensity and defines the dark-state population. With illumination of the secondary laser, the fluorescence intensity would increase to a higher level due to depopulation of the dark state (Figure 3.3 A). As seen in Section 2.6.2.1, the difference between the two laser fluorescence intensity and primary only fluorescence intensity is used to calculate

enhancement (Equation 2.8). At a single primary intensity, a finite population builds up in the dark state and an appropriate secondary intensity for depopulating can be determined. Keeping the primary intensity fixed at a relatively low 500 W/cm^2, the secondary laser (514 nm) was varied over an order of magnitude (Figure 3.3 B). As the secondary laser intensity is increased, there is an increase in enhancement reaching somewhat of a plateau at 30 kW/cm^2. In this plateau region, the secondary intensity has surpassed the intensity needed to depopulate the dark state and thus results in no change in enhancement. It is important to note that at this high secondary intensity there is a small proportion of secondary only fluorescence recorded (~1%).

Additionally, an expected increase in primary laser intensity results in increased rate into the dark state and a high population residing in the dark state. Consequently, increased primary excitation should increase modulation depth. In order to find the best primary intensity for enhancement, the secondary laser was fixed at the optimal 36 kW/cm^2 and the primary intensity was varied recording the enhancement (Figure 3.3 C). Interestingly, an experimental increase in primary intensity decreases total enhancement for all emitters studied. As fluorescence enhancement is defined as fluorescence with two lasers divided by fluorescence with primary excitation only, any dark state absorption at the primary wavelength will reduce steady-state dark state population, resulting in decreased secondary laser-induced enhancement.[19] Thus, a balance between populating the dark state without increasing its rate of decay must be reached, resulting in maximum enhancement being observed at relatively low ~70 W/cm^2 primary excitation intensity. An optimal intensity combination of 500 W/cm^2 primary and 36 kW/cm^2 secondary was chosen for experiments. Though better enhancement is achieved at lower intensities, the

primary intensity chosen gives good fluorescence and increasing the protein concentration for lower intensities could lead to aggregation or other unwanted side effects.

3.4.2 Enhancement and Characteristic Frequency

With the appropriate intensities gathered in the Section 3.4.1, the enhancement for modBFP and the mutants can be determined. While all variants exhibit a 390 nm absorbance maximum (Figure 3.2), dual laser fluorescence enhancement was greatly affected by these mutations. Almost all the tested variants were modulatable, ranging between 2% and 15% (Table 3.2). The single variants of modBFP: H148G (6%), V150A (10%), and H148K (15%), each further increased fluorescence enhancement under 514-nm co-illumination over that of modBFP (4%) while F165L diminished the modulation. The possible reasons are discussed later in Chapter 5.

Table 3.2 Modulation and Characteristic Frequency of modBFP and Variants. Primary intensity (405 nm) held at 560 W/cm^2 and secondary (514 nm) is at 36 kW/cm^2.

Fluorescent Protein	Enhancement	Characteristic Freq. (Hz)
modBFP	4%	16
H148D	4%	24
H148G	6%	30
H148K	15%	37
H148R	3%	5
H148Y	2%	6
V150A	10%	31
F165H	2%	10
F165L	0	N/A

Modulating the secondary laser intensity increases and decreases the detected emission, the result is modulated time trace in which the frequency of the secondary laser can be extracted by Fourier transform. The demodulated signal can then be recovered from

the Fourier amplitude at the modulation frequency and the enhancement calculated as described in Section 2.6.2.1. Analogous to frequency domain lifetime measurements,[178] the buildup and decay of steady state population takes a finite time and as the modulation frequency becomes faster than this the depopulation becomes faster than the buildup, reducing the effectiveness of the secondary laser. The competition between the rate into and out of the dark state determines the characteristic frequency. Using intensities for modulation, the secondary laser was varied from a low frequency of 1 Hz to a high frequency of 3 kHz. At each frequency, the enhancement was calculated and then plotted as a function of the secondary modulation frequency. Figure 3.4 is an example of modBFP/H148K enhancement versus modulation frequency dependence. To quantitatively identify a rate in and out of the dark state to compare between proteins, the data was fit to Equation 2.10 for each of the proteins. The modulation characteristic frequency was extracted at half the original value and was recorded as the characteristic frequency (ν_c). The characteristic frequency of modBFP and variants are summarized in Table 3.2. For all the proteins, the characteristic frequency is low ($\leq$ ~40 Hz) suggesting the rate constants into and out of the dark state are likely relatively slow. As the characteristic frequency is equivalent to $k_{on} + k_{off}$, the off time for the recorded excitation intensities of Table 3.2 is the inverse of k_{off} and this is consistent with 10-millisecond *cis-trans* interconversion timescales in other fluorescent proteins.[179]

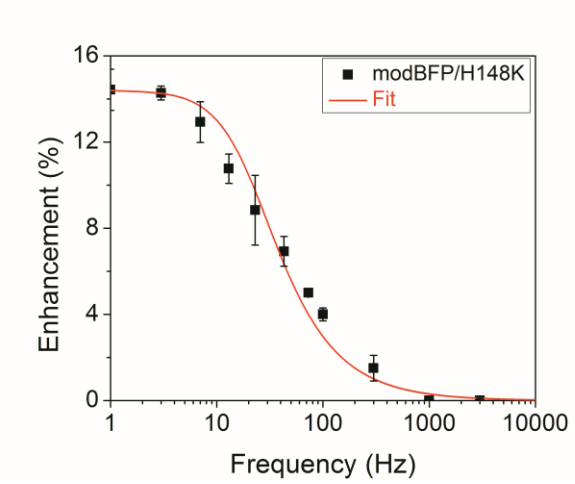

Figure 3.4 modBFP/H148K enhancement as a function of modulation frequency fitted to phase-resolved lifetime equations.

3.4.3 Extraction of Modulated State Photophysical Timescales

The slow characteristic modulation frequency of all the variants was intriguing. Investigating the dark state lifetime as a function of mutation may lead to an understanding of the factors controlling modulation. As discussed in Section 1.6, the characteristic frequency is the sum of the intensity-dependent rate out of the bright manifold and the natural rate constant of dark state decay, $k_{on} + k_{off}$. Thus, as the modulation frequency of modBFP and variants is $\leq$ ~40 Hz (Table 3.2) and the inverse of the frequency is characteristic time (τ_c), this suggested a modulatable process on the order of tens of milliseconds. The first approach to extracting the natural dark state decay was to eliminate the k_{on} contribution of the characteristic frequency. The k_{on} is the product of excitation rate, k_{exc}, and dark state quantum yield, Φ_{dark}. Varying primary excitation intensity should alter the k_{on} and subsequently change the characteristic modulation frequency. Linearly fitting the characteristic frequency versus primary intensity curve yielded a line that, when extrapolated to zero primary intensity, extracts k_{off} as the y-intercept. Figure 3.5 shows this

method with modBFP and modBFP/H148K. As the primary intensity decreases, the characteristic frequencies of both modBFP and modBFP/H148K decrease. The low primary intensity k_{off}'s of both variants are very similar at ~ 6 Hz.

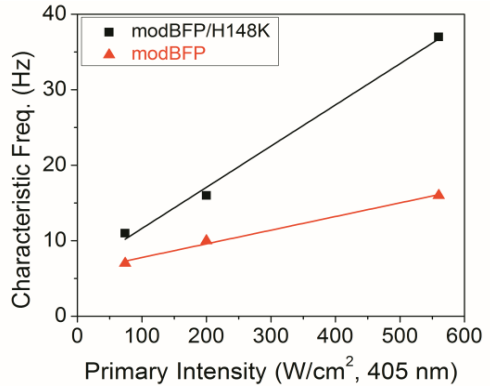

Figure 3.5 Characteristic frequencies are plotted as a function of 405 nm primary excitation for modBFP and modBFP/H148K. The y-intercept yields the natural dark state decay rate of each protein.

The inverse of this rate constant gives the natural dark state decay time, τ_{off}. When coupled with the measured characteristic frequency, the average time spent in the fluorescent manifold can also be determined. The characteristic times for 560 W/cm^2 excitation conditions are given in Table 3.3. Mutants with lower than 4% enhancement were not measured as higher intensities showed no enhancement and fluorescence levels were too low for additional measurements at extremely low primary excitation intensities. Of the measured proteins, the natural dark state off times seem relatively consistent with each other, ~170 ms. However, the reduction of τ_{on} compared to modBFP is clear. Comparing the τ_{on} of modBFP and modBFP/H148K, the 32 ms on time of modBFP/H148K indicated more efficient photoinduced dark state formation in that mutant compared to that in modBFP (100 ms). As enhancement is dictated by the ratio of the single and dual laser-

illuminated off and on times, the extracted photophysical times bolster the observed enhancement improvement due to the H148K mutation (Table 3.2).

Table 3.3 Extracted Photophysical On and Off Times for modBFP and Variants.

Fluorescent Protein	τ_{on} (ms)	τ_{off} (ms)
modBFP	100 (± 5)	167 (± 14)
H148D	66 (± 5)	113 (± 16)
H148G	57 (± 2)	222 (± 28)
H148K	32 (± 2)	162 (± 35)
V150A	40 (± 3)	164 (± 56)

With timescales on the order of hundreds of milliseconds, the role of diffusion in determined times or enhancement factors was investigated and efforts were made to immobilize the proteins in a polymer matrix to verify the calculated on and off times. The first attempt was with polyacrylamide which has been used previously for the immobilization of single molecules.[140] With appropriate cross-linking concentrations and conditions, the matrix creates pore sizes appropriate for protein molecules allowing for rotational freedom but restricting diffusion. However, bulk polyacrylamide displayed background levels similar to modBFP fluorescence with 405 nm excitation and a small contribution from the secondary laser. An alternative was low-melting agarose ($T_m \leq$ 65°C) in which polymer is melted and mixed with the protein and allowed to repolymerize. While agarose alone contributed no background, this method had two other disadvantages. First, the reported pore size for the chain length used was much bigger than compared to the polyacrylamide matrix, meaning diffusion could still occur. Second, though most fluorescent proteins are impervious to temperatures up to 70°C, the modified proteins being tested resulted in elimination of the fluorescence after repolymerization. An alternative to

the use of immobilizing matrices would be an FCS experiment with an expanded the focal volume. Additionally, fluorescent proteins can be modified to have a linker with a biotin molecule on the end so that the protein can be immobilized on a glass coverslip modified with streptavidin.

3.5 Long-Wavelength Modulation: Pulsed Excitation

As discussed in 3.4.1, the uncharacteristic primary intensity dependence with continuous wave excitation indicated the probability that the 405 nm laser was also depopulating the modulatable dark state. The result was a decreased observed enhancement for modBFP and variants at higher primary intensities. Previous studies have shown the advantage of pulsed excitation for improved enhancement. Akin to studies with heavy atom-substituted xanthene dyes, pulsed primary excitation offers the opportunity to increase k_{on}, and therefore dark state population without increasing dark state decay, $k_{off.}$[19]

3.5.1 Intensity Dependence

The appropriate excitation intensities for the primary and secondary laser were investigated again for modBFP and variants with a 372 nm pulsed (90 ps FWHM) diode and continuous wave (CW) 514 nm secondary. Similar intensity dependent experiments to the continuous wave were done to examine the optimal conditions with the pulsed primary laser. Though the overall enhancement had increased, the primary and secondary responses were the same. An important point to note is that as the rep rate is so such faster than characteristic time of the modulatable state the 372 nm may have the same effect as a CW laser. Though increased enhancement is seen regardless, the difference in spectral line for excitation should be taken into consideration.

3.5.2 Secondary Wavelength Dependence

Alternatively, a more appropriate secondary wavelength matching the absorption cross-section may increase the modulation. For a constant secondary excitation at 372 nm pulsed at 200 W/cm^2 and a varying primary laser 488, 496, and 514 nm (all at 37 kW/cm^2 CW), the enhancement was recorded for modBFP and its variants (Table 3.4). Using 90 ps FWHM pulses at 372 nm, the primary excitation only populates dark states within a short time window, allowing the modulated CW secondary laser to depopulate the dark state over longer periods, with lower primary laser-induced dark state absorption. As long as primary-induced dark state creation is more efficient than dark state decay, such pulsed excitation quickly generates the dark state with a single pulse, allowing the secondary laser to optically regenerate the emissive manifold. Thus, switching from the CW 405 nm to a pulsed 372 nm primary excitation, each with secondary illumination at 514 nm, a marked increase in enhancement was observed across all proteins. However, there is no visible trend to indicate that the dark state action cross section of the fluorescent proteins is affected by any secondary wavelength excitation. Many of the variants maintained a constant enhancement value over all three wavelengths investigated (Table 3.4). A comparison of modBFP and modBFP/H148K suggested that modBFP may benefit from the use of 496 nm over the previously used 514 nm while there is no difference observed in modBFP/H148K. Of note, secondary-induced fluorescence was higher as the secondary wavelength approached the fluorescence window. Additionally, the secondary-induced fluorescence intensity observed was dependent on the identity and concentration of the protein. This phenomenon is still a mystery as fluorescence from possibly exciting the anionic chromophore would not result in fluorescence in the detection window. Because

of this prominent secondary-induced fluorescence, the 514 nm wavelength was used for all subsequent experiments with 372 nm excitation.

Table 3.4 Secondary Wavelength Dependence on Modulation for modBFP and Variants.

Fluorescent Protein	488 nm	496 nm	514 nm
modBFP	29 ± 1%	42 ± 2%	20 ±1%
H148D	13 ± 2%	15 ± 1%	15 ± 3%
H148G	14 ± 1%	15 ± 2%	11±7%
H148K	25 ± 1%	40 ± 1%	37 ± 3%
H148R	10 ± 1%	15 ± 2%	15 ± 2%
H148Y	6 ± 1%	9 ± 2%	5 ± 2%
V150A	24 ± 2%	29 ± 1%	20 ± 1%
F165H	5 ± 1%	6 ± 2%	5 ± 1%
F165L	2 ± 1%	0	0

3.5.3 Characteristic Frequency

With the increased enhancement at 372 nm excitation, the k_{on} and k_{off} rates may also change to reflect this. As the primary laser now effectively excites the molecule with little dark state depopulation, a more accurate description of the on time and dark state off time could be obtained. The same method of varying primary intensity for extrapolation to the zero intensity intercept was used with pulsed 372 nm excitation and 514 nm secondary (for lowest secondary-induced fluorescence interference). Proteins with higher than 5% enhancement are shown in Table 3.5. As seen with CW excitation, the characteristic frequencies for all tested proteins are < 30 Hz indicating an even slower process than predicted with CW. An extraction of on and off times (Section 3.4.3) reveals, again, times in the milliseconds. Similar to CW off times, the off times are relatively

unchanged across the mutants. Unlike the CW extracted photophysical data, recorded on times show no trend and do not explain the difference in enhancement.

Table 3.5 Extracted Photophysical On and Off Times for modBFP and Variants with Pulsed Excitation.

Fluorescent Protein	ν_c (Hz)	τ_{on} (ms)	τ_{off} (ms)
modBFP	11	357	122
H148D	19	212	71
H148G	14	434	88
H148K	28	115	81
H148R	23	179	57
V150A	24	120	90

The possibility exists that the 372 nm diode used for excitation may be less than optimal for determining on and off times with the current method used. The output beam cross-section was not a symmetric Gaussian of light, but elliptical in shape. This focal spot was larger than the secondary 514 nm laser spot, thus could create a large bath of excited molecules primed into the dark state. When the secondary is turned on not only is it immediately depopulating the fluorescent proteins within the laser focus, but also fluorescent proteins diffusing into the laser focus. The recorded on and off times may be a reflection of these two processes altering the measurable timescales and thus lengthening the calculated times. Thus, alternative methods that reduce the effect of diffusion on calculated photophysical parameters should be investigated for better understanding of the timescales involved in pulsed excitation.

3.6 mKalama1 Modulation

mKalama1 is a brighter and more photostable tyrosine-based blue fluorescent protein commonly used in cellular studies. The protein has the same key mutations as modBFP and stabilizes the neutral chromophore. We predicted that fluorescence enhancement in mKalama1 would also exhibit improved long-wavelength modulation, and studies with both CW and pulsed excitation were carried out. While exciting mKalama1 yields bright emission centered around 456 nm, co-illumination at all tested wavelengths (488, 496, and 514 nm) did not lead to enhancement of the fluorescence. As modulation results from significant steady-state dark state population buildup, any photoaccessed mKalama1 dark states either do not absorb at 488-514 nm or are too inefficiently populated to yield measureable fluorescence enhancements. However, informed by the studies of modBFP, the marked improvement of modulation depth in mod-BFP/H148K suggested that mutation of the corresponding residue in mKalama1 (glycine in position 149) may similarly confer modulatability. Both mutations, G149H to represent the original amino acid in modBFP and G149K which reflected the mutation that conferred increased enhancement, were made. Both proteins, mKalama1/G149H and mKalama1/G149K displayed similar absorbance and emission maxima to mKalama1, but only the G149K mutation resulted in fluorescence enhancement of 6% upon co-excitation with 514 nm. Plotting the G149K fluorescence enhancement versus modulation frequency reveals a characteristic frequency of ~90 Hz, again consistent with the slow ~10 millisecond modulation timescales seen for modBFP and its variants. The consistent ms timescale of modulation suggests a common mechanism for all the blue fluorescent proteins.

3.7 Imaging of Blue Fluorescent Proteins

Cellular imaging is often plagued by autofluorescence stemming from endogenous fluorophores and has, in part, limited the use of blue-emitting proteins. However, blue fluorescent proteins are useful in terms of multicolor imaging and modulatable BFPs would be instrumental in circumventing endogenous fluorescence. To demonstrate the utility of modulatable BFPs we investigated selective recovery of modBFP/H148K fluorescence in the presence of non-modulatable background, distinguishing its emission from that of autofluorescence present in cellular imaging. In collaboration with the Bommarius group and Dr. Bettina Bommarius at the Georgia Institute of Technology, NIH-3T3 cells were transfected with a plasmid encoding modBFP/H148K fused to a mitochondrial targeting peptide (modBFP/H148K-mito). Wide field epifluorescence imaging and modulation were performed with the overlapped, defocused primary (405 nm) and a smaller secondary laser excitation (514 nm) (Section 2.8.3). To maintain the high kW/cm^2 intensities necessary for modulation, the secondary laser excitation area was approximately one-third the area of primary excitation. The slow characteristic modulation frequency dictated the use of a low modulation frequency for imaging and the secondary laser was modulated at 2Hz, and emission was imaged at least 5 times faster using a CCD detector. A variety of exposure rates and total frames were investigated and in order to collect enough data for demodulation and not have significant photobleaching ~100 frames at an 80 millisecond exposure rate (total time was ~8 seconds) was most appropriate for imaging modBFP/H148K. The resulting average image displays both modBFP/H148K-mito emission and autofluorescence. After demodulation (2.8.3), images display enhanced signal matching the modulation frequency used.

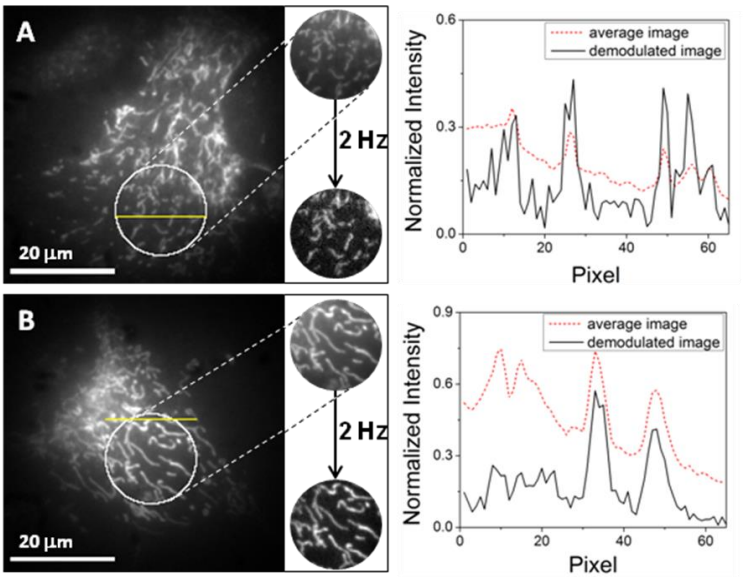

Figure 3.6 Demodulation of mitochondria-targeted modBFP/H148K in (A) fixed and (B) live cells. Upon 405 nm illumination, blue fluorescence is collected from modBFP/H148K-mito and autofluorescence. Co-illumination at 514nm, modulated at 2 Hz (white circle) recovers only the modBFP/H148K-mito signal (lower circle). Line graphs (yellow line) display the improved contrast of signal from background. Scale bar is 20 μm.

Done first in cells fixed with 4% formaldehyde (Figure 3.6 A), images suggested the ability to modulate at the working intensities and showed improved signal (line graph), but the low level of background in the cellular environment limited the improvement that could be achieved. Thus, live cells transfected for 48 hours were also imaged and exhibited higher autofluorescent background (Figure 3.6 B). Demodulation at 2 Hz directly yields images with an average 5-fold improvement in signal to background as autofluorescent background is removed. Signal visibility gains are further improved when raw fluorescence contrast is lower.

To ensure the modulated signal recovered in cells was not due to photobrightening of the protein relative to the background, a control with constant 405 nm and 514 nm co-illumination was performed. Live cells were illuminated with the same conditions used in

the modulation image recovery of Figure 3.6. However, instead the secondary laser was on and unmodulated during the data acquisition. The image frames are processed similarly to those in Figure 3.6, selectively looking for the 2 Hz FT amplitude. While the raw image appeared slightly brighter, demodulated images plotting the 2 Hz amplitude showed no signal resembling mitochondrial structure (Figure 3.7 A). This second control checks that cells or other structures are not excited or modulated by the secondary 514 nm laser, and could be registered as a false positive. Cells were cultured and maintained exactly as those in the previous cellular modulation experiments but not transfected with modBFP/H148K-mito. After modulated excitation and demodulation, images demonstrated no signal other than noise (Figure 3.7 B).

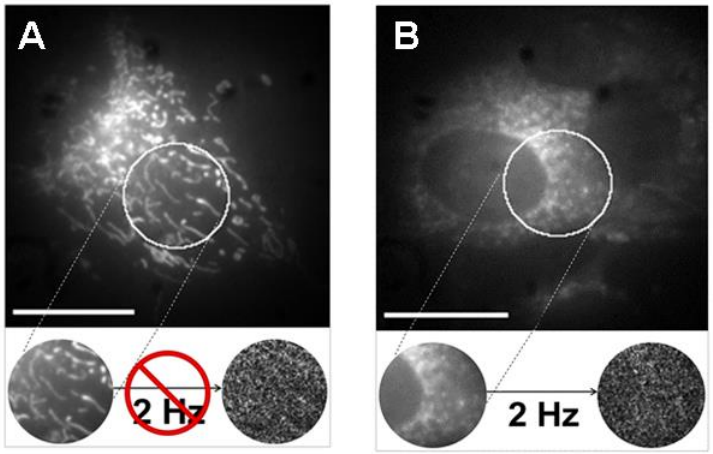

Figure 3.7 Control cells to modBFP/H148K modulation imaging. (A) Cells expressing modBFP/H148K were co-illuminated with 405 nm and 514 nm without 2 Hz modulation of the secondary laser. (B) Untransfected cells excited with 405 nm primary and 2 Hz modulated secondary 514 nm. Scale bar is 20 μm.

3.8 Conclusions

To circumvent the sensitivity issues in cellular imaging, the investigation of selectively shifting signals to unique detection frequencies with long-wavelength modulation was undertaken with BFPs. Mutations to BFP and BFP variants are thought to create changes in the immediate chromophore environment which stabilize the neutral cis excited and anionic trans ground states. This change in chromophore environment directly alters the enhancement and modulation frequency. Thus, BFPs are conducive to significant signal improvements over autofluorescent background through modulation. Further modulation gains may also be possible through additional mutation of the chromophore environment. Specifically, an increased efficiency of creating dark, trans anionic state directly would increase fluorescence enhancement, visible in the comparison of modBFP and its H148K variant and the creation of modulatable species, mKalama1/G149K. Most interesting is the ability to improve the fluorescence enhancement with mutations and characterize each in terms of on and off times reflecting the inverse rates into and out of the dark state. The ~100-ms modulation timescale is postulated to involve cis/trans photoisomerization, coupled with neutral cis- and anionic trans-chromophore forms, or other photoreversible processes. The understanding of these photophysics will inform the development of fluorophores with better signal to noise. The low utility of blue fluorescent proteins due to weak fluorescence, poor photostability, and high background upon UV excitation was improved upon by the use of modulation. Demodulation of modBFP/H148K exhibited a 5-fold improvement over the UV-induced background and provided an avenue for future applications utilizing BFPs such as better multi-color imaging.

CHAPTER 4

Aequorea coerulescens GREEN FLUORESCENT PROTEIN (AcGFP)

In working towards understanding the fluorescent properties, the first studies of the spectral properties revealed that wild-type green fluorescent protein (WT-GFP) had a major excitation peak at a wavelength of 395 nm, and a minor one at 475 nm associated with the chromophore and its conjugate base, respectively.[86,104,139] Previously discussed was the simple case of blue fluorescent proteins in which the role of ESPT was negated, the tyrosine chromophore remained neutral, and the 395 nm was the primary focus.[98] Here, the anionic chromophore of the green fluorescent protein is investigated. With the emission shifted from a spectral region of high background such as with BFPs and copious amounts of characterization, green fluorescent proteins have become a staple in biological imaging. Of specific interest is the GFP derived from the *Aequorea coerulescens* whose specific photophysical properties make it an interesting target for optical modulation.[180,181] The optical modulation and photophysical parameters of modulatable states are discussed. Additionally, the utility of modulatable GFPs in inhomogeneous background environments was demonstrated in cells.

4.1 Introduction

After studies of the WT-GFP revealed the dual excitation nature of the chromophore, work began to engineer a protein with a single excitation band for green emission and better photophysical properties for possible applications in biological imaging. The first major improvement was reported by the Tsien group.[105] A single mutation of serine (position 65) near tyrosine chromophore to a threonine (designated

S65T) causing the ionization of the phenol of the chromophore.[88,104,105] The result was a suppression of the 395 nm peak due to the neutral chromophore and shift and amplification of the major excitation peak to 488 nm without altering the green emission. Additionally, the mutation resulted in increased relative brightness and photostability as compared to the WT-GFP. There has been continuing research to improve the properties of green fluorescent proteins, many taking advantage of the S65T mutation.[100] One commonly used green emitter is enhanced GFP (EGFP) that contains the S65T mutation and F64L to give greater brightness at warmer temperatures expected in mammalian expression.[91,182] With a moderate extinction coefficient and quantum yield (55,000 $M^{-1}cm^{-1}$ and 0.60, respectively),[91] EGFP has been one of the preferred GFPs in fluorescence imaging.[148]

In addition, other GFP homologues have been discovered. Recently, Gurskaya and colleagues isolated a GFP homologue from a non-fluorescent jellyfish *Aequorea coerulescens* that had the same three amino acid motif as GFP.[180,181] This protein, aceGFPL, was initially colorless with only a very minor absorption at 390 nm; however, random mutagenesis identified an E222G mutation that leads to fluorescent derivative (aceGFP or AcGFP) with a single 480 nm excitation peak and emission centered at 505 nm (Figure 4.1).[180] This bright GFP has a fluorescence quantum yield (0.55) and extinction coefficient (50,000 $M^{-1}cm^{-1}$).[180] To further study the fluorescent properties and effect of mutation, an aceGFP-G222E variant was created with only the G222E mutation.[181] The protein returned to being colorless but upon illumination with UV light photoconversion of the protein took place, generating an anionic species, with the same spectra as aceGFP.[181] This kindling behavior involves proton transfer coupled with a cis/trans isomerization that is controlled by the short wavelength absorption. However, if this

photoisomer has a possible long-wavelength absorptions, though harder to predict, one may be able to use long-wavelength light instead of 405nm for photoreversion.

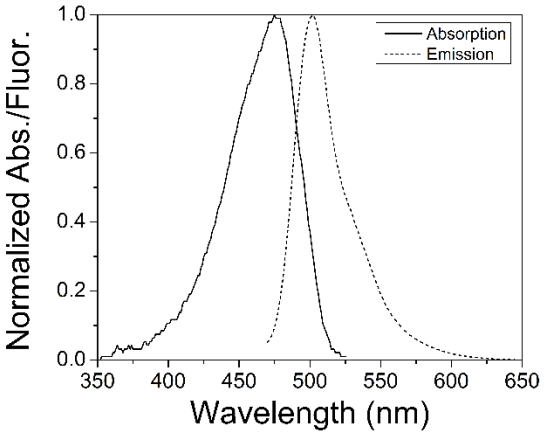

Figure 4.1 Absorption and emission spectra of purified AcGFP in PBS pH 7.4.

4.2 Fluorescent Enhancement of AcGFP

For fluorescent proteins to be optically modulated, a dark state that sufficiently absorbs the secondary illumination must exist. Motivated by the optical photoconversion seen in AcGFP studies,[181] the fluorescence enhancement of AcGFP was investigated. The purified AcGFP, kindly provided by Dr. Pritha Bagchi of the Fahrni group at the Georgia Institute of Technology, was diluted to a working concentration of approximately 100 nM. Based on the spectra of AcGFP (Figure 4.1), the protein has a single absorption peak at 480 nm and thus an Ar^+ ion laser line of 476 nm was used to excite the protein. As the collected fluorescence ranges from 500 to 530 nm, a secondary wavelength was chosen by finding a suitable spectral line outside of the fluorescence window. A solid-state 561 nm laser was first chosen as it was outside the fluorescence collection window and sufficiently away from the absorption band to result in excitation of the protein by the secondary laser alone.

The primary laser excites the electrons to the excited state and can either fluoresce or non-radiatively decay to a fluorescence-sapping dark state. The fraction in the dark state is controlled by the rates into and out of that state. An increase in primary laser intensity results in increased rate into the dark state and a high population residing in the dark state. In order to find the best primary intensity for enhancement, the secondary laser was fixed at 23.5 kW/cm^2 and the primary intensity was varied recording the enhancement at each point. As seen in Figure 4.2 A, an increase in the primary intensity results in an increase in fluorescence enhancement which is unlike the BFPs (Figure 3.3). The slight decrease seen at high intensities may be a result of photobleaching or saturation and ground state depletion. Inversely, at a single primary intensity, a finite population builds up in the dark state and an appropriate secondary intensity for depopulating this must be determined. Keeping the primary intensity fixed at 2 kW/cm^2, the secondary laser (561 nm) was varied over an order of magnitude (Figure 4.2 B). As the secondary laser intensity in increased, there is an increase in enhancement, until a plateau. In this plateau region, the secondary intensity has surpassed the intensity needed to depopulate the dark state and thus results in no change in enhancement. Thus, from these studies the appropriate laser intensity ratio for maximum enhancement requires a secondary:primary ratio of about 10:1. It is also important to note that no emission is detected from secondary illumination alone. The 2 kW/cm^2 primary and 23 kW/cm^2 secondary resulting in 8% enhancement serves as an internal "standard" when using these wavelengths with other proteins.

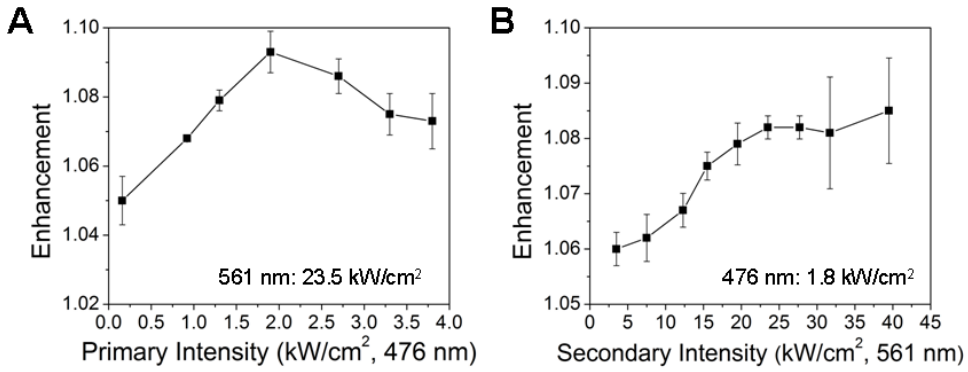

Figure 4.2 Enhancement as a function of (A) primary and (B) secondary laser intensity. Error is calculated from triplicate experiments.

As enhancement depends on the sufficient depopulation of the dark state by the secondary laser, diffusion of the protein out of the focal volume before depopulation can occur could result in a decrease of fluorescence enhancement. The protein was immobilized in PAA to limit this effect and the fluorescence enhancement was recorded. AcGFP showed a 13% enhancement, almost twice the recorded enhancement in solution at the optimal conditions. Of note for later imaging studies (Section 4.6), EGFP was also studied under these conditions for fluorescence enhancement. As a similarly emitting fluorescent protein, EGFP has the same chromophore and photophysical properties (Section 4.1) as AcGFP which suggested the optical modulation may be achievable. However, EGFP showed no fluorescence enhancement or modulation upon secondary laser co-illumination. Possible reasons for this difference are discussed in Chapter 5.

4.3 Secondary Wavelength Dependence

While 561 nm was the first wavelength investigated for modulation, other wavelengths may be more optimally absorbed by the optical dark state of AcGFP. Efficient repopulation of the emissive manifold is characterized by large action cross sections which

are defined by the product of the dark state quantum yield and absorption cross section. As these parameters are not directly measurable with fluorescence techniques, the dark state action spectrum for AcGFP can be visualized by the enhancement at varying longer wavelengths. Initial studies to determine the optimal secondary wavelength for AcGFP enhancement were performed. AcGFP protein solutions were excited with a 476 nm primary laser (2 kW/cm^2) and the secondary wavelength was scanned from 561 nm to 950 nm, maintaining a constant intensity of 22 kW/cm^2. Figure 4.3 shows the resulting secondary laser scan, which reflects the relative action cross section for the dark state. This dark state action spectrum indicates that the modulatable state absorbs a wide range of wavelengths. While enhancement is observed over much of the scanned region, maxima occur at ~560 nm, ~780 nm, and 900 nm. Spectral overlap between the secondary laser and the collected emission limits the high energy side of the 561 nm "peak" so the true maximum was not observed. The dark state has the greatest absorption at the wavelengths corresponding to each maximum, and thus these wavelengths are best suited for optical modulation experiments.

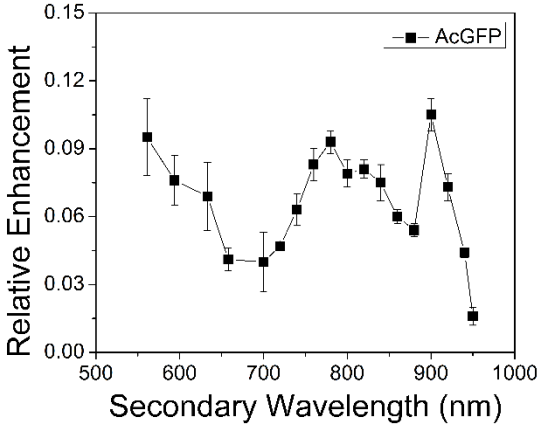

Figure 4.3 AcGFP fluorescence enhancement dependence on secondary laser wavelength.

4.4 Characteristic Modulation Frequency

While knowing AcGFP can be optically modulated is important to its use in biological imaging, another parameter that dictates its utility is the rate at which the protein can be modulated. As seen previously, co-illumination with the secondary 561 nm laser increased the detected fluorescence. By modulating the secondary laser, this dynamically increases and decreases the AcGFP emission. The result is an encoded secondary laser modulation waveform on the higher-energy fluorescence that can be extracted by Fourier transform. The demodulated signal can then be recovered from the Fourier amplitude at the modulation frequency and the enhancement calculated as described in Section 2.6.2. Accelerating dark state decay, secondary laser excitation alters relative emissive and dark state populations to establish a new steady-state fluorescence intensity in a time that directly depends on the new rates in and out of the dark state manifold. Analogous to frequency domain lifetimes,[178] the buildup and decay of steady state population takes a finite time and as modulation frequencies become faster than this the depopulation becomes faster than the buildup. This is seen as a decrease in enhancement at frequencies higher than the inverse time to establish these populations. Using optimal intensities for AcGFP modulation, the secondary laser was varied from a low frequency of 1 Hz to a high frequency of 10 kHz. At each frequency, the enhancement was calculated and then plotted as a function of the secondary modulation frequency (Figure 4.4). At high modulation frequencies, the enhancement of AcGFP is decreased.

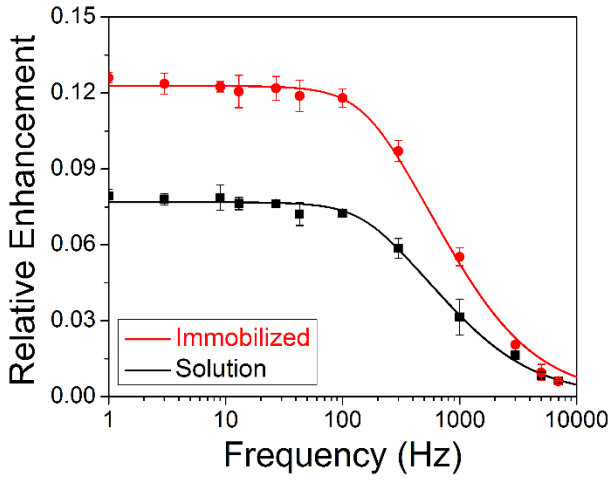

Figure 4.4 Enhancement frequency dependence of purified AcGFP either in solution (black) or immobilized in polyacrylamide gels (red).

The frequency that corresponds to a 50% decrease in the initial recorded amplitude yields a characteristic lifetime for the modulated fluorophore. Data in Figure 4.4 was fit to Equation 2.10 and the modulation frequency at half the original value was recorded as the characteristic frequency. In solution, the AcGFP characteristic frequency is 760 Hz which corresponds to an approximately millisecond timescale. Fluorescent proteins are known to have an approximate millisecond diffusion time in water.[183,184] Thus, to confirm the characteristic frequency determined with AcGFP in solution, the frequency dependence of immobilized AcGFP was also investigated (Figure 4.4, red). The characteristic frequency for immobilized protein is 830 Hz confirming that the millisecond timescale is unique to the protein and not an artifact of diffusion. It is important to note that these characteristic frequencies are intensity dependent. As discussed earlier when studying the enhancement intensity dependence, the dark state being probed in modulation is dependent not only on the rate out but also the rate in, the latter of which is primary intensity dependent. Thus,

characteristic frequencies will change depending on the primary and secondary intensities used and can be utilized later to determine other photophysical parameters (Section 4.5.2).

4.5 Extraction of Photophysical Parameters

As discovered with the investigation of optically modulated blue fluorescent proteins, understanding the photophysical parameters of the optical dark state involved is important in a number of other facets of modulation. The photophysical on and off times can inform about the possible state involved in modulation and limitations of using AcGFP as a modulatable probe. The following section discusses methods used to extract these parameters for AcGFP using both bulk and single molecule techniques. Bulk characterization is relatively easy and, with the appropriate fitting, can provide a look into the timescales associated with modulation. However, single molecule spectroscopy is a powerful experimental technique that does average over the ensemble of behaviors, thereby yielding characteristic timescales and insight into possible complex fluctuations in AcGFP.

4.5.1 Fluorescence Correlation Spectroscopy: One Laser versus Two Laser

Fluorescence correlation spectroscopy (FCS) is an experimental technique using statistical analysis of the fluctuations of fluorescence in a system in order to decipher dynamic molecular events.[48] As discussed in Sections 1.2.3.1 and 2.4, the basic concept is that as fluorescent molecules diffuse in and out of the detection volume the fluorescence fluctuations are recorded and then a proper correlation function is taken. FCS has been used previously to investigate the photodynamics of green fluorescent proteins.[50,185,186] Thus, FCS seemed an appropriate method to begin teasing out the photophysical parameters of the dark state of AcGFP. Initial characteristic frequency measurements suggest a timescale of ~1 millisecond. However, previous reports of EGFP triplet states

suggested lifetimes of hundreds of microseconds.[50] The possibility existed that the modulatable state was a longer-lived triplet state that was short enough to be resolved from diffusion in FCS. To begin, primary illumination alone was investigated to see the unperturbed dynamics of AcGFP. As seen in Figure 4.5 A, the correlation fits of AcGFP contain a diffusion component in the millisecond time range and a "triplet" fraction in the microsecond time frame. As expected, increased primary intensity resulted in an increased fraction in the dark state along with the better contrast of the triplet and diffusion components. Using the fitting parameters for the triplet fraction and associated time (Section 2.4), the calculated on and off times for the varying primary intensity were plotted (Figure 4.5 B). Thus, initial evidence pointed to a ~300 microsecond dark state.

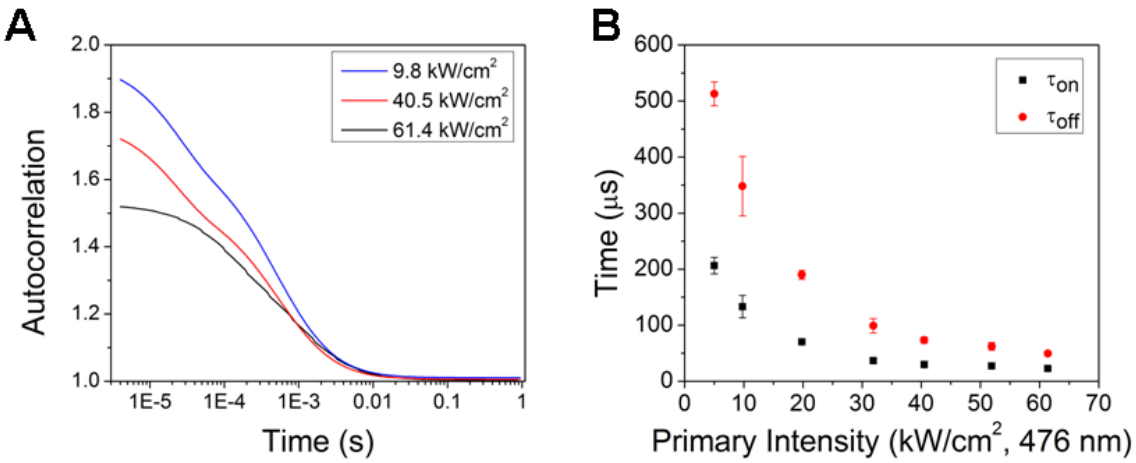

Figure 4.5 Single laser FCS curves of AcGFP. (A) FCS fits for varying primary intensities in the absence of the 561 nm secondary. (B) Calculated on and off times for AcGFP from extracted fitting parameters assuming a single state model with diffusion of (A).

If this is the state being modulated, co-illumination with secondary laser should show a reduction in the dark state population. However, upon investigating the effect of the secondary laser on this dark state lifetime, the results were inconclusive as to any

change in the FCS-measured off time. Additionally, the lack of contrast change in the correlation curve seemed to be accompanied by a change in apparent diffusion time (Figure 4.6). This change could be due to a photinduced process on the millisecond time scale but is convolved with the diffusion of the protein suggesting more techniques capable of probing long-lived states.

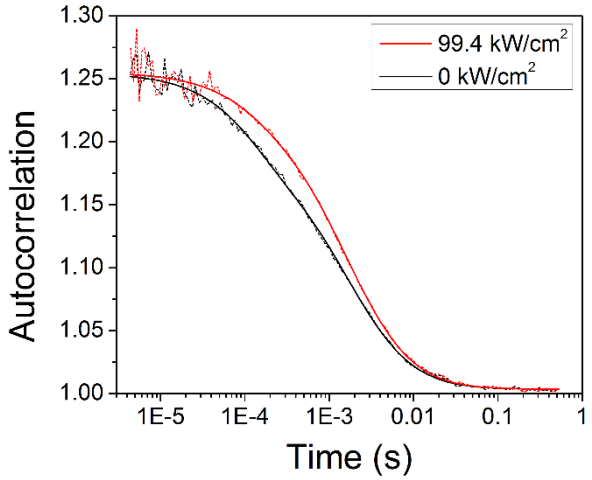

Figure 4.6 FCS fits with (red) or without (black) 561 nm secondary illumination. The primary laser excitation was fixed at 10 kW/cm^2.

4.5.2 Modulation Frequency Intensity Dependence

FCS measurements were inconclusive in the investigation of on and off times associated with the modulatable optical state. Thus, the method used to investigate these times in BFPs was used. As previously mentioned, the characteristic frequency is primary intensity dependent as it is a function of both the rate in and out of the dark state. Thus, the natural off time of the modulatable dark state can be extracted from bulk solution of AcGFP. This is done by recording the modulation frequency dependence at varying primary intensities. The characteristic frequency is the sum of rate constant out of the

bright manifold and the natural rate constant of dark state decay, $k_{on} + k_{off}$. In theory, extrapolation to the zero intensity is equivalent to no primary illumination and thus k_{on} becomes zero and the characteristic frequency reflects the natural off rate, k_{off}, of the dark state. Thus, by plotting the inverse of the characteristic lifetime (ν_c) as a function of primary laser intensity (secondary held constant at 30 kW/cm^2), the natural off time (τ_{off}) can be determined using the y-intercept as was done with the modBFP mutants. By doing so, a frequency of 550 Hz is extrapolated and is predictive of an off time (1/y-intercept) of the modulatable state of AcGFP which is 1.8 (± 0.9) ms. It is important to note that the best results for this technique are gathered when the primary intensity can be varied by an order of magnitude and the enhancement is high enough to get a good fit for the characteristic frequency.

Additional data can be gathered from the fluorescence time traces of modulation as well. In the case of very fast response of the molecule to secondary waveform imposed on it, the fluorescent time trace would perfectly reflect the waveform. However, there is a molecular response and there is a decay that is present once the secondary laser is turned off. A square waveform was used as we wanted an immediate removal of the secondary to view the response with primary. The decay on the falling edge of the square waveform is related to the $k_{on} + k_{off}$ similarly to the characteristic frequency. Thus, as was done with the previous modulation frequency experiments, the primary intensity was varied and the falling edge decays in the fluorescence time trace were measured. After binning the data for the modulation frequency used, the individual decays were fit to the appropriate exponential decay and averaged together. However, to make analysis faster, the time trace was converted into a histogram of the binned fluorescence in one period. This one period

is the result of overlapping all the recorded cycles for a given time and the average photon counts and is used to find the decay of a single falling edge representative of all cycles (Figure 4.7 A). The decay times ($1/\tau_c$) are then plotted versus the primary intensity (Figure 4.7 B). At the zero primary intensity, a frequency of 620 Hz is extrapolated, which is consistent with the modulation frequency data of a state with an off time of 1.6 (± 0.1) ms.

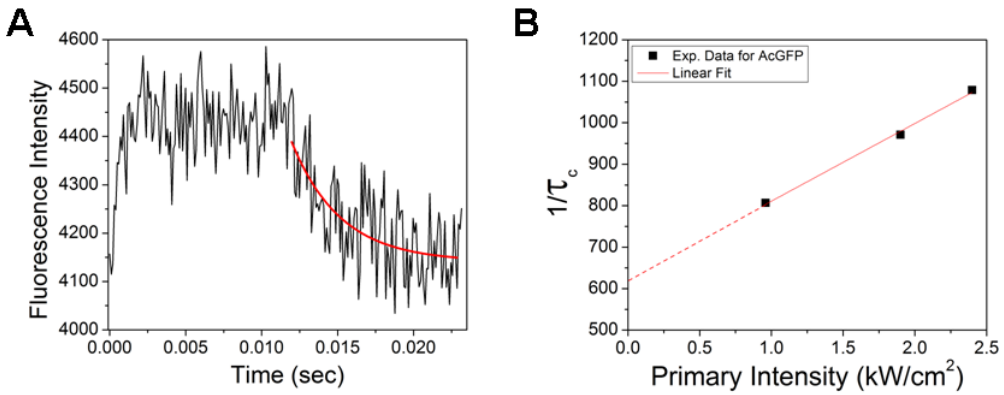

Figure 4.7 Extraction of natural dark state off time using modulated time traces for AcGFP. (A) Histogram of 43 Hz modulated AcGFP signal and fit (red line) to a single exponential decay. (B) The inverse of the characteristic time are plotted as a function of 476 nm primary excitation. Secondary is held constant at 30 kW/cm^2.

4.5.3 Immobilized Single Molecules

While FCS was inconclusive, and bulk intensity dependent modulation techniques pointed to a possible millisecond component that would have been unresolved in FCS, a new approach was needed to verify the longer-lived millisecond dark state off time for AcGFP. Many longer time dynamics have been probed with single molecule techniques in which information is collected molecule by molecule. The dark state responsible for modulation in silver nanoclusters were investigated in this way.[74] By immobilizing single AcGFP proteins in a matrix of PAA, this removes the limitation that was present in FCS:

diffusion. Thus, after collecting the fluctuations of the protein an autocorrelation can be fit without worrying about the diffusional component that normal FCS correlations account for. Additionally, as predicted by the bulk experiments, it is likely that the autocorrelation will reveal a component on the millisecond timescale. Data was collected for 100 AcGFP molecules with primary illumination alone to get an average. The resulting averaged autocorrelation revealed two components: one on the ~300 microsecond timescale and another on the ~1 millisecond timescale (Figure 4.8). Co-illuminating with both the primary and secondary laser (561 nm) showed a marked reduction in the millisecond component in the average autocorrelation of 30 molecules (Figure 4.8). It was determined from the single molecule data that AcGFP has a 1.5 millisecond and 350 microsecond natural off time confirming the previous data taken from bulk experiments and FCS.

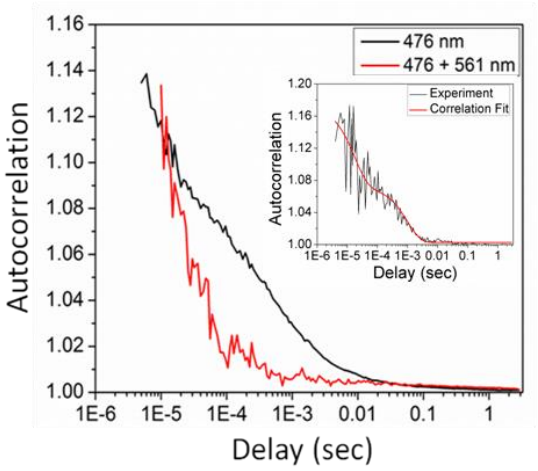

Figure 4.8 Single molecule autocorrelations without (black) and with (red) illumination of the secondary 561 nm laser.

4.6 Signal Recovery in High Background

Motivated by the ability to optically modulate the AcGFP fluorescence by longer wavelength illumination, we investigated selective recovery of AcGFP fluorescence in

cells. Previously reported in Section 3.7, a blue fluorescent protein, modBFP/H148K, was selectively recovered over the high autofluorescent background of the cell under UV illumination. Here, we also demonstrate the recovery of AcGFP in the presence of a non-modulatable background distinguishing its emission from that of autofluorescence and from the similarly emitting, yet unmodulatable, EGFP. For this purpose, NIH-3T3 cells were co-transfected with two plasmids, the first encoding AcGFP fused to a mitochondrial targeting peptide (mito-AcGFP), and the second to express EGFP as fluorescent background (transfection done by Dr. Pritha Bagchi) in fixed and live cells. Imaging was performed in a stage-scanning confocal geometry utilizing 476 nm primary excitation and spatially overlapped, intensity-modulated secondary excitation at 561 nm. Fluorescence was collected between 500 and 530 nm. To generate cell images, the average fluorescence intensity and lock-in amplitude (intensity of the modulated fluorescence component) were recorded at each stage position (Section 2.8.2). No emission was observed from secondary laser illumination alone, and background in blank or EGFP-only cells was non-modulatable.

Lock-in-based fluorescence demodulation at each stage position within the AcGFP-expressing cells improves the visibility of fluorescence associated with mitochondria, primarily by suppressing the heterogeneous, unmodulated background. Control mito-AcGFP-only cells exhibit largely mito-AcGFP fluorescence, with other subcellular locations showing only dim residual background, resulting in modest (< 10%) contrast improvements upon background-removing demodulation (Figure 4.9). When co-expressed with untargeted EGFP, cells show much higher overall emission that obscures much of the mitochondria-associated AcGFP fluorescence. As only AcGFP fluorescence is modulated

by the secondary laser, selective recovery of the AcGFP signal over EGFP was readily achieved through demodulation, revealing the AcGFP-labeled mitochondria (Figure 4.10 A & B) with a maximum signal-to-background ratio indistinguishable from that of the AcGFP-only control. The most promising gain in signal visibility was observed in areas with low AcGFP presence and hence weak emission signals. In formaldehyde-fixed co-transfected cells, mitochondria were barely visible over background in the raw fluorescence images, exhibiting an average 1.4:1 ratio. However, in the demodulated image the ratio increased to an average of 18.8:1, yielding a ~13-fold improvement of signal visibility. Similarly, in live co-transfected cells, the raw fluorescence ratio of weakly emissive AcGFP signal was 1.2:1. Upon demodulation, the average ratio increased to 12.1:1, again yielding a ~10-fold improvement upon demodulation.

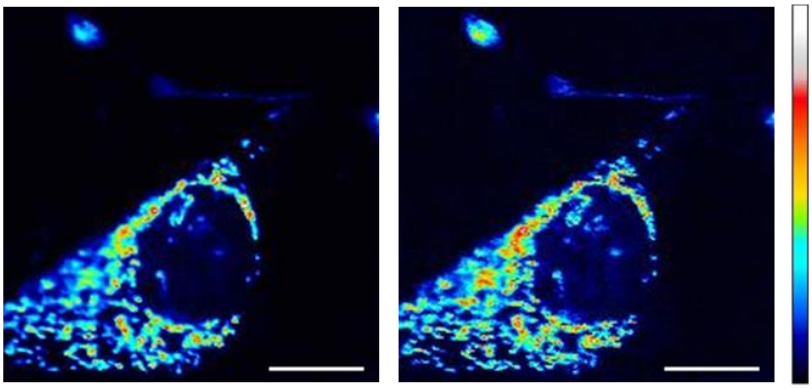

Figure 4.9 Fixed NIH-3T3 cells expressing mitochondria-targeted AcGFP. Primary intensity was held at 5.9 kW/cm^2 and the secondary intensity (64 kW/cm^2) was modulated at 300 Hz. (Left) Raw fluorescence image of AcGFP-labeled mitochondria. Min to max color bar is 0 to 10 × 105 photons counts. (Right) Demodulated image of AcGFP as lock-in amplitude. The color map on the right is linear from min to max in each image, with no threshold applied. The raw fluorescence image intensity is in photon counts, and the demodulated image intensity is in mV after lock-in amplification. Scale bar: 10 μm.

Selective recovery of mitochondrial signal is also seen when both fluorescent proteins, AcGFP and EGFP, are targeted to different locations (Figure 4.10 C& D). By targeting EGFP to the nucleus, the EGFP emission is much higher than that of AcGFP targeted to the mitochondria. In formaldehyde-fixed co-transfected cells, mitochondria exhibited noticeably weaker fluorescence than did the nuclear EGFP in the raw fluorescence images, yielding an average 0.27:1 ratio. However, in the demodulated image the ratio increased to an average of 6.6:1, yielding a ~24-fold improved signal recovery. Similarly, in live co-transfected cells, the raw fluorescence ratio of weakly emissive AcGFP signal was 0.25:1. Upon demodulation, the average ratio increased to 5:1, again yielding a ~20-fold improvement upon demodulation. The higher fluorescence exhibited in the nucleus created a larger lock-in noise level; thus, the visual effect of demodulation was not as pronounced as in the untargeted EGFP case. However, a ratio image of the normalized demodulated signal to the normalized raw signal revealed that the mito-AcGFP signal was being modulated (Figure 4.10 E). Based on the different dark state residences and selective long-wavelength optical recovery of fluorescence, AcGFP signals are readily distinguished from both autofluorescent background and the otherwise indistinguishable EGFP emission in fixed and live cells.

The frequency employed in with this point-by-point scanning technique is controlled by the modulation frequency response curve; the faster the characteristic frequency, the shorter the dwell time. In this case, the 300 Hz is utilized allowing for a dwell time on each pixel for 50 ms. However, to recreate an image of 40 × 40 μm dimensions total time can be ~ 30 minutes. This imaging time is quite long for applications with faster diffusing characteristics. In order to image faster, optical demodulation

microscopy could be readily combined with other techniques (e.g., total internal reflection microscopy or spinning disk confocal microscopy) to further expand the scope, sensitivity, and speed of live cell imaging.

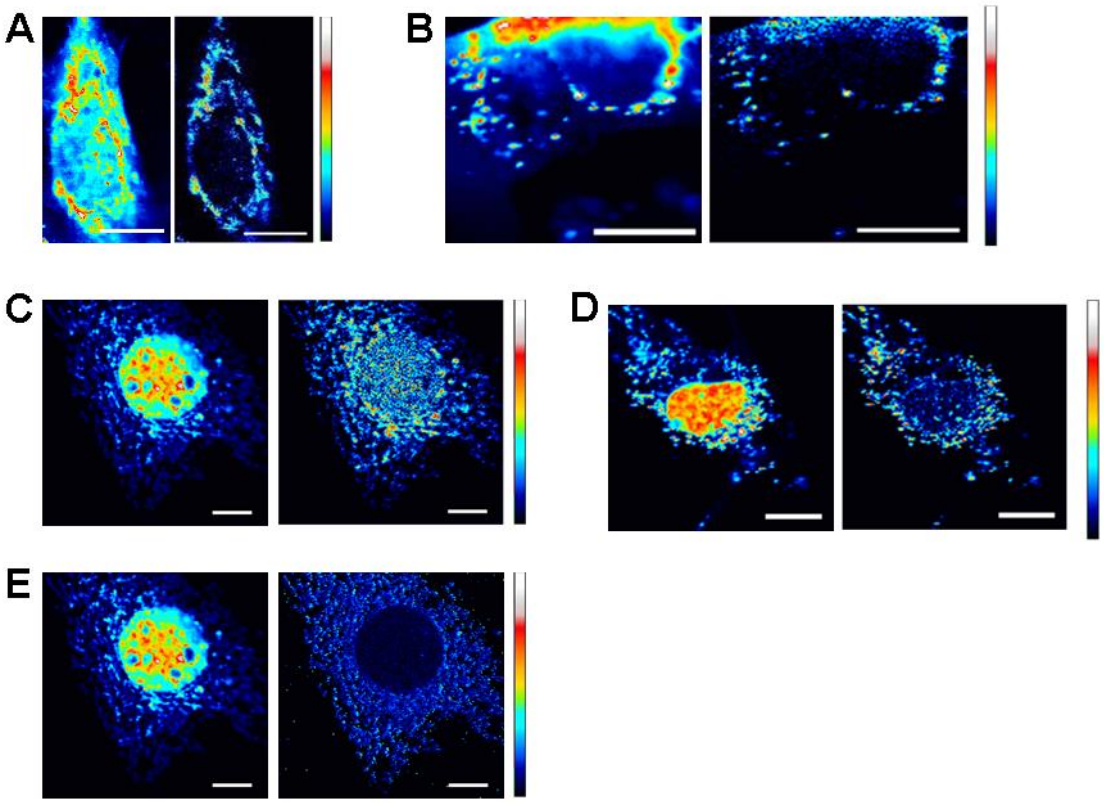

Figure 4.10 Selective fluorescence recovery of mitochondria-targeted AcGFP in the presence of high EGFP background fluorescence in NIH 3T3 mouse fibroblasts. In all cases, the primary laser intensity was held at 5.9 kW/cm^2 and the secondary intensity (64 kW/cm^2) was modulated at 300 Hz. EGFP was untargeted and measured in (A) fixed cells and (B) live cells or EGFP was targeted to the nucleus in (C) fixed and (D) live cells. (Left) Raw fluorescence image of AcGFP-labeled mitochondria and EGFP. (Right) Demodulate image of lock-in signal to raw fluorescence. (Left) Raw fluorescence image of AcGFP-labeled mitochondria and EGFP. (Right) Ratio image of lock-in signal to total fluorescence image. (E) Ratio image of (C). The color map is linear from min to max in each image, with no threshold applied. The raw fluorescence image is reproduced in units of photon counts. Scale bar: 10 μm.

4.7 Conclusions

Expanding modulation to fluorescent proteins offers greatly improved sensitivity by removing the spatially heterogeneous background typically encountered in biological imaging, and the opportunity to further distinguish signals from multiple proteins with strongly overlapping spectra. Because secondary illumination is lower in energy than the collected fluorescence, no additional background is introduced, and heterogeneous cellular fluorescence and obscuring fluorophore signals are readily removed to yield order-of-magnitude increased signal visibility in fixed and live cells. The already-demonstrated 10- to 20-fold sensitivity improvement provides motivation for even more dramatic gains as proteins are bred for modulation depth and characteristic frequency, thereby greatly expanding signal recovery applications in biological and medical imaging. Additionally, long-wavelength modulation expands the dimensionality to discriminate FP emitters based on dark state lifetimes. Once fully mechanistically understood and optimized, this would allow for similarly emitting modulatable proteins to be selectively modulated by varying the modulation frequency, thereby inherently offering an additional dimension for multispectral imaging.

CHAPTER 5

SPECTRAL VARIANTS & PROPOSED MECHANISM FOR OPTICAL MODULATION IN FLUORESCENT PROTEINS

In previous chapters, two proteins of different spectral properties were found to be capable of long wavelength fluorescence modulation. Along with their usefulness in cellular imaging, the proteins were studied for photophysical parameters that are characteristic of the modulated state. Evidence pointed towards the presence of a long-lived dark state that allowed for modulation and the presence of a long-lived dark state was consistent across proteins. This leads to two questions: 1) are there proteins within other spectral regions capable of long-wavelength modulation and 2) what is the possible mechanism for modulation in fluorescent proteins? This chapter explores the modulation capability of other spectral variants containing tyrosine chromophores. In order to better understand the modulatable state, the chromophore environment is probed with structural changes that could be controlled through mutation and environmental factors such as pH and deuterated solvent to provide insight into modulation factors. Additionally, contrasts between unmodulatable and modulatable proteins in the same spectral region and modulatable proteins across spectral regions are considered. A proposed mechanism derived from these results is discussed.

5.1 Introduction

As reviewed in the Introduction, these spectral variants are derived from various sources. While some are created from the WT-GFP[107,110], others have been identified from other organisms[32,117]. All of the proteins discussed here are similar in their inclusion of a

tyrosine chromophore that is present within the β-barrel. While the blue fluorescent proteins (Chapter 3) and most green fluorescent proteins (Chapter 4) were previously introduced, a short description of the other proteins investigated is given.

5.1.1 Padron*

In order to expand the dual color imaging of photoswitchable proteins, researchers worked to create proteins with different switching properties. Many photoswitchable proteins are controlled by "negative" switching in which UV illumination primes the protein to the on state and blue (488 nm) illumination converts the protein to the dark, off state while emitting green fluorescence.[118-120,124] The problem with most photoswitchable proteins is that they all use the same illumination for switching. To broaden the number of labels in dual color imaging, proteins were modified to have "positive" switching capabilities in which the protein has the opposite reaction to illumination sources.[119] While the green emission still comes from blue (488 nm) photons, this excitation also results in the protein being in the on state and can be reverted to off with UV light. The first protein to be found with these properties was Padron (indicative of the reverse switching properties of Dronpa).[119,122] While Padron was a great advancement, a few more mutations (N94H, I100S, P141R) for low temperature monomer creation for applications lead to the protein known as Padron*.[119] Padron* has an absorption maximum at 500 nm, a lesser absorption peak at 400 nm at room temperature, and gives good green fluorescence at 525 nm (Figure 5.1).

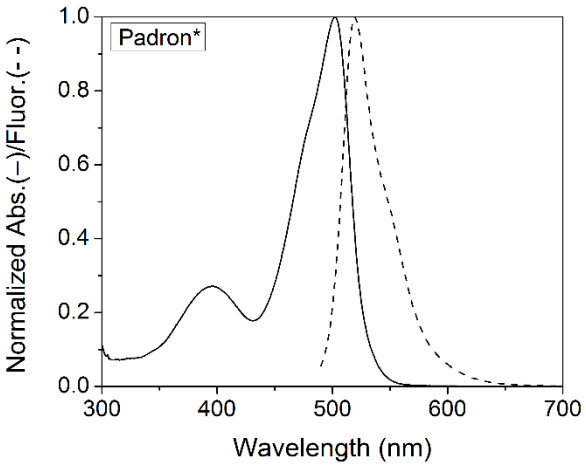

Figure 5.1 Absorption (solid) and emission (dash) spectra of room-temperature equilibrated Padron* in PBS at pH 7.4. Emission spectra taken with excitation at 470 nm.

5.1.2 Yellow Fluorescent Proteins

Created for use in FRET experiments because of the favorable overlapping spectral properties with its partner, cyan fluorescent protein, and yellow fluorescent proteins (YFPs) are characterized by their 515 nm excitation and 525 nm emission peaks (Figure 5.2). The red-shifted spectral properties are suggested to arise from the T203Y substitution in the GFP variant as the tyrosine results in π-stacking interactions between the chromophore and the highly polarizable phenol.[88,91,110,187] Unfortunately, for use in cellular imaging studies early YFPs were plagued by excessive pH sensitivity, halide interference, and poor photostability.[107,111] Venus, developed by introducing five mutations into the well characterized variant, enhanced yellow fluorescent protein (EYFP), improved maturation and brightness and greatly reduced environmental dependence.[109,188,189] Of all the fluorescent proteins derived from the *Aequorea* genus, yellow fluorescent proteins are the most red-shifted possible that maintain the original chromophore.

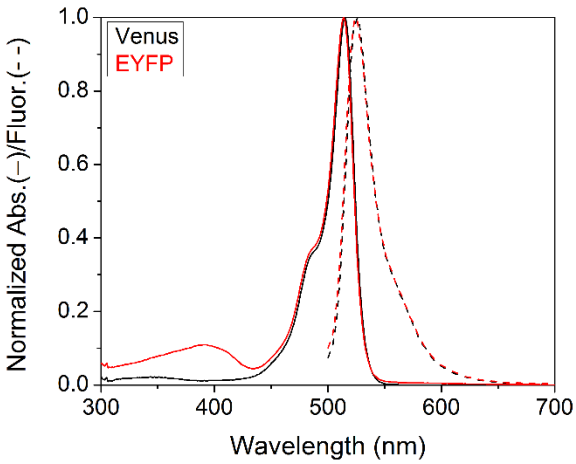

Figure 5.2 Absorption (solid) and emission (dash) spectra of yellow fluorescent proteins, EYFP (red) and Venus (black) in PBS at pH 7.4. Emission spectra taken with excitation at 480 nm.

5.1.3 Red Fluorescent Proteins

To further extend the fluorescent protein palette into a spectral region of low autofluorescent background, researchers continue to develop fluorescent proteins with redder emission than that of the YFP variants. Six proteins from the non-bioluminescent Anthozoa class corals were isolated and determined to only share a 26-30% identity to *Aequorea* GFP.[117,190] However, the proteins displayed the same β-barrel structure first seen in GFPs and, more importantly, the two most crucial residues contributing to the chromophore of GFP, Y66 and G67.[117] Some of the important polar residues contacting the chromophore, such as R96 and E222, were conserved in the coral proteins. The species tested exhibited fluorescence from blue to red. However, DsRed was from a red portion of a *Discosoma* species[92,113] and had excitation and emission maxima at 558 and 583 nm, respectively (Figure 5.3). This was the first report of a wild-type red fluorescent protein and work began to modify the protein for improved photophysical characteristics and decreased oligomerization.[114-116] The first attempts created mRFP1 which improved the

quantum yield, photostability, and maturation compared to DsRed.[30-32] However, mCherry of the "mFruits" showed the most promise with even greater red shift to an excitation of 587 nm and 610 nm emission, and featured superior photostability to that of the other mutants.[33]

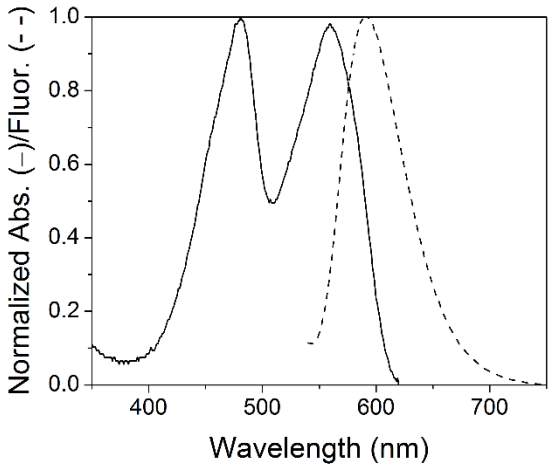

Figure 5.3 Absorption (solid) and emission (dash) spectra of red fluorescent protein, dsRed-monomer in PBS at pH 7.4. Emission spectra taken with excitation at 594 nm.

5.2 Spectral Variants Modulation Summary

The prospect of other tyrosine-based fluorescent proteins led to the investigation of fluorescent proteins across the visible spectral range. However, the investigation of every fluorescent protein and possible variants available would be an arduous task and beyond the scope of this work. Instead, a representative group of fluorescent proteins were chosen based on the following criteria (in order): tyrosine-based chromophore, commercially available, high use in cellular studies, and available, solved crystal structures or other structural data. The blue fluorescent proteins selection was discussed in Chapter 3. In the green fluorescent protein family, EGFP and AcGFP are highly used for cellular imaging

and have resolved structures in the RCSB Protein Data Bank (PDB) as seen in Chapter 4. An additional green fluorescent protein, Padron*, was added to the collection as the Tolbert group was working on researching excited state transient absorption of Padron* and its variants to determine dark states in the protein. This could add insight into modulation states and possible timescales so Padron* is useful for this study. The additional proteins studied are red-shifted from the blue and green fluorescent proteins already investigated. The yellow fluorescent proteins chosen were EYFP, Venus, and YPet. The red fluorescent proteins selected were dsRed-monomer, mRFP1, and mCherry.

While the blues and most of the greens were extensively investigated previously in this work, the yellow and red fluorescent proteins had not been tested for optical modulation. As the end goal is the use of these proteins in cellular studies, the six remaining proteins were transfected into cells, fixed, and tested for fluorescence enhancement via long-wavelength modulation. The yellow fluorescent proteins were studied with 476 nm primary and 594 nm secondary while collecting fluorescence at 500-535 nm. The red fluorescent proteins were investigated with 561 nm primary and 700 nm secondary illumination, while collecting fluorescence at 550-600 nm. Despite the fact that an absolute enhancement and appropriate characteristic timescales may be muddled with the background of the cell, this approach allows for a fast determination of secondary laser enhancement without the purification of all the proteins. Initial experiments suggested that all yellow fluorescent proteins tested and only dsRed-monomer of the red fluorescent proteins were modulatable.

Table 5.1 Spectral Variant Modulation Summary. Information was obtained from purified protein at pH 7.4 though † indicates data obtained for protein in fixed cells.

Fluorescent Protein	$\lambda_{ex}/\lambda_{em}$ (nm)	Primary λ (nm)	Secondary λ (nm)	Enhancement (%)	ν_c (Hz)
modBFP	390/450	405	514	4	16
mKalama1	385/456	405	514	0	—
EGFP	488/507	476	561	0	—
AcGFP	480/505	476	561	8	760
Padron*	503/522	476	561	12	750
EYFP	514/527	476	594	12	800
Venus	515/528	476	594	16	816
YPet†	517/530	476	594	9	—
dsRed-m	556/586	561	700	27	3000
mRFP1†	587/610	561	700	0	—
mCherry†	587/610	561	700	0	—

Based on the cellular modulation experiments, the group of proteins to be purified for further modulation characterization was narrowed. The purified EYFP, Venus, and dsRed-monomer were prepared by Dr. Irina Issaeva of the Fahrni group and the purified Padron* was prepared by Dr. Russell Vegh of the Tolbert group. With these proteins, optical modulation and characteristic frequencies can be measured and compared to the blue and green fluorescent proteins already studied. Table 5.1 is a summary of those results. For the greens and yellows, a primary intensity of 1.9 kW/cm^2 and secondary intensity of 25 kW/cm^2 was used. DsRed-monomer required a high primary intensity of 13 kW/cm^2 and a secondary of 100 kW/cm^2 for both 543 nm and 561 nm excitation. Padron* has the same characteristic frequency as AcGFP, but slightly higher enhancement. The yellow fluorescent proteins have between 12-16% enhancement, and a characteristic frequency slighter higher than the greens and an order of magnitude faster than the blues. The red fluorescent proteins exhibit the highest enhancement at 27% with 561 nm excitation, and the fastest characteristic frequency, though 543 nm excitation also resulted in enhancement but at 17% for similar excitation intensities. These results yield a basis for

the comparative analysis of structural features important for optical modulation. The blue, green, and red-emitting proteins are of particular interest for mechanistic determination as these groups contain at least one modulatable protein and one non-modulatable.

5.3 Secondary Wavelength Dependence

In BFPs and GFPs, the proteins exhibited a dependence on the secondary laser wavelength. AcGFP exhibited a dark state action spectrum far into the red (~900 nm). As select yellow and red fluorescent proteins also show modulation and frequencies similar to AcGFP, the possibility existed that these proteins may also have dark state action spectrums far into the red region. Studies were carried out with Padron*, EYFP, and Venus solutions and excited with a 476 nm primary laser (2 kW/cm^2) while the secondary wavelength was scanned from 594 nm to 950 nm (22 kW/cm^2). Figure 5.4 shows the resulting secondary laser scan (700 to 950 nm), which reflects the relative action cross section for the dark state. This dark state action spectrum indicates that the modulatable state absorbs a wide range of wavelengths similar to AcGFP. Interestingly, whereas AcGFP peaked at 780 nm, Padron*, EYFP, and Venus had the similar peak shifted by ~20 nm to 800 nm. DsRed-monomer was excited at 561 nm primary laser (18 kW/cm^2) and the secondary wavelength was scanned from 700 nm to 850 nm (113 kW/cm^2). There is an apparent peak at 720 nm.

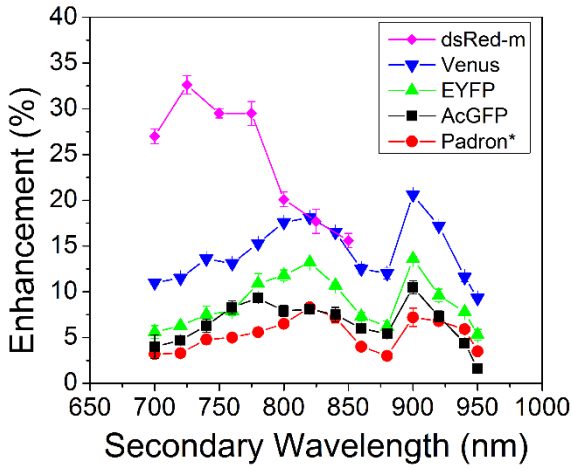

Figure 5.4 Dark state action cross section spectra scanned by secondary laser wavelength of AcGFP, Padron*, EYFP, Venus, and dsRed-monomer. Green and yellow proteins are excited with 476 nm and dsRed is excited with 561 nm.

Work was done to confirm the dark state spectrum of the fluorescent proteins in collaboration with Ariel Marshall of the Perry group at Georgia Institute of Technology. Previous transient absorption experiments of silver nanoclusters had proven useful in understanding the excited state dynamics and explaining the secondary wavelengths in modulation. Ultrafast transient absorption spectroscopy is commonly used to investigate the excited state absorption of a molecule. Briefly, a femto- or nanosecond laser is used to excite sample and prime the molecules to a higher energy level ("pump"). After a defined delay time, the sample is scanned with another continuous light source to "probe" the spectrum of molecules in the lowest excited state. However, conclusive information for the green and yellow fluorescent proteins could not be obtained. The time resolution of the nanosecond transient absorption was a possible limitation. After the nanosecond pulse, the probe delay capability was only hundreds of microseconds before the next pulse. Initial information gathered from the frequency dependence data suggested a 1-2 millisecond time component for the optically modulated state. Though, if the dark state is efficiently

populated, a small transient absorption would likely be present on the hundreds of microsecond timescale. Thus, dark state transition must not be as efficient as expected resulting in a relatively small intersystem crossing quantum yield to the modulatable state. A quick calculation of the dark state quantum yield using other extracted timescales revealed the dark state quantum yield to be ~0.01%. With low probability of entering the dark state from one pulse of the pump laser it is unlikely to see a distinct spectrum upon visible light probing.

5.4 Structural Dependence

Just as site-directed and random mutagenesis of fluorescent proteins investigations have revealed that fluorescence is highly dependent on the three-dimensional structure of amino acid residues surrounding the chromophore, so is the optical dark state responsible for long-wavelength modulation. Not only do these mutations alter spectral characteristics of fluorescent proteins, mutations and structural differences of green, yellow, red, and photoswitchable proteins have demonstrated the change in photophysical lifetimes. Using protein structure visualization software such as Swiss PDB Viewer, the proteins having similar emitting characteristics were aligned and compared. Of particular note were the amino acids within 4 Å of the tyrosine chromophore, as at these distances hydrogen bonding and steric interactions are likely to affect the chromophore most.

5.4.1 Blue Fluorescent Proteins

As seen in Chapter 3, altering interactions between the chromophore and the surrounding amino acid residues enabled tuning fluorescence enhancement. Based on the prediction of a cis/trans isomerization, coupled with a photo-induced protonation/deprotonation, mutations to the H148 positions were made to test the

hydrogen-bonding amino acids that better stabilize the anionic trans-chromophore in the ground and excited states, increasing population and residence of this kinetically trapped, but photo- and thermally reversible dark state. Such H-bonding and steric bulk near the chromophore are likely to raise the barrier separating cis and trans forms, increasing the dark state lifetime. Coupling photoisomerization with different chromophore protonation states rationalizes the observed red-shift of the dark state absorption relative to the ground state absorption spectrum, enabling the observed optical modulation. This initial hypothesis resulted in the marked improvement of modulation depth in mod-BFP/H148K and production of modulation in mKalama1. Additionally, the modulation differences were supported by altered optical on and off times (Section 3.4.3). The structural mutation for bright emission of mKalama1 may limit the production of the long-wavelength absorbing dark state. To date, there are no solved crystal structures of mKalama1 or modBFP. The closest crystal structure was published by Shu et al. with the S205V mutation.[98] However, as mutations can result in amino acid rearrangement within the pocket, better assumptions could be made with solved x-ray structures.

5.4.2 Green Fluorescent Proteins

The extensive work with GFPs has resulted in a wealth of information on the structural dependence on spectral changes and timescales. Three GPFs have been tested for modulation in this work, resulting in discovery that AcGFP and Padron* are modulatable while EGFP is not. In an attempt to further understand these differences past the simplified BFP case, this section discusses similar mutagenesis results on the photoswitchable green-emitting protein Padron* and the comparison of AcGFP and EGFP.

In BFPs, the mutation of H148 was based on the proximity and hydrogen bonding of the histidine to the phenol of the Y66. Mutation was made to increase and decrease the pK_a of the surrounding amino acid seen by the chromophore to stabilize one conformer over its conjugate. This approach was also taken for Padron*, mutating the histidine in the 194 position (H194) which aligned with H148 in the modBFP sequence. Random mutagenesis with all the natural amino acids was carried out by the Tolbert group and targets were selected by bright green emitters. Using 2 kW/cm^2 primary and 25 kW/cm^2 secondary, the enhancement of the proteins were compared. The variants were all modulatable ranging from 11-15% (Padron* = 12%) for the tested primary and secondary intensities (Figure 5.5). Unlike the mutations made to modBFP, the Padron* mutations showed little effect. As many of the variants have side chain residues that cannot be protonated or deprotonated, the discussion may be focused more on the steric bulk of the 194 position. Padron* is a known photoswitch and can undergo cis/trans isomerization; x-ray crystallographic data on closely related Padron 0.9 confirms the π-stacking of the histidine with the hydroxyphenyl ring of the cis chromophore.[122] Thus, steric hinderance may alter the energy barrier of switching. A smaller amino acid may free the chromophore environment to lower the barrier to the higher energy trans state sapping from the lower energy absorbing state (modulatable state). If the lower energy absorbing state does not build up an efficient population then the secondary laser would not significantly depopulate the state leading to a reduction in fluorescence enhancement. However, Padron* has additional mutations to that of Padron[119] or Padron 0.9[122] and resolved structures may better explain the changes in fluorescent enhancement.

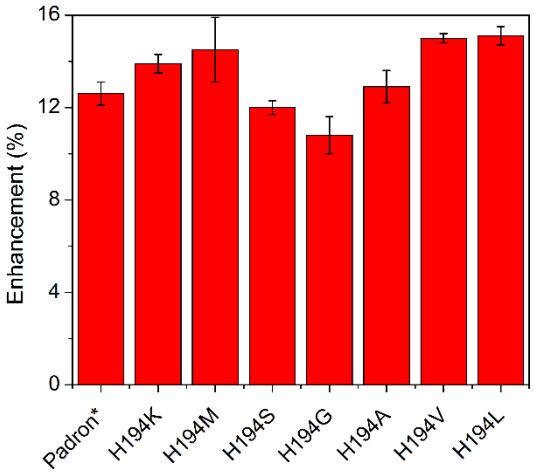

Figure 5.5 Fluorescence enhancement of Padron* and H194 variants at 2 kW/cm^2 (476 nm) and 25 kW/cm^2 (594 nm).

Taking another approach to the discussion of structural dependence on modulation, a comparison between the modulatable AcGFP and unmodulatable EGFP is made. One advantage of this comparison is the known ground state configurations of the amino acids, which allows for structural comparison that can lead to structural tuning of modulation depth. As mentioned in detail in Chapter 4, the AcGFP structure was solved by Gurskaya et al. and listed under PDB identity 3LVA.[180] Enhanced GFP (EGFP) was studied by Royant et al. for the stabilizing role of glutamic acid 222 and is listed under PDB identity 2Y0G.[191] Swiss PDB Viewer was used to align the two proteins around the chromophore Y66 that they share in common. Figure 5.6 displays the amino acids residing 4 Å from the ground state chromophore and the structural alignment between the two proteins. EGFP is 92% homologous with AcGFP and the most notable differences within the 4 Å sphere are Y220 and G222 (L220 and E222 in EGFP). These noted mutations were the amino acids engineered to turn the colorless acGFPL into the single band green emitter.[180] Compared with EGFP, the AcGFP chromophore resides in a different stabilizing

environment with structural rearrangements to surrounding interacting amino acids such as the T203. The stabilizing effects of E222 and proton pathway exchange of T203 are well studied.[192,193] The engineering in EGFP to stabilize the cis anionic chromophore may eliminate dark state populating processes that are facilitated in AcGFP. This could lead to inefficient dark state population at which long wavelength modulation could work. One disadvantage of examining only the ground state configuration is it does not tell anything about excited state structure or interaction.

Figure 5.6 Structural alignment and rendering of AcGFP (3LVA, cyan)[180] and EGFP (2Y0G, green)[191]. Amino acids within 4 Å of the chromophore (blue) are highlighted in the image and in yellow in the structural alignment. Differences within this distance are indicated in green in the alignment.

5.4.3 Red Fluorescent Proteins

Despite the low overall homology between *Aequorea* GFPs and *Discosoma* RFP, the tyrosine chromophore is protected by a surrounding amino acid network in both proteins. Previous investigations of AcGFP and EGFP showed the structural differences and their possible relation to modulation. The same was done with dsRed and mCherry with the advantage that each is from the same species (as mCherry was directly evolved from dsRed). Similarly, mCherry is mutated to exhibit favorable photophysical parameters

for cellular imaging such as further red-shift, brightness, and photostability.[33] These rounds of mutagenesis resulted in an 80% homology with dsRed and a 30 nm shift in absorption. Again, two amino acids within the 4 Å distance around the chromophore are different between dsRed and mCherry (Figure 5.7). The pK_a of the amino acid in the 163 position has changed from a positively charged, high pK_a (K163) that may favor more of a neutral chromophore to a negatively charged, low pK_a (Q163) that may favor the anionic chromophore. Additionally, serine in the 197 position in dsRed is the aliphatic amino acid, isoleucine, in mCherry that may eliminate a stabilizing force or proton pathway that was available in dsRed. As a point of reference to GFPs, the amino acids corresponding to Y66 and E222 are numbered Y67 and E215, respectively, in dsRed.

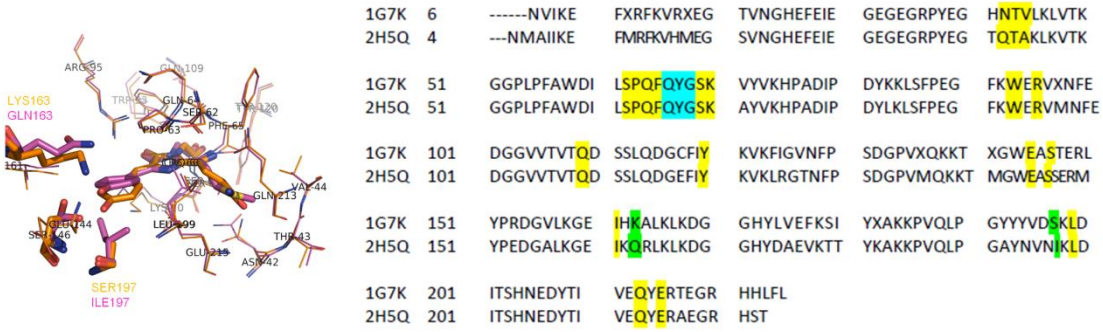

Figure 5.7 Structural alignment and rendering of dsRed (1G7K, orange)[116] and mCherry (2H5Q, magenta)[33]. Amino acids within 4 Å of the chromophore (blue) are highlighted in the image and in yellow in the structural alignment. Differences within this distance are indicated in green in the alignment.

5.5 pH Dependence

While the structural organization of the chromophore environment is important, comparison of structural differences are only a part. Examination of ground state structures give the first glimpse at possible long-wavelength shifted dark states, but they are static and give limited information of dynamic processes such protonation/deprotonation events

in the protein. Numerous studies have investigated the dark state dynamics of various fluorescent proteins and have shown the dependence of photophysical lifetimes on pH or other environments.[50-52,140,143,144,194-196] Dark state conversion can be both pH-sensitive and pH-insensitive, with photophysical processes taking place on the μs to 1 ms timescales. To further investigate photophysical timescales and processes of modulatable proteins, the PBS (pH 7.4) that the proteins were stored in was exchanged for buffered solutions with pH values from 4.5 to 10.5 (Section 2.2.3). The fluorescence enhancements were measured and the photophysical on and off times extracted for green, yellow, and red fluorescent proteins.

As the absorption spectra and resulting fluorescence intensity is dependent on pH, the fluorescence enhancement is calculated by the Fourier transform at a modulation frequency of 1 Hz (Section 2.6.2.1). This allows for the normalization of the enhancement to the fluorescence intensity of the solution. A marked reduction in fluorescence enhancement at low pH values was noted in all proteins (Figure 5.8). However, the range in which the protein enhancement becomes the most sensitive varies. In green fluorescent proteins, the enhancement is reduced at low pH, regained at neutral pH, and seems to rise again at more basic pH (Figure 5.8 A). Though in yellow fluorescent proteins, enhancement is reduced at low pH, is regained at neutral pH, and stays constant through basic pH (Figure 5.8 B). Interestingly, other than at very low pH (pH 4.5) where protein denaturation could begin to occur, the fluorescence enhancement is not significantly changed with enhancement being only slightly higher at neutral pH (Figure 5.8 C). The overall trends are compared in Figure 5.8 D.

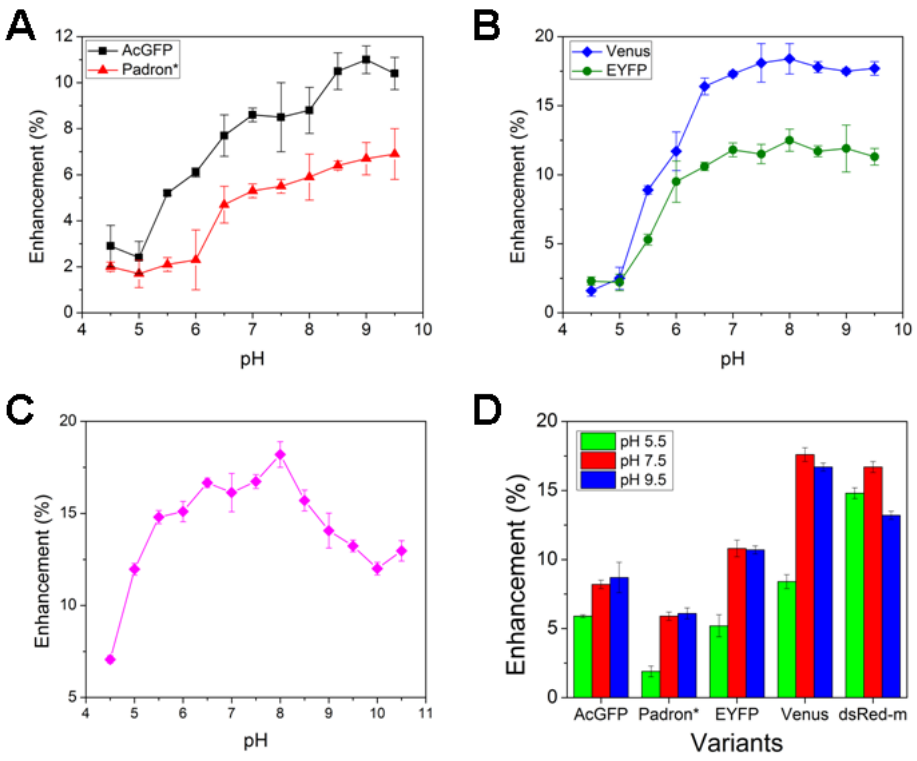

Figure 5.8 pH dependence of fluorescence enhancement for (A) green, (B) yellow, and (C) red fluorescent proteins. (A) and (B) were recorded with 476 nm at 1.8 kW/cm^2 and 800 nm at 22 kW/cm^2. (C) was recorded with 543 nm (13 kW/cm^2) and 720 nm (130 kW/cm^2). (D) Comparison of all proteins at pH 5.5, 7.5, and 9.5.

This change in modulation can be quantitatively measured in the change of fluorescence enhancement and the on and off times. As total observed enhancement is dictated by the on and off times (Enhancement = τ_{off}/τ_{on}), a change in fluorescence enhancement results of alterations in ground state on and off times. In addition to the measurement of fluorescence enhancement, the on and off times of the fluorescent proteins was measured as a function of pH. Doing so, the potential for understanding the role of protonation/deprotonation dynamics on the dark state lifetime can lead back to a reason for loss of enhancement and thus, an understanding of the mechanism involved in optical modulation.

As discussed in previous chapters, the on and off times can be extracted from the characteristic frequency. The extrapolation to the zero primary intensity reflects the natural off rate, k_{off}, of the dark state. Thus, the characteristic frequency of the proteins for pH 5.5, 7.5, and 9.5 were measured with the same parameters in Figure 5.8 D (476 nm/800 nm at 22 kW/cm^2 for greens and yellows, and 543 nm/720 nm at 130 kW/cm^2 for red). The characteristic frequency (ν_c) was plotted as a function of primary laser intensity and the natural off time (τ_{off}) was determined by the y-intercept (Table 5.2). For most proteins, a lower pH (pH 5.5) displayed a shorter off time compared to pH 7.5. This is one possible explanation for the decrease in observed enhancement as faster natural decay ($1/\tau_{off}$) of the protein results in less population in the dark state to be affected by the secondary laser. As the pK_a of the chromophore environment changes, the protonation state of the chromophore or surrounding animo acids could change. As a result, the stabilization of the chromophore is altered. However, the change is not very significant and the protonation states may play a small role in dark state lifetimes.

Table 5.2 Extracted Off Times of Green, Yellow, and Red Fluorescent Proteins as a Function of pH. All times are in milliseconds. Recorded with the parameters used in Figure 5.8D, color coding corresponds to the colors in Figure 5.8D.

Protein	pH 5.5	pH 7.5	pH 9.5
AcGFP	1.6 (± 0.1)	2.4 (± 0.6)	2.8 (± 1.6)
Padron*	3.0 (± 0.5)	2.4 (± 0.1)	2.9 (± 0.1)
EYFP	0.9 (± 0.2)	1.5 (± 0.1)	1.2 (± 0.1)
Venus	1.5 (± 0.2)	2.6 (± 0.9)	1.5 (± 0.4)
dsRed-m	0.9 (± 0.1)	1.3 (± 0.2)	0.7 (± 0.1)

Previous reports have studied the pH-dependent dynamics of dark states in green and red fluorescent proteins. Some flickering was pH-dependent as seen in GFPs[50,51,185,197]

and some RFPs[52,195], while others were pH-independent as dsRed[51]. The fast (< 100 μs) dynamics were attributed to the protonation/deprotonation of the chromophore. However, long-lived timescales associated with flickering in fluorescent proteins has also been observed. These longer-lived timescales may be convolved with conformational rearrangements and cis/trans isomerization.[198] In the case of dsRed, the dsRed crystal structure exhibits an extensive hydrogen bond network with reduced conformational freedom than many other RFPs.[195] The observed pH-dependence may stem from the structure configuration of the chromophore. At a neutral pH, a hydrogen bond between the chromophore and Q215 exists, which pulls the chromophore out of its planar conformation causing a red shift of the spectrum and a decreased brightness. At a pH that causes the hydrogen bond between the Q215 and the chromophore to be broken, conformational rearrangements will be favored. A similar pH-dependence has been recently observed in a related chromoprotein.

Transferable to the other fluorescent proteins, extensive hydrogen bond networks exist in many of the proteins investigated. As the pK_a of the chromophore environment changes, the protonation state of the chromophore or surrounding amino acids could change. At acidic pH, a population of fluorescent proteins do exhibit a protonated chromophore as an increase in the 400 nm absorption peak is observed. However, as dark state absorption occurs at longer wavelength than fluorescence, a protonation of the chromophore is not likely the probed species in modulation. As seen in the structural information (Section 5.4.), there are many surrounding amino acids within 4 Å of the chromophore with the possibility of protonation. For example in GFPs, T203 and T205 contain hydroxyl groups and R96, Y145, H148, and E222 contain side chains with varying

pK_a (Figure 5.6). The alteration of the protonation state of these may decrease the ground stabilizations of the chromophore which was observed with the decrease in τ_{off} and reduction in enhancement. However, modulation may be more than the change in protonation of amino acids in the ground state configuration and that interactions in the excited state are also important.

5.6 Deuterated Solvent Dependence

Deuterium exchange has been used to examine the reaction dynamics in a number of systems. In fluorescent proteins, researchers observed the marked isotope effect on the excited state dynamics of WT-GFP which was attributed to an excited state proton transfer (ESPT).[138] They noted a reduction in excited state proton transfer rate with deuterium, for a kinetic isotope effect of ~5.[193,199] Many other fluorescent proteins and their ESPT processes have also been studied. Thus, the kinetic isotope effect has an essential role in the mechanistic determination of optical states in fluorescent proteins and is useful to study with modulation.

As such, the PBS at pH 7.5 was exchanged with deuterated buffer (DPBS) at pD 7.5 (2.2.4) and the fluorescence enhancement and characteristic dark state off times measured. Similar to the conditions for measuring pH dependence, green and yellow fluorescent proteins were recorded with 476 nm at 1.8 kW/cm^2 and 800 nm at 22 kW/cm^2. DsRed was recorded with 543 nm (13 kW/cm^2) and 720 nm (130 kW/cm^2). Unlike the absorption spectra change in pH studies, exchange with DPBS at pD 7.5 does not result in a change of the absorption spectra of the proteins. However, the fluorescence enhancement decreases for all proteins to a varying degree (Figure 5.9). Interestingly, while most proteins show a reduction by half in enhancement, Padron* showed a negligible decrease.

This may point to a slight difference in the pathways for modulation in relation to the other proteins.

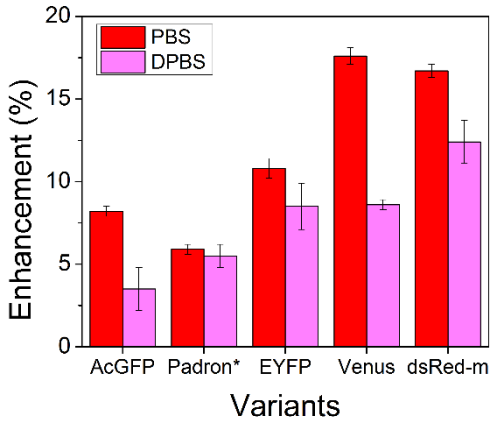

Figure 5.9 Deuterated buffer effect on fluorescence enhancement of green, yellow, and red modulatable fluorescent proteins.

The characteristic frequency (ν_c) was measured as a function of primary laser intensity and the natural off time (τ_{off}) was calculated for the proteins in DPBS (Table 5.3). Unlike the pH dependence that showed a decrease in off times with low pH, the off times are not altered with DPBS exchange. Additionally, the characteristic frequency at a constant primary intensity is similar for proteins in PBS and DPBS. For example, the characteristic frequency of AcGFP is 855 (± 208) Hz in PBS and 856 (± 222) Hz in DPBS. Thus, as ν_c is the sum of k_{on} and k_{off}, there was no observable change in the dark state lifetimes that explained the recorded reduction in enhancement. Thus, the reduction in fluorescence enhancement may be a result of alterations in excited state proton transfer.

Table 5.3 Extracted Off Times of Green, Yellow, and Red Fluorescent Proteins as a Function of Deuterium Oxide. All times are in milliseconds. Recorded with the parameters used in Figure 5.9, color coding corresponds to the colors in Figure 5.9.

Protein	PBS	DPBS
AcGFP	2.4 (± 0.6)	2.3 (± 0.3)
Padron*	2.4 (± 0.1)	2.5 (± 0.4)
EYFP	1.5 (± 0.1)	1.6 (± 0.1)
Venus	2.6 (± 0.9)	2.3 (± 0.2)
dsRed-m	1.3 (± 0.2)	1.4 (± 0.8)

The proton transfer dynamics of surrounding amino acids can either shift the dark state spectrum or affect the energy barrier of the ground and/or excited state. Examination of the dark state action spectrum of AcGFP in DPBS (pD 7.5) revealed the spectrum was unaltered (Figure 5.10). Thus, this along with the unaltered timescales suggests that the modulatable state is present and that ground state dynamics may be unaffected leading to the probability of a key role of the excited state. ESPT is much faster than the slow dynamics (~ 1 ms dark state) probed in modulation and may not be captured in ground state dark state lifetime. Along these lines, deuterium exchange may be altering the excited state proton transfer (which is still relatively fast compared to modulation) which results in a change of the barrier which is ultimately recorded with the change in enhancement.

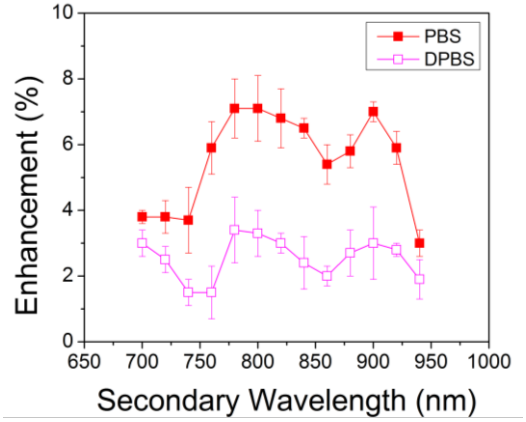

Figure 5.10 Dark state action cross section spectra scanned by secondary laser wavelength of AcGFP in PBS at pH 7.5 (red) and DPBS at pD 7.5 (pink). Primary laser is 476 nm.

5.7 Proposed Mechanism of Fluorescent Protein Modulation

The information gathered here suggests an optically modulated dark state that is controlled by both ESPT and cis/trans photoisomerization. Protonation dynamics have been reported in a number of proteins and are useful in the generation of proteins with different spectral emissions. While modification of excited state proton transfer rates leads to emission wavelength control, photoinduced isomerization ("trans/cis") is a parallel but low quantum yield process. The isomerization by itself is insufficient to significantly shift wavelengths in fluorescent proteins implying the joint control of the coupled proton transfer relay with this to create the long-wavelength absorbing dark state needed for modulation. When coupled to the proton transfer process, the combined long-lived isomerization and wavelength-shifting (proton transfer) processes has yielded several photoactivatable proteins, as well as switching proteins. Although published crystal structures of the fluorescent proteins all indicate a ground-state in the cis conformation, the trans conformation, coupled with proton transfer to yield the neutral chromophore leads to the presence of dark states from which anionic fluorescence is recoverable upon re-irradiation at 405 nm. Several recent crystal structures of both stereoisomers have been obtained, including the photoswitchable protein Dronpa, providing further evidence that the so-called dark state of GFP and some of its derivatives is the trans isomer.

Altering fluorescence enhancement stems from tuning interactions between the chromophore and the surrounding amino acid residues. As balanced rates in and out of the dark state are crucial for modulation, a hypothesis about possible states conferring modulatability can be made. While k_{on} is the product of excitation rate and dark state quantum yield, k_{off} is the natural decay out of the dark state and is associated with an energy

barrier for back reversion to the fluorescent manifold (Figure 5.11). Consistent with our observed long dark state lifetimes and known roles of photoisomers in photoswitches and other fluorescent proteins, the hydrogen-bonding amino acids that better stabilize the trans-chromophore in the ground and excited states increase population and residence of this kinetically trapped, but photo- and thermally reversible dark state. These interactions would thereby enhance modulatability. Such hydrogen-bonding and steric bulk near the chromophore are likely to raise the barrier separating cis and trans forms, increasing dark state lifetime. Coupling photoisomerization with different chromophore protonation states rationalizes the observed large red-shift of the dark state absorption relative to the ground state absorption spectrum, enabling the observed optical modulation.

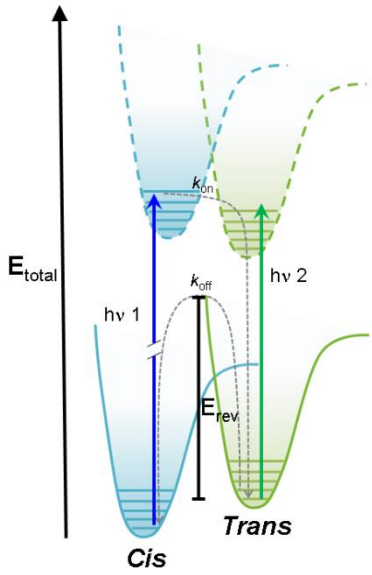

Figure 5.11 A possible schematic of energy levels involved in optical modulation. Excitation of cis state forms an excited state that can interconvert into the trans state that is coupled with ESPT to create a long-wavelength absorbing state. The natural decay out of that state is k_{off} and can be related to the activation energy for back reversion, E_{rev}.

Mutations of residues near the chromophore are likely to affect the energy barrier inhibiting back reversion. Conversely, mutation of residues near the trans configuration could have a more direct impact on the trans back reversion energy barrier. The data presented supports the possible mechanism. Differences in ground state x-ray crystal structures between modulatable and non-modulatable proteins point to different stabilized cis ground states that are also reflected in altered enhancement. pH and deuterated buffer dependence of the enhancement points to an excited state proton transfer that affects the E_{rev}. This is important for the optimization of modulatable proteins as done with non-modulatable mKalama1 (Section 3.6).

5.8 Conclusions

In the quest to understand the mechanism of optical modulation, the spectrum of fluorescent proteins capable of optical modulation has been extended to yellow and red fluorescent proteins. In addition to the modBFP and AcGFP fluorescent proteins identified and characterized in previous chapters, Padron*, EYFP, Venus, and dsRed-monomer have been identified with modulation depths up to 27%. Interestingly, the identified green, yellow, and red fluorescent proteins have dark state absorptions far into the red (~ 900 nm) as exhibited in the dark state action spectrum of the studied proteins. While initial photophysical timescales extracted for modBFP and AcGFP suggested cis/trans isomerization as a contributing factor to the modulation mechanism, photoisomerization may not have been sufficient enough to cause the far red-shift of the dark state absorption. Thus, further studies were done to understand the complete picture of modulation including conditions effecting the protonation of the chromophore pocket. The pH dependence of modulation suggested that protonation plays a role in natural photophysical off time of all

proteins. However, the deuterated solvent dependence supports an ESPT associated with the back reversion of the transient dark to the ground state. This informs the proposed modulation mechanism that is the result of coupled cis/trans isomerization and protonation of surrounding amino acids. In this system, fluorescent proteins capable of modulation have a transiently trans isomer that is stabilized by the hydrogen bond network increasing the barrier of reversion. Knowledge of this proposed mechanism allows for the manipulation of the dark state to engineer better and more specific proteins of modulation.

CHAPTER 6

PHOTOSWITCHABLE PROTEINS IN DUAL MODULATION

Fluorescent proteins have become indispensable tools in fluorescent imaging. With the discovery of photoswitchable fluorescent proteins, imaging modalities expanded into applications to investigate subcellular organization and dynamics. These phototransformable proteins allow repeated switching between a fluorescent and a non-fluorescent state in response to specific wavelengths of light, resulting in processes known as photoactivation, photoconversion, or photoswitching. As discussed in the Introduction, these proteins have led to advancements in spatial resolution and imaging contrast. Of particular interest to this fluorescent protein research is the photoswitchable protein Dronpa and similar variants. The photophysics and imaging applications of these particular photoswitchable proteins are investigated.

6.1 Introduction

Dronpa, a 28.8 kDa monomer, is 76% similar in sequence to GFP and shares a similar structure with an 11 stranded β-barrel.[127] Dronpa exhibits an absorption maximum at 503 nm (arising from the anionic, deprotonated chromophore) with a minor peak at 392 nm (from the neutral, protonated chromophore).[123,124] The anionic chromophore emits green fluorescence with a maximum at ~520 nm and has a brightness level almost 2.5 times that of EGFP.[119] Dronpa photoswitching occurs in part by interconversion between the deprotonated (on state; bright) and protonated (off state; dark) forms.[118,120] Illumination at 488 nm drives Dronpa to the dark species after which the fluorescent protein can be subsequently switched back on by brief illumination at 405nm (Figure 6.1). The primary

mechanism of fluorescent protein photoswitching is thought to arise from *cis-trans* isomerization of the tyrosine-chromophore moiety that accompanies the changes in the protonation state and this cycle can be repeated several hundred times.

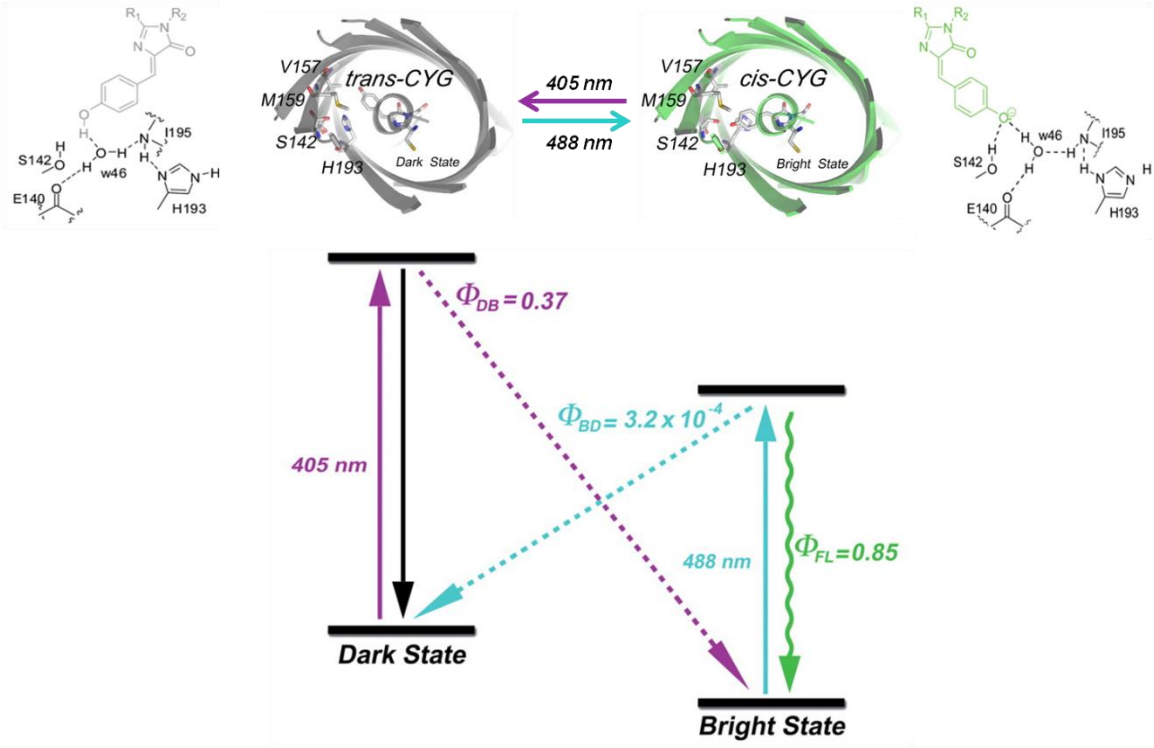

Figure 6.1 Schematic of reversible photoswitching of Dronpa adapted from Sample et al. and Kao et al.[200,201] Upon irradiation at 405 and 488 nm, Dronpa switches between dark and bright states (grey and green, respectively). The tyrosine chromophore adapts *cis* (bright) and *trans* (dark) configurations coupled with protonation/deprotonation of the phenol moiety.

Photoswitchable proteins are characterized by a number of factors including reversibility, mode of switching, and switching times. Of the reversible proteins, many are characterized by a 'negative' mode of switching indicating that irradiation of the protein with blue light not only excites the fluorescence, but also converts the proteins from the fluorescent on-state to the nonfluorescent off-state.[118,125,202] Dronpa, a reversibly

photoswitchable fluorescent protein with negative mode switching, has a switch-off half-time (488 nm irradiation) of several seconds. However, several variants of Dronpa with faster switching times, reversed photoswitching properties, and broader spectra have been reported.[118] Table 6.1 lists some examples of these proteins and their photophysical properties reported from the literature. While Dronpa is currently the most widely studied and used for most cell biology applications, alterations to Dronpa have been done to generate new proteins with different switching properties. Dronpa-2 and rsFastLime, which contain mutations to the 159 and 157 position, respectively, have significantly reduced switch-off half-times compared to Dronpa; thus, accelerating the switching kinetics of these proteins.[118] bsDronpa, also with mutations to the 157 and 159 positions, exhibited a broad asymmetric absorption spectrum that was shifted to a shorter wavelength.

Table 6.1 Photophysical characteristics of negative-mode, reversibly photoswitchable green fluorescent proteins investigated.

Protein	Mutations	Abs. Max On/Off (nm)	Em. Max (nm)	488/405 switching $t_{1/2}$	Ref.
Dronpa		503/392	522	115 s/0.12 s	[119]
Dronpa-2	Dronpa-M159T/E218G	489/396	515	0.23 s/0.05 s	[118]
rsFastLime	Dronpa-V157G	496/384	518	2.6 s/0.03 s	[119]
rsEGFP	EGFP-Q69L/V150A/V163S/S205N/A206K	489/396	504	1 ms/< 20 μs	[141]

These different photophysical properties allow for many different applications based on experimental constraints. Commonly combined with super-resolution techniques, multiple groups have reported sub-diffraction-limited spatial resolution of

cellular structures in the literature.[14,16,18,35,62,149] Additionally, Dronpa and other photoswitches have been useful in optical imaging. Using optical lock-in detection (OLID), Marriott et al. have demonstrated a 20-fold improvement of Dronpa signal over background.[17] Unfortunately, some of the disadvantages of photoswitchable proteins still exist in imaging. The first is that two higher energy lasers are required in most techniques for switching. The second is the need for a background-free environment. In super-resolution, most samples must be free of obscuring background to ensure fluorescent signal can be detected from the limited number of switched proteins. In OLID, while samples themselves do not have to be background-free, a pure reference dye must be placed in a background-free area to get the model waveform. In this chapter, some of these imaging issues are addressed by introducing a dual optical modulation methodology. In addition to the modulation of the secondary laser, the primary laser (the one responsible for fluorescence) is also modulated, and the technique is deemed dual modulation.

6.2 One Laser versus Two Laser Switching

The normal switching control for negative-mode switching fluorescent proteins is 405 nm laser irradiation to prime the fluorescent on-state, and 488 nm laser irradiation to induce fluorescence and switch the protein back to the dark, non-fluorescent state. With constant 488 nm illumination the photoswitchable protein will eventually become dark; thus, in most experimental setups the 405 nm laser is switched on, or pulsed, to switch it back. The number of switching occurrences is not unlimited; eventually the protein will become either photobleached or irreversibly damaged. However, constant, weak 488 nm illumination combined with switching the 405 nm at a specific frequency will result in fluorescent time traces that mirror the waveform used for 405 nm switching. This is

demonstrated in Figure 6.2A, which shows the switching of Dronpa-2 with 488 nm (50 W/cm^2 intensity) and 405 nm (900 W/cm^2 intensity) modulated a 1 Hz. Fourier transform of the time traces shows a 1 Hz signal of the Dronpa-2 switching (Figure 6.2 B). However, at the same intensities and frequencies, cells not transfected with a photoswitchable protein also produced a 1 Hz signal from endogenous fluorophore background (Figure 6.2 C). Thus, an imaging modality based on image reconstruction using the Fourier transform signal from only 405 nm modulation frequency will have problems with signal to background contrast.

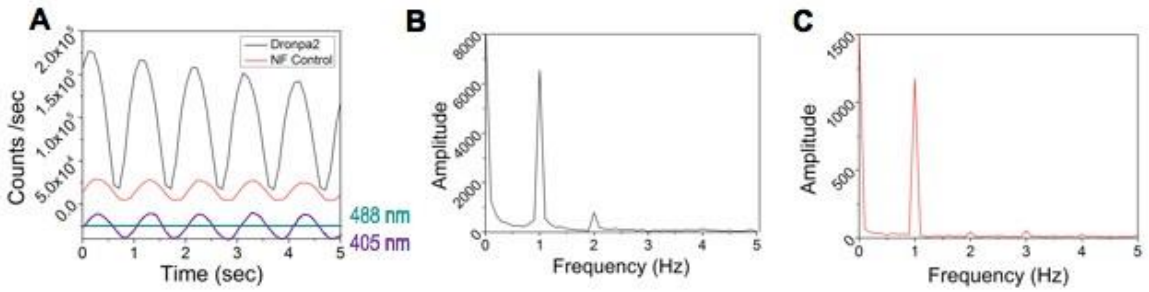

Figure 6.2 Photoinduced switching of Dronpa-2 in fixed NIH 3T3 cells with 1 laser. (A) Fluorescent time traces Dronpa-2 (black) and non-fluorescent NIH 3T3 cells (red). The bottom graphic represents the switching pattern used. Dark cyan represents the constant 488 nm illumination and purple represents the applied 405 nm 1 Hz sine wave. (B) Fourier transform of Dronpa-2 time trace and (C) non-fluorescent control cells shown in (A).

In an attempt to overcome this, the modulation technique was modified so that the photoswitchable protein displays a unique signal after Fourier transform of the time trace. In long-wavelength modulation, the second laser, which is responsible for the increased enhancement, is of longer wavelength than emission; however, in the case of the photoswitchable proteins the "secondary" laser (405 nm) is the laser responsible for creating the fluorescent state. Thus, the 488 nm laser, which is responsible for the

fluorescent signal, becomes the “primary” laser. By modulating both the secondary and primary lasers, the resulting Fourier transform of the photoswitchable protein will display both the fundamentals of each laser frequency but also additional sidebands at the sum and difference frequencies. Since this signal is unique to only the protein, the cellular background will show the fundamental frequencies but not the sum and difference frequencies. In the Dronpa-2 1 laser example, only the 405 nm laser is modulated resulting in one waveform imprinted on the time trace. However, in the 2 laser modulation case there are two frequencies. As seen in Figure 6.3, the secondary laser is modulated at 2 Hz and the primary laser is modulated at another frequency, 25 Hz. After Fourier transform of the signals both Dronpa-2 and the non-fluorescent control have the 2 Hz and 25 Hz peaks (Figure 6.3 B and C). However, only Dronpa-2 Fourier transform has the sidebands of 23 Hz and 27 Hz (Figure 6.3 D).

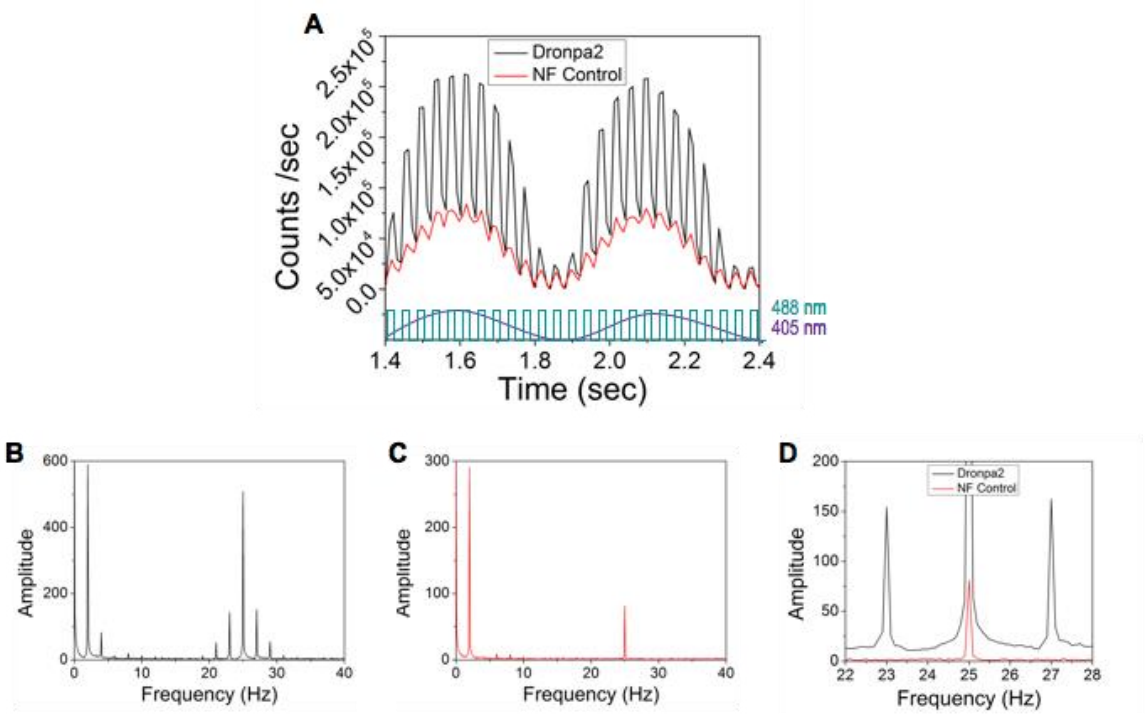

Figure 6.3 Dual modulation switching of Dronpa-2 in fixed NIH 3T3 cells. (A) Fluorescent time traces Dronpa-2 (black) and non-fluorescent NIH 3T3 cells (red). The bottom graphic represents the switching pattern used. Dark cyan represents the 488 nm illumination at 25 Hz and purple represents the 405 nm 2 Hz sine wave applied. (B) Fourier transform of Dronpa-2 time trace and (C) non-fluorescent control cells shown in (A). (D) The overlay of (B) with 10 offset and (C) to showcase the lack of peaks at 23 Hz and 27 Hz in non-fluorescent control cells.

To this point, the examples shown have been of Dronpa-2; however, other photoswitchable variants (e.g., rsFastLime and rsEGFP) also exhibited this sideband characteristic, though the magnitude of the effect differs for each protein. To compare the proteins, the intensities of the 488 nm and 405 nm were held constant and the two lasers are modulated at relatively low modulation frequencies. The enhancement of each protein was calculated as described in the Experimental section (2.7).

Table 6.2 Dual Modulation Enhancement of Photoswitchable Proteins.

Protein	Enhancement (%)
Dronpa-2	25
rsFastLime	10
rsEGFP	10

6.3 Controlling Optical Switching

As seen in Table 6.1, each photoswitchable variant has an inherent off switching and on switching half-time associated with the particular protein. As previously noted, the chromophore environment controls the kinetic switching observed. The times reported in Table 6.1 are the intensity dependent lifetimes taken from a high intensity pulse of the 405 nm laser and then low illumination with 488 nm light. However, actual values are intensity dependent and result in inconsistent values depending on intensities and methods used. To avoid inconsistencies in comparing variants with dual modulation, the frequency response of the individual proteins under the same intensities was taken. Understanding the photophysics and response times of each protein is important to understanding the dynamics and applications the photoswitchable proteins can investigate.

Similar to long-wavelength modulation, the characteristic frequency of a protein has proven useful in understanding its photophysics and possible applications. Thus, the first experiment was to ascertain the characteristic frequency for the photoswitchable proteins that exhibited the sideband effect. Holding the 488 nm frequency constant and with the intensity at 500 W/cm^2, the frequency of the secondary 405 nm laser (900 W/cm^2) was scanned and the enhancement at each frequency was plotted. As the primary frequency can also affect the amplitude of the sidebands, this was repeated with other 488 nm frequencies (Figure 6.4). In general, for all the proteins tested the characteristic frequencies recorded were all below 100 Hz. Dronpa-2 exhibited the fastest characteristic frequency

of ~30 Hz. rsEGFP and rsFastLime had lower characteristic frequencies ~5 Hz. This information becomes the first step for understanding the limitations of the dual modulation for imaging purposes. However, the 488 nm intensity dependence was also important to investigate.

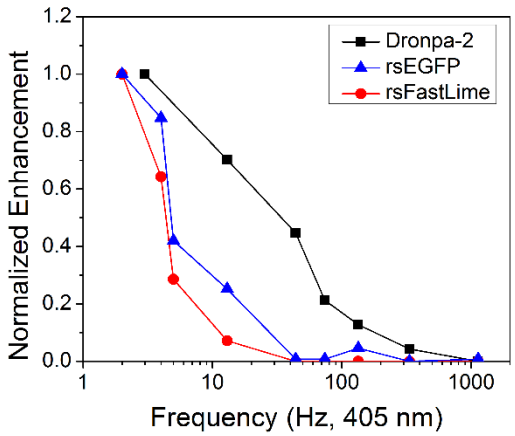

Figure 6.4 Frequency dependence of photoswitchable proteins. The 488 nm intensity is fixed at 360 W/cm^2 (43Hz) and the 405 nm frequency is varied (900 W/cm^2).

Thus, it became apparent that in order to understand the photoswitchable protein photophysics it is more important to change the 488 nm intensity at constant 488 nm frequency. At a fixed 43 Hz modulation of the 488 nm laser, the intensity is varied over an order of magnitude and the 405 nm laser frequency is scanned (Figure 6.5). At higher 488 nm intensity, the signal from the photoswitchable protein is stronger, as reflected in larger amplitude of the sidebands. Thus, the maximum enhancement recorded is larger. While the 488 nm intensity dependence is very prominent with Dronpa-2 and rsEGFP, the intensity dependence is less noticeable with rsFastLime.

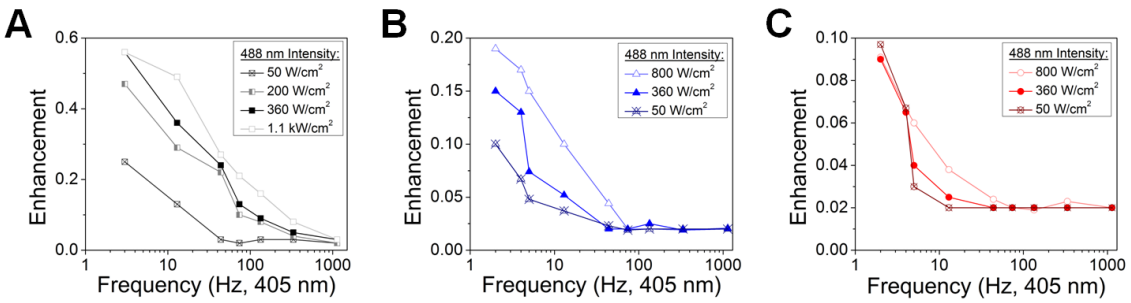

Figure 6.5 Intensity dependent frequency response of photoswitchable proteins. The 405 nm intensity is fixed at 900 W/cm^2 and the frequency varied for (A) Dronpa-2, (B) rsEGFP, and (C) rsFastLime.

6.4 Dual Modulation Imaging

As shown in Section 6.2 of this chapter, the advantage of dual modulation is the selective modulation of the photoswitchable protein over endogenous (or non-modulatable exogenous) background. In contrast to the reference dye used with OLID cross-correlation, the sum/difference sidebands arising from this make reconstruction of an image possible using only the amplitude of one of the sidebands frequencies. We demonstrated this advantage with NIH-3T3 cells transfected with rsFastLime localized to the mitochondria. In the case of 405 nm laser modulation only, the 488 nm laser is held at a constant 50 W/cm^2 and a total of 1200 frames were collected on a CCD with a frame rate of 90 frames/sec. When the image of the average fluorescence per pixel is displayed, the resulting image showed not only rsFastLime-mito but also other endogenous fluorophores present in the cell (Figure 6.6 A). Upon Fourier transform of each pixel in the time series, an image was reconstructed based on the amplitude of the 2 Hz signal (Figure 6.6 C). Though an image can be made, the signal improvement of the demodulated image was not improved from the raw fluorescence image. Alternatively, a model time trace (Figure 6.6 B, inset) can be used to correlate to each pixel in the image series (Figure 6.6 D). In this

OLID-like image reconstruction, the signal improvement of rsFastLime signal to background is ~5:1.

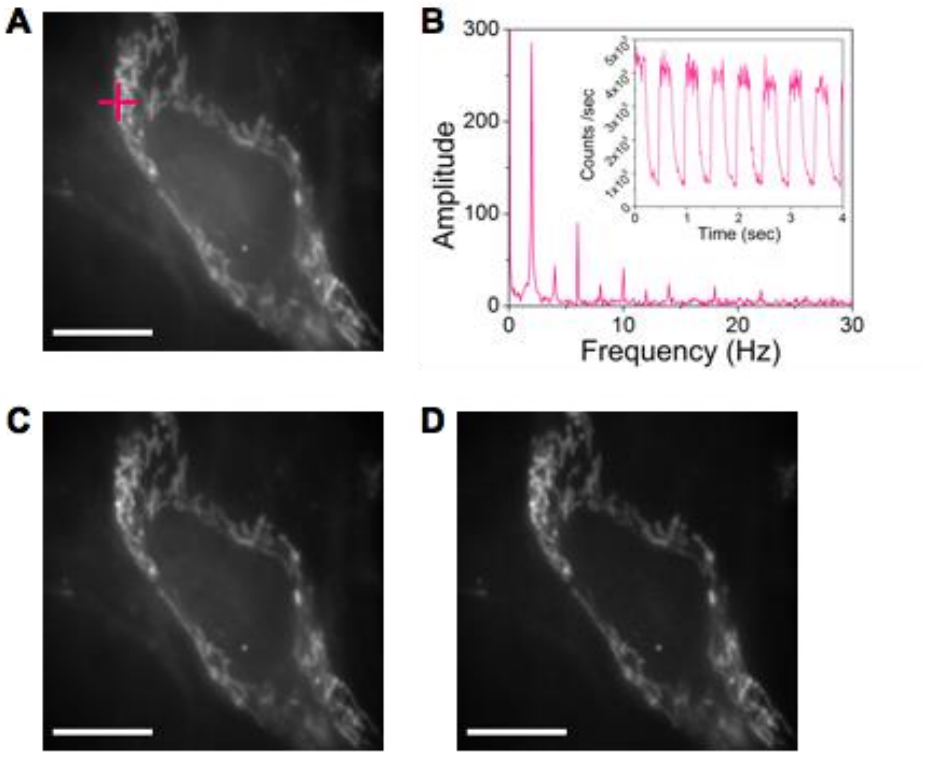

Figure 6.6 OLID-like image reconstruction of rsFastLime-mitochondria with one laser modulation. (A) Average fluorescence image of all frames in the time series. (B) Fourier transform of pixel at pink point, inset: time trace at the same spot. (C) Image plotting amplitude of the 2 Hz signal in FT. (D) Correlation amplitude when correlated with the time trace of B inset. Scale bar: 15 μm.

Our dual modulation method does not rely on finding a model waveform with good signal to background. Instead, the data was collected the same as in single laser modulation and the only additional requirement is the external modulation of both lasers. The raw fluorescence image of the average fluorescence intensity per pixel was similar to that seen in the one laser case (Figure 6.7 A). However, upon Fourier transform of each pixel in the time series, the pixels with rsFastLime-mito now displayed the fundamental frequency of

the two lasers, but also the sidebands (Figure 6.7 B). By plotting the amplitude at one of the sideband frequencies (15 Hz) a clearer image of rsFastLime-mito was revealed (Figure 6.7 C). This post-processing takes minimal time and results in a signal to background improvement of ~6-fold (using only one sideband), the same or more than achieved with the OLID-like correlation. However, the addition of both sidebands together would likely achieve a √2 improvement beyond this. Also, the images recreated here are limited to only the autofluorescent background generated. More significant background from a similar emitting background would result in even better signal to background improvement using dual modulation versus using OLID-like correlation.

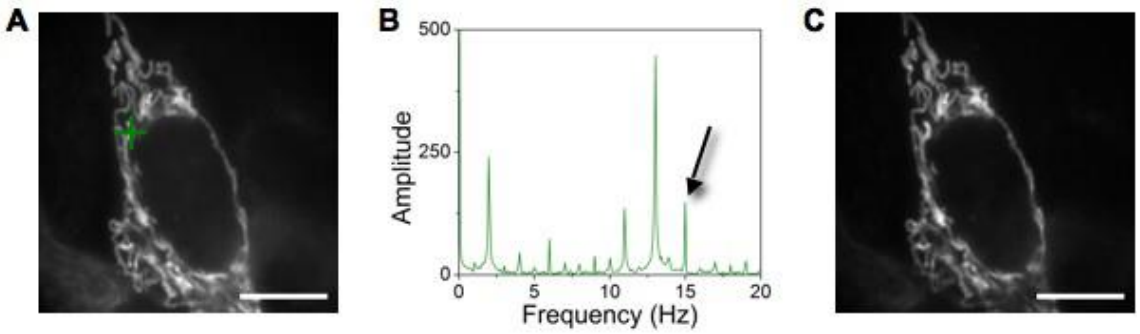

Figure 6.7 Image reconstruction of rsFastLime-mitochondria with two laser modulation. (A) Average fluorescence image of all frames in the time series. (B) Fourier transform of pixel at green point. (C) Image plotting amplitude of the 15 Hz signal in FT as pointed out with black arrow. Scale bar: 15 μm.

6.5 Future Applications of Dual Modulation

While the advantages of dual modulation in imaging have been shown, the possibility for applications is abundant. As seen in Section 6.3, the switching of particular proteins can be controlled with the 488 nm intensity. This allows the protein to be tailored to a particular application depending on the dynamics being investigated. Dual modulation

can benefit fluorescence imaging two ways: improved contrast imaging and sensitive detection of slow dynamics such as protein binding. As seen previously in this chapter, dual modulation can be used in imaging. The use of high primary intensity results in larger sideband height, leading to better enhancement. Images with high heterogenous background can show greater improved contrast in this case.

Another application in which the slow dynamics of the photoswitchable proteins is useful is in the discrimination of immobilized and diffusing populations. In a diffraction-limited spot, the residence time of a diffusing protein is limited to ~1 millisecond. A slow switching fluorescent protein must reside in the focal spot for a relatively long period of time in order to be affected by both slow modulating lasers. Freely diffusing proteins will move through before the protein can have this effect. However, proteins that are immobilized or limited in movement will reside long enough to have an effect. Thus, in cells of diffusing rsFastLime, the resulting Fourier transform will display no sidebands. Cells with rsFastLime immobilized in the mitochondria, the lasers adequately switch the protein to create desired sidebands (Figure 6.8).

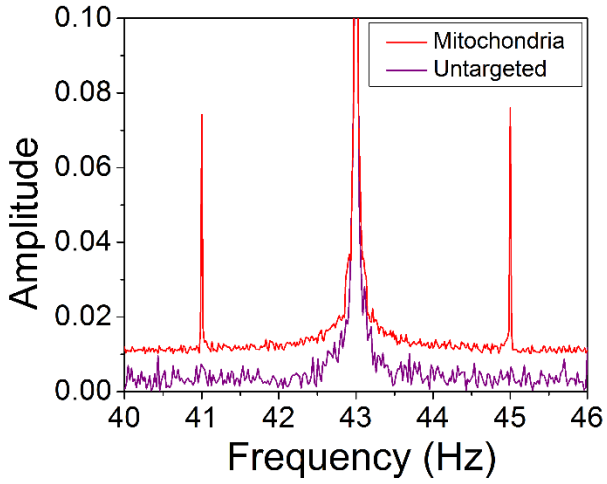

Figure 6.8 Fourier transform of rsFastLime freely diffusing (purple) or targeted to the mitochondria (red). The 488 nm intensity is 50 W/cm^2 and the 405 nm intensity is 900 W/cm^2.

6.6 Conclusions

Reversible photoswitchable proteins have been used extensively in super-resolution imaging. However, the utility of these proteins in other imaging modalities has been quite limited. The use of two higher energy lasers for switching leads to problems with the autofluorescent background in cellular imaging. Our lab has approached these problems with using two modulated higher energy lasers. Investigation of the Dronpa variant photophysical properties reveals slow characteristic frequencies which are consistent with the long timescales previously reported. The main advantage of the dual modulation technique in cellular imaging is the suppression of heterogeneous autofluorescent background. Unlike other similar techniques, dual modulation does not need an internal, background-free reference. Reconstruction of the modulation image takes minimal time and results in signal to background improvement similar to correlation techniques. However, additional work needs to be done to completely understand the photophysical parameters. Additonally, proof-of-principle work has been done with using rsFastLime in

distinguishing diffusing and immobilized populations. However, attempts to image the two populations in a single cell have been unsuccessful. Though imaging techniques such as total internal reflection limit the imaging dimension in the z-direction, the motion in x and y dimensions still result in sidebands from diffusing protein. There are specific biological questions that can be answered through using diffraction limited spot and the dual modulation, but they have yet to be investigated.

CHAPTER 7

CONCLUSIONS AND OUTLOOK

Fluorescence microscopy in cellular imaging has become an essential tool for the investigation of subcellular locations and dynamics. While many fluorophores have been created to visualize targets of interest, the minimally invasive, biocompatible fluorescent proteins have become the preferred fluorophores for many cellular applications. Fluorescent proteins have been developed with a broad range of fluorescence emission spectral profiles covering most of the visible light spectrum. However, despite these advantages, fluorescent protein use is still limited in some applications. Firstly, cellular imaging is messy and full of inherent background fluorescence and although work has been done to brighten or change the spectrum to less absorbing wavelength low population levels in the cell suffer from sensitivity issues in the background. Additionally, most multi-label schemes depend on the spectral discrimination between fluorescent proteins limiting the number of fluorescently labeled targets at one time. The expansion of optical modulation to fluorescent proteins to increase sensitivity and dimension in imaging would make great strides in overcoming these disadvantages and aiding understudied cellular dynamics.

While previous reports of modulation with nanoparticles and dyes, this is the first demonstration of optical modulation of fluorescent proteins for the purpose of imaging. We have demonstrated that a number of proteins across the spectrum experience an increase of fluorescence with second long-wavelength excitation; however, not all proteins do. We have elucidated the photophysical characteristic parameters that point to a ~millisecond timescale. Additionally, modulate the signal to dynamically shift the signal

of interest away for total fluorescence and that extracting this signal increases sensitivity not only in autofluorescent background, but up to 20-fold in the presence of high, heterogeneous background. The sensitivities of the chromophore environment to structural and sometimes solvent conditions allows for the study of possible mechanisms which likely involve a cis/trans coupled to a protonation/deprotonation.

An alternative approach to high sensitivity of a target protein over background is change the technology to extract an even better signal. Modulating both lasers shifts the extracted signal away from background and only specific protein of interest is seen. Extremely advantageous in the case of normal photoswitches that utilize two higher energy lasers, we have demonstrated improved sensitivity in imaging relative to traditional ways. Additionally, we have shown that this method can be used to control the timescales of switching to tailor to specific applications. Harnessing these advantages in better imaging technologies allows for difficult cellular system, such as low-copy number concentration of proteins or weak transient interactions, to be studied in vivo.

Fluorescent proteins coupled with this technology is in its infancy and require more development and understanding to truly outweigh the traditional approaches to imaging. While the modulatable proteins is nice, the reported modulation depths are still significantly less than reported in engineered nanoparticles and organic dyes. Additionally, the approximately one millisecond timescale for modulation limits the speed of imaging for looking at fast dynamics. These can be addressed in protein engineering. In order to do so, better understanding of the mechanism is needed. The results reported here strongly agree with the proposed mechanism; however, more traditional techniques lack in the ability to investigate this transient state. X-ray crystallography need longer lived or

permanent states such as studied with photoswitches. Transient absorption lacks time resolution to one millisecond and detection of low quantum yield dark states. Evolving technologies could eventually come to light, such as computational methods to help.

Despite this, the groundwork has been laid for great potential in cellular imaging. This project has the potential to expand in two directions. One being the improvement of modulatable fluorescent proteins and the other being the study of cellular applications that would benefit from this. The potential for even greater sensitivity improvement provides motivation for proteins established for modulation depth and characteristic frequency, thereby greatly expanding signal recovery in multiple applications. Additionally, long-wavelength modulation expands the dimensionality to discriminate FP emitters based on dark state lifetimes. This would allow for similarly emitting modulatable proteins to be selectively modulated by varying the modulation frequency, thus inherently offering an additional dimension for multispectral imaging. Taking advantage of the technology can be expanding the biological understanding. Weak interactions that need to restrict the information or low copy number that are hard to see. Have great potential for helping these systems.

APPENDIX A

OPTICAL MODULATION OF NON-TYROSINE CHROMOPHORE PROTEINS: CYAN FLUORESCENT PROTEINS

A.1 Introduction

While many spectral shifts have been effected through tuning the tyrosine chromophore environment, other approaches have altered the chromophore. Cyan fluorescent proteins are created from replacement of the tyrosine 66 (Y66) with a tryptophan (W66) leading to an absorption maximum of 436 nm and broad emission centered at 485 nm.[86] Further mutations incorporating the F64L and S65T that improved WT-GFP resulted in the production of an enhanced version (ECFP) with greater brightness and photostability.[104,203] The most successful applications using ECFP have been coupling it with yellow fluorescent protein (YFP) and derivatives to generate FRET biosensors capable of monitoring a wide spectrum of intracellular processes.[160,204,205] Among the improved cyan fluorescent proteins, CyPet[55] and an enhanced cyan variant termed Cerulean[103] show the most promise as fusion tags, FRET biosensors, and for multicolor imaging. The Cerulean fluorescent probe was engineered by site-directed mutagenesis of enhanced cyan fluorescent protein to yield a higher extinction coefficient, improved quantum yield, and a fluorescence lifetime decay having a single exponential component for better FLIM-FRET measurements.[101-103,189]

The frequently used fluorescent proteins for FRET experiments (ECFP, EGFP, EYFP, and Citrine) are all susceptible to reversible photobleaching leading to the generation of a nonfluorescent species, which recovers spontaneously or through

illumination.[134,196,206] These processes may cause significant artifacts in a number of commonly applied quantitative imaging techniques. Sinnecker et al. documented a dynamic equilibrium between reversible photobleaching, spontaneous recovery and light-induced recovery.[206] Of particular interest to this work was the co-illumination of ECFP cells with 430 nm and 500 nm light that resulted in a partial recovery of the fluorescence intensity.

A.2 Modulation of Cyan Fluorescent Proteins

As with the survey of proteins investigated in Chapter 5, ECFP, mCerulean, and CyPet were transfected into NIH 3T3 cells and studied for long-wavelength modulation before purification. The expressing cells were excited with a primary 405 nm diode and a secondary 514 nm Ar^+ laser collecting fluorescence 430-474 nm. Initial studies with 500 W/cm^2 405 nm and 35 kW/cm^2 514 nm showed ~5-8% enhancement for all tested CFPs validating the observed reports of Sinnecker et al.[206] As with many of the proteins in this thesis, Irina Isseava of the Fahrni group purified ECFP and mCerulean for further studies of absolute enhancement and characteristic frequency. However, studies of ECFP and mCerulean in PBS (pH 7.4) showed no enhancement at 480 W/cm^2 405 nm and 26 kW/cm^2 514 nm (similar intensities used for enhancement in cells). As Sinnecker et al. performed these experiments in cells equilibrated at pH 5.5[206] and our fixation method may also lower the pH of the protein environment, ECFP and mCerulean were diluted into acetate buffer at pH 5.4. At the same intensities used to investigate the proteins in PBS pH 7.4, ECFP showed ~20% enhancement at pH 5.4. This suggested a pH dependence of the modulation in CFPs. Thus, ECFP and mCerulean were diluted in a pH range of 4 to 8 (Section 2.2.3) and the enhancement was recorded. Enhancement at pH 4 was not recorded as there was

no fluorescence (at 405 nm excitation) after equilibrating in pH 4 buffer; however, all other pH dilutions showed a strong absorbance band at 433 nm with little shift in maximum.

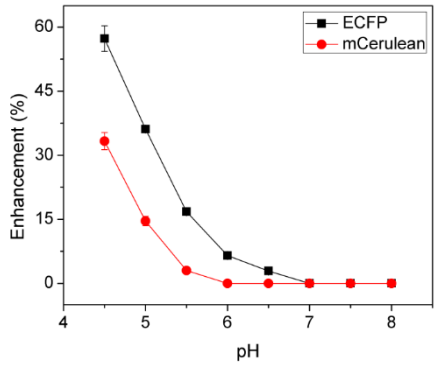

Figure A.1 Fluorescence normalized pH dependence of ECFP and mCerulean enhancement at 480 W/cm^2 (405 nm) and 26 kW/cm^2 (514 nm).

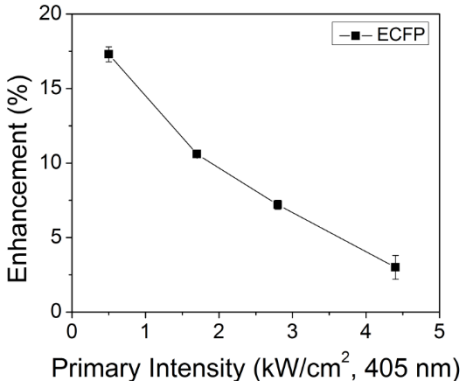

Figure A.2 Primary (405 nm) intensity dependence of ECFP enhancement at pH 5.5. Secondary is held at 30 kW/cm^2.

For both ECFP and mCerulean, enhancement is increased at low pH (Figure A.1). However, ECFP enhancement is gained at a higher pH (~pH 6.0) than mCerulean enhancement (~pH 5.4). Interestingly, as seen in Figure A.2, the power dependence of ECFP (at pH 5.5) reflects a similar trend to modBFP and variants (Section 3.4.1). The

modulation frequency dependence was also recorded for ECFP and mCerulean. Examination of the frequency response showed a slow response with the characteristic frequency ~100 Hz (Figure A.3). However, the response was not able to be fit to Equation 2.10 because of a shallow slope and plateau points lacking at low frequency. This suggests that a better model will need to be made to understand the true photophysics of modulation in cyan fluorescent proteins.

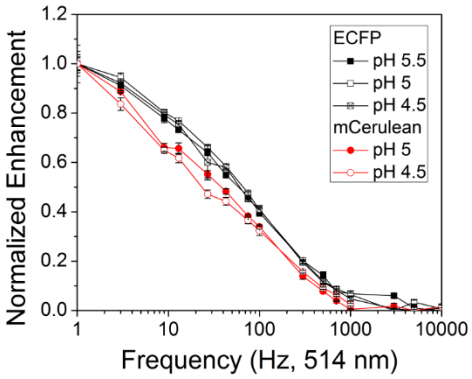

Figure A.3 Normalized modulation frequency dependence as a function of pH for ECFP (black) and mCerulean (red). Primary was 480 W/cm^2 and secondary was 30 kW/cm^2.

A.3 Comparison of ECFP and mCerulean

The difference in apparent pK_a of modulatable state between ECFP and mCerulean may lead to an understanding of modulation in fluorescent proteins. As the chromophore of CFPs, tryptophan, is not protonatable, the protonation state of the chromophore may not be as a factor in modulation. Though, as surrounding amino acids do have pK_a, the protonation of those amino acids and the immediate chromophore environment pK_a may change with pH. Using the crystal structures of ECFP and Cerulean,[101] an investigation of the structural difference and rearrangement of Cerulean compared to ECFP was done. A

major difference is the replacement of the histidine in the 148 position of ECFP to aspartic acid in Cerulean (H148D). Structural data suggests the H148D mutation results in a favored cis conformation in Cerulean likely triggering a switch in indole hydrogen-bonding partner from S205 in ECFP to D148 in Cerulean, at least in acidic media.[101] H148 was also an important point of mutation in modBFP (Section 3.4), conferring better modulation by destabilizing the cis configuration. Additionally, the difference in pK_a of histidine (pK_a = 6) and aspartic acid (pK_a = 3.65) could explain the pH dependence in ECFP and mCerulean. These factors point to a change in the chromophore environment that may explain the pH dependence between ECFP and mCerulean, but further studies are needed.

A.4 Conclusions and Future Outlook

The light-induced reversible photobleaching first reported by Sinnecker et al. was also seen in our results. However, modulation of ECFP and mCerulean could only be achieved at low pH and low primary intensity (< 5 kW/cm^2). The modulation of tryptophan chromophore proteins expands on the understanding of modulatable states in fluorescent proteins. The unprotonatable chromophore, but similar structure, may help predict key mutations for better modulation or more stable modulation across a pH range. Additionally, the pH dependence of modulation of CFPs can be developed as a sensor for in vivo experiments. Of interest may be FRET systems that need improved sensitivity. Our lab has shown the advantage of modulation in FRET systems previously,[207] this could be extended to protein FRET systems using the CFP-YFP partners such as calmodulin.[159,160,208] However, better models for photophysical determination is still needed to completely understand modulation in CFPs.

REFERENCES

[1] Lippincott-Schwartz, J.; Snapp, E.; Kenworthy, A. Studying protein dynamics in living cells. *Nat. Rev. Mol. Cell Biol.* **2001**, *2*, 444-456.

[2] Chudakov, D. M.; Matz, M. V.; Lukyanov, S.; Lukyanov, K. A. Fluorescent proteins and their applications in imaging living cells and tissues. *Physiol. Rev.* **2010**, *90*, 1103-1163.

[3] Day, R. N.; Schaufele, F. Fluorescent protein tools for studying protein dynamics in living cells: a review. *J. Biomed. Opt.* **2008**, *13*, 6.

[4] Chudakov, D. M.; Lukyanov, S.; Lukyanov, K. A. Fluorescent proteins as a toolkit for in vivo imaging. *Trends Biotechnol.* **2005**, *23*, 605-613.

[5] Giepmans, B. N. G.; Adams, S. R.; Ellisman, M. H.; Tsien, R. Y. Review - The fluorescent toolbox for assessing protein location and function. *Science* **2006**, *312*, 217-224.

[6] Newman, R. H.; Fosbrink, M. D.; Zhang, J. Genetically encodable fluorescent biosensors for tracking signaling dynamics in living cells. *Chem. Rev.* **2011**, *111*, 3614-3666.

[7] Rao, J.; Dragulescu-Andrasi, A.; Yao, H. Fluorescence imaging in vivo: recent advances. *Current Opinion in Biotechnology* **2007**, *18*, 17-25.

[8] Weissleder, R.; Ntziachristos, V. Shedding light onto live molecular targets. *Nat. Med.* **2003**, *9*, 123-128.

[9] Sako, Y.; Minoguchi, S.; Yanagida, T. Single-molecule imaging of EGFR signalling on the surface of living cells. *Nat. Cell Biol.* **2000**, *2*, 168-172.

[10] Wouters, F. S.; Verveer, P. J.; Bastiaens, P. I. H. Imaging biochemistry inside cells. *Trends Cell Biol.* **2001**, *11*, 203-211.

[11] Ibraheem, A.; Campbell, R. E. Designs and applications of fluorescent protein-based biosensors. *Curr. Opin. Chem. Biol.* **2010**, *14*, 30-36.

[12] Meyer, T.; Teruel, M. N. Fluorescence imaging of signaling networks. *Trends Cell Biol.* **2003**, *13*, 101-106.

[13] Nienhaus, G. U.; Wiedenmann, J. Structure, dynamics and optical properties of fluorescent proteins: Perspectives for marker development. *ChemPhysChem* **2009**, *10*, 1369-1379.

[14] Betzig, E.; Patterson, G. H.; Sougrat, R.; Lindwasser, O. W.; Olenych, S.; Bonifacino, J. S.; Davidson, M. W.; Lippincott-Schwartz, J.; Hess, H. F. Imaging intracellular fluorescent proteins at nanometer resolution. *Science* **2006**, *313*, 1642-1645.

[15] Dertinger, T.; Colyer, R.; Iyer, G.; Weiss, S.; Enderlein, J. Fast, background-free, 3D super-resolution optical fluctuation imaging (SOFI). *Proc. Natl. Acad. Sci. U. S. A.* **2009**, *106*, 22287-22292.

[16] Huang, B.; Bates, M.; Zhuang, X. W. In *Annu. Rev. Biochem.*; Annual Reviews: Palo Alto, 2009; Vol. 78, p 993-1016.

[17] Marriott, G.; Mao, S.; Sakata, T.; Ran, J.; Jackson, D. K.; Petchprayoon, C.; Gomez, T. J.; Warp, E.; Tulyathan, O.; Aaron, H. L.; Isacoff, E. Y.; Yan, Y. L. Optical lock-in detection imaging microscopy for contrast-enhanced imaging in living cells. *Proc. Natl. Acad. Sci. U. S. A.* **2008**, *105*, 17789-17794.

[18] Patterson, G.; Davidson, M.; Manley, S.; Lippincott-Schwartz, J. In *Annual Review of Physical Chemistry, Vol 61*; Leone, S. R., Cremer, P. S., Groves, J. T., Johnson, M. A., Richmond, G., Eds.; Annual Reviews: Palo Alto, 2010; Vol. 61, p 345-367.

[19] Richards, C. I.; Hsiang, J. C.; Dickson, R. M. Synchronously Amplified Fluorescence Image Recovery (SAFIRe). *J. Phys. Chem. B* **2010**, *114*, 660-665.

[20] Olenych, S. G.; Claxton, N. S.; Ottenberg, G. K.; Davidson, M. W. In *Current Protocols in Cell Biology*; John Wiley & Sons, Inc.: 2001.

[21] Crivat, G.; Taraska, J. W. Imaging proteins inside cells with fluorescent tags. *Trends Biotechnol.* **2012**, *30*, 8-16.

[22] Day, R. N.; Davidson, M. W. The fluorescent protein palette: tools for cellular imaging. *Chem. Soc. Rev.* **2009**, *38*, 2887-2921.

[23] Nienhaus, K.; Nienhaus, G. U. Fluorescent proteins for live-cell imaging with super-resolution. *Chem. Soc. Rev.* **2014**, *43*, 1088-1106.

[24] Shcherbakova, D. M.; Subach, O. M.; Verkhusha, V. V. Red fluorescent proteins: Advanced imaging applications and future design. *Angew. Chem.-Int. Edit.* **2012**, *51*, 10724-10738.

[25] Jayaraman, S.; Haggie, P.; Wachter, R. M.; Remington, S. J.; Verkman, A. S. Mechanism and cellular applications of a green fluorescent protein-based halide sensor. *J. Biol. Chem.* **2000**, *275*, 6047-6050.

[26] McAnaney, T. B.; Park, E. S.; Hanson, G. T.; Remington, S. J.; Boxer, S. G. Green fluorescent protein variants as ratiometric dual emission pH sensors. 2. Excited-state dynamics. *Biochemistry* **2002**, *41*, 15489-15494.

[27] Baudendistel, N.; Muller, G.; Waldeck, W.; Angel, P.; Langowski, J. Two-hybrid fluorescence cross-correlation spectroscopy detects protein-protein interactions in vivo. *ChemPhysChem* **2005**, *6*, 984-990.

[28] Kenworthy, A. K. Imaging protein-protein interactions using fluorescence resonance energy transfer microscopy. *Methods* **2001**, *24*, 289-296.

[29] Oyama, R.; Takashima, H.; Yonezawa, M.; Doi, N.; Miyamoto-Sato, E.; Kinjo, M.; Yanagawa, H. Protein-protein interaction analysis by C-terminally specific fluorescence labeling and fluorescence cross-correlation spectroscopy. *Nucleic Acids Res.* **2006**, *34*, 8.

[30] Campbell, R. E.; Tour, O.; Palmer, A. E.; Steinbach, P. A.; Baird, G. S.; Zacharias, D. A.; Tsien, R. Y. A monomeric red fluorescent protein. *Proc. Natl. Acad. Sci. U. S. A.* **2002**, *99*, 7877-7882.

[31] Jach, G.; Pesch, M.; Richter, K.; Frings, S.; Uhrig, J. F. An improved mRFP1 adds red to bimolecular fluorescence complementation. *Nat. Methods* **2006**, *3*, 597-600.

[32] Shaner, N. C.; Campbell, R. E.; Steinbach, P. A.; Giepmans, B. N. G.; Palmer, A. E.; Tsien, R. Y. Improved monomeric red, orange and yellow fluorescent proteins derived from Discosoma sp red fluorescent protein. *Nat. Biotechnol.* **2004**, *22*, 1567-1572.

[33] Shu, X. K.; Shaner, N. C.; Yarbrough, C. A.; Tsien, R. Y.; Remington, S. J. Novel chromophores and buried charges control color in mFruits. *Biochemistry* **2006**, *45*, 9639-9647.

[34] Hofmann, M.; Eggeling, C.; Jakobs, S.; Hell, S. W. Breaking the diffraction barrier in fluorescence microscopy at low light intensities by using reversibly photoswitchable proteins. *Proc. Natl. Acad. Sci. U. S. A.* **2005**, *102*, 17565-17569.

[35] Rust, M. J.; Bates, M.; Zhuang, X. W. Sub-diffraction-limit imaging by stochastic optical reconstruction microscopy (STORM). *Nat. Methods* **2006**, *3*, 793-795.

[36] Shaner, N. C.; Patterson, G. H.; Davidson, M. W. Advances in fluorescent protein technology. *J. Cell Sci.* **2007**, *120*, 4247-4260.

[37] Richards, C. I.; Hsiang, J. C.; Senapati, D.; Patel, S.; Yu, J. H.; Vosch, T.; Dickson, R. M. Optically modulated fluorophores for selective fluorescence signal recovery. *J. Am. Chem. Soc.* **2009**, *131*, 4619-4621.

[38] Gest, H. The discovery of microorganisms by Robert Hooke and Antoni van Leeuwenhoek, fellows of the Royal Society. *Notes and Records of the Royal Society* **2004**, *58*, 187-201.

[39] Hooke, R. *Micrographia; or, some physiological descriptions of minute bodies made by magnifying glasses. with observations and inquiries thereupon. by r. hooke*; Bruxelles, Culture et Civilisation, 1966., 1966.

[40] *Optical microscopy : emerging methods and applications*; Herman, B.; Lemasters, J. J., Eds.; Academic Press, Inc.: San Diego, CA., 1993.

[41] Rost, F. W. D. *Fluorescence microscopy*; Cambridge University Press: Cambridge, UK, 1992; Vol. 2.

[42] Valeur, B.; Berberan-Santos, M. N. *Molecular fluorescence : principles and applications*; 2nd ed. ed.; Wiley-VCH: Weinheim Germany, 2012.

[43] Lakowicz, J. R. *Principles of fluorescence spectroscopy*; 3rd ed. ed.; New York: Springer, 2006.

[44] Herman, B. *Fluorescence microscopy*; 2nd ed. ed.; BIOS Scientific Publishers: New York: Oxford, UK, 1998.

[45] Masters, B. R. *Confocal microscopy and multiphoton excitation microscopy : the genesis of live cell imaging*; SPIE Press: Bellingham, Washington, 2005.

[46] Mertz, J. *Introduction to optical microscopy*; Roberts and Company Publishers: Greenwood Village, Colorado, 2010.

[47] Denk, W.; Strickler, J. H.; Webb, W. W. 2-Photon laser scanning fluorescence microscopy. *Science* **1990**, *248*, 73-76.

[48] Schwille, P. Fluorescence correlation spectroscopy and its potential for intracellular applications. *Cell Biochem. Biophys.* **2001**, *34*, 383-408.

[49] Fitzpatrick, J. A. J.; Lillemeier, B. F. Fluorescence correlation spectroscopy: linking molecular dynamics to biological function in vitro and in situ. *Curr. Opin. Struct. Biol.* **2011**, *21*, 650-660.

[50] Haupts, U.; Maiti, S.; Schwille, P.; Webb, W. W. Dynamics of fluorescence fluctuations in green fluorescent protein observed by fluorescence correlation spectroscopy. *Proc. Natl. Acad. Sci. U. S. A.* **1998**, *95*, 13573-13578.

[51] Heikal, A. A.; Hess, S. T.; Baird, G. S.; Tsien, R. Y.; Webb, W. W. Molecular spectroscopy and dynamics of intrinsically fluorescent proteins: Coral red (dsRed) and yellow (Citrine). *Proc. Natl. Acad. Sci. U. S. A.* **2000**, *97*, 11996-12001.

[52] Schenk, A.; Ivanchenko, S.; Rocker, C.; Wiedenmann, J. R.; Nienhaus, G. U. Photodynamics of red fluorescent proteins studied by fluorescence correlation spectroscopy. *Biophys. J.* **2004**, *86*, 384-394.

[53] Widengren, J.; Terry, B.; Rigler, R. Protonation kinetics of GFP and FITC investigated by FCS - aspects of the use of fluorescent indicators for measuring pH. *Chem. Phys.* **1999**, *249*, 259-271.

[54] Foo, Y.; Korzh, V.; Wohland, T. In *Fluorescent Proteins II*; Jung, G., Ed.; Springer Berlin Heidelberg: 2012; Vol. 12, p 213-248.

[55] Nguyen, A. W.; Daugherty, P. S. Evolutionary optimization of fluorescent proteins for intracellular FRET. *Nat. Biotechnol.* **2005**, *23*, 355-360.

[56] Piston, D. W.; Kremers, G. J. Fluorescent protein FRET: the good, the bad and the ugly. *Trends Biochem.Sci.* **2007**, *32*, 407-414.

[57] Mattheyses, A. L.; Axelrod, D. Direct measurement of the evanescent field profile produced by objective-based total internal reflection fluorescence. *J. Biomed. Opt.* **2006**, *11*, 7.

[58] Toomre, D.; Manstein, D. J. Lighting up the cell surface with evanescent wave microscopy. *Trends Cell Biol.* **2001**, *11*, 298-303.

[59] Brandenburg, B.; Zhuang, X. W. Virus trafficking - learning from single-virus tracking. *Nat. Rev. Microbiol.* **2007**, *5*, 197-208.

[60] Thompson, N. L.; Steele, B. L. Total internal reflection with fluorescence correlation spectroscopy. *Nat. Protoc.* **2007**, *2*, 878-890.

[61] Bates, M.; Huang, B.; Dempsey, G. T.; Zhuang, X. W. Multicolor super-resolution imaging with photo-switchable fluorescent probes. *Science* **2007**, *317*, 1749-1753.

[62] Lippincott-Schwartz, J.; Patterson, G. H. Photoactivatable fluorescent proteins for diffraction-limited and super-resolution imaging. *Trends Cell Biol.* **2009**, *19*, 555-565.

[63] Mao, S.; Benninger, R. K. P.; Yan, Y. L.; Petchprayoon, C.; Jackson, D.; Easley, C. J.; Piston, D. W.; Marriott, G. Optical lock-in detection of FRET using synthetic and genetically encoded optical switches. *Biophys. J.* **2008**, *94*, 4515-4524.

[64] Gill, S. C.; Vonhippel, P. H. Calculation of protein extinction coefficients from amino-acid sequence data. *Anal. Biochem.* **1989**, *182*, 319-326.

[65] Ramanujam, N.; Richards-Kortum, R.; Thomsen, S.; Mahadevan-Jansen, A.; Follen, M.; Chance, B. Low temperature fluorescence imaging of freeze-trapped human cervical tissues. *Opt. Express* **2001**, *8*, 335-343.

[66] Skala, M. C.; Riching, K. M.; Gendron-Fitzpatrick, A.; Eickhoff, J.; Eliceiri, K. W.; White, J. G.; Ramanujam, N. In vivo multiphoton microscopy of NADH and FAD redox states, fluorescence lifetimes, and cellular morphology in precancerous epithelia. *Proc. Natl. Acad. Sci. U. S. A.* **2007**, *104*, 19494-19499.

[67] Lavis, L. D.; Raines, R. T. Bright ideas for chemical biology. *ACS Chem. Biol.* **2008**, *3*, 142-155.

[68] Li, A. D. Q.; Zhan, C. L.; Hu, D. H.; Wan, W.; Yao, J. N. Photoswitchable nanoprobes offer unlimited brightness in frequency-domain imaging. *J. Am. Chem. Soc.* **2011**, *133*, 7628-7631.

[69] Medintz, I. L.; Uyeda, H. T.; Goldman, E. R.; Mattoussi, H. Quantum dot bioconjugates for imaging, labelling and sensing. *Nat. Mater.* **2005**, *4*, 435-446.

[70] Michalet, X.; Pinaud, F. F.; Bentolila, L. A.; Tsay, J. M.; Doose, S.; Li, J. J.; Sundaresan, G.; Wu, A. M.; Gambhir, S. S.; Weiss, S. Quantum dots for live cells, in vivo imaging, and diagnostics. *Science* **2005**, *307*, 538-544.

[71] Derfus, A. M.; Chan, W. C. W.; Bhatia, S. N. Probing the cytotoxicity of semiconductor quantum dots. *Nano Lett.* **2004**, *4*, 11-18.

[72] Lovric, J.; Bazzi, H. S.; Cuie, Y.; Fortin, G. R. A.; Winnik, F. M.; Maysinger, D. Differences in subcellular distribution and toxicity of green and red emitting CdTe quantum dots. *J. Mol. Med.* **2005**, *83*, 377-385.

[73] Petty, J. T.; Story, S. P.; Hsiang, J. C.; Dickson, R. M. DNA-templated molecular silver fluorophores. *J. Phys. Chem. Lett.* **2013**, *4*, 1148-1155.

[74] Vosch, T.; Antoku, Y.; Hsiang, J. C.; Richards, C. I.; Gonzalez, J. I.; Dickson, R. M. Strongly emissive individual DNA-encapsulated Ag nanoclusters as single-molecule fluorophores. *Proc. Natl. Acad. Sci. U. S. A.* **2007**, *104*, 12616-12621.

[75] Petty, J. T.; Fan, C. Y.; Story, S. P.; Sengupta, B.; Iyer, A. S.; Prudowsky, Z.; Dickson, R. M. DNA encapsulation of 10 silver atoms producing a bright, modulatable, near-infrared-emitting cluster. *J. Phys. Chem. Lett.* **2010**, *1*, 2524-2529.

[76] Petty, J. T.; Fan, C. Y.; Story, S. P.; Sengupta, B.; Sartin, M.; Hsiang, J. C.; Perry, J. W.; Dickson, R. M. Optically enhanced, near-IR, silver cluster emission altered by single base changes in the DNA template. *J. Phys. Chem. B* **2011**, *115*, 7996-8003.

[77] Zimmer, M. Green fluorescent protein (GFP): Applications, structure, and related photophysical behavior. *Chem. Rev.* **2002**, *102*, 759-781.

[78] Labas, Y. A.; Gurskaya, N. G.; Yanushevich, Y. G.; Fradkov, A. F.; Lukyanov, K. A.; Lukyanov, S. A.; Matz, M. V. Diversity and evolution of the green fluorescent protein family. *Proc. Natl. Acad. Sci. U. S. A.* **2002**, *99*, 4256-4261.

[79] Shimomura, O.; Johnson, F. H.; Saiga, Y. Extraction, purification and properies of Aequorin, a bioluminescent protein from luminous hydromedusan, Aequorea. *Journal of Cellular and Comparative Physiology* **1962**, *59*, 223-&.

[80] Morin, J. G.; Hastings, J. W. Energy transfer in a bioluminescent system. *J. Cell. Physiol.* **1971**, *77*, 313-&.

[81] Morise, H.; Shimomur.O; Johnson, F. H.; Winant, J. Intermolecular energy-transfer in bioluminescent system of Aequorea. *Biochemistry* **1974**, *13*, 2656-2662.

[82] Shimomura, O. Structure of the chromophore of Aequorea green fluorescent protein. *FEBS Lett.* **1979**, *104*, 220-222.

[83] Ward, W. W.; Cormier, M. J. Energy-transfer protein in coelenterate bioluminescence - characterization of the Renilla green-fluorescent protein. *J. Biol. Chem.* **1979**, *254*, 781-788.

[84] Prasher, D. C.; Eckenrode, V. K.; Ward, W. W.; Prendergast, F. G.; Cormier, M. J. Primary structure of the Aequorea-victoria green-fluorescent protein. *Gene* **1992**, *111*, 229-233.

[85] Chalfie, M.; Tu, Y.; Euskirchen, G.; Ward, W. W.; Prasher, D. C. Green fluorescent protein as a marker for gene-expression. *Science* **1994**, *263*, 802-805.

[86] Heim, R.; Prasher, D. C.; Tsien, R. Y. Wavelength mutations and posttranslational autoxidation of green fluorescent protein. *Proc. Natl. Acad. Sci. U. S. A.* **1994**, *91*, 12501-12504.

[87] Tsien, R. Y. Constructing and exploiting the fluorescent protein paintbox (Nobel Lecture). *Angew. Chem.-Int. Edit.* **2009**, *48*, 5612-5626.

[88] Ormo, M.; Cubitt, A. B.; Kallio, K.; Gross, L. A.; Tsien, R. Y.; Remington, S. J. Crystal structure of the Aequorea victoria green fluorescent protein. *Science* **1996**, *273*, 1392-1395.

[89] Yang, F.; Moss, L. G.; Phillips, G. N. The molecular structure of green fluorescent protein. *Nat. Biotechnol.* **1996**, *14*, 1246-1251.

[90] Remington, S. J. Green fluorescent protein: A perspective. *Protein Sci.* **2011**, *20*, 1509-1519.

[91] Tsien, R. Y. The green fluorescent protein. *Annu. Rev. Biochem.* **1998**, *67*, 509-544.

[92] Gross, L. A.; Baird, G. S.; Hoffman, R. C.; Baldridge, K. K.; Tsien, R. Y. The structure of the chromophore within DsRed, a red fluorescent protein from coral. *Proc. Natl. Acad. Sci. U. S. A.* **2000**, *97*, 11990-11995.

[93] Cody, C. W.; Prasher, D. C.; Westler, W. M.; Prendergast, F. G.; Ward, W. W. Chemical-structure of the hexapeptide chromophore of the Aequorea green-fluorescent protein. *Biochemistry* **1993**, *32*, 1212-1218.

[94] Cubitt, A. B.; Woollenweber, L. A.; Heim, R. Understanding structure-function relationships in the Aequorea victoria green fluorescent protein. *Methods in Cell Biology, Vol 58* **1999**, *58*, 19-+.

[95] Ai, H. W.; Shaner, N. C.; Cheng, Z. H.; Tsien, R. Y.; Campbell, R. E. Exploration of new chromophore structures leads to the identification of improved blue fluorescent proteins. *Biochemistry* **2007**, *46*, 5904-5910.

[96] Kremers, G. J.; Goedhart, J.; van den Heuvel, D. J.; Gerritsen, H. C.; Gadella, T. W. J. Improved green and blue fluorescent proteins for expression in bacteria and mammalian cells. *Biochemistry* **2007**, *46*, 3775-3783.

[97] Mena, M. A.; Treynor, T. P.; Mayo, S. L.; Daugherty, P. S. Blue fluorescent proteins with enhanced brightness and photostability from a structurally targeted library. *Nat. Biotechnol.* **2006**, *24*, 1569-1571.

[98] Shu, X.; Leiderman, P.; Gepshtein, R.; Smith, N. R.; Kallio, K.; Huppert, D.; Remington, S. J. An alternative excited-state proton transfer pathway in green fluorescent protein variant S205V. *Protein Sci.* **2007**, *16*, 2703-2710.

[99] Yang, T. T.; Sinai, P.; Green, G.; Kitts, P. A.; Chen, Y. T.; Lybarger, L.; Chervenak, R.; Patterson, G. H.; Piston, D. W.; Kain, S. R. Improved fluorescence and dual color detection with enhanced blue and green variants of the green fluorescent protein. *J. Biol. Chem.* **1998**, *273*, 8212-8216.

[100] Heim, R.; Tsien, R. Y. Engineering green fluorescent protein for improved brightness, longer wavelengths and fluorescence resonance energy transfer. *Curr. Biol.* **1996**, *6*, 178-182.

[101] Malo, G. D.; Pouwels, L. J.; Wang, M. T.; Weichsel, A.; Montfort, W. R.; Rizzo, M. A.; Piston, D. W.; Wachter, R. M. X-ray structure of cerulean GFP: A

tryptophan-based chromophore useful for fluorescence lifetime imaging. *Biochemistry* **2007**, *46*, 9865-9873.

[102] Markwardt, M. L.; Kremers, G. J.; Kraft, C. A.; Ray, K.; Cranfill, P. J. C.; Wilson, K. A.; Day, R. N.; Wachter, R. M.; Davidson, M. W.; Rizzo, M. A. An improved Cerulean fluorescent protein with enhanced brightness and reduced reversible photoswitching. *PLoS One* **2011**, *6*, 11.

[103] Rizzo, M. A.; Springer, G. H.; Granada, B.; Piston, D. W. An improved cyan fluorescent protein variant useful for FRET. *Nat. Biotechnol.* **2004**, *22*, 445-449.

[104] Cubitt, A. B.; Heim, R.; Adams, S. R.; Boyd, A. E.; Gross, L. A.; Tsien, R. Y. Understanding, improving and using green fluorescent proteins. *Trends Biochem.Sci.* **1995**, *20*, 448-455.

[105] Heim, R.; Cubitt, A. B.; Tsien, R. Y. Improved green fluorescence. *Nature* **1995**, *373*, 663-664.

[106] Elsliger, M. A.; Wachter, R. M.; Hanson, G. T.; Kallio, K.; Remington, S. J. Structural and spectral response of green fluorescent protein variants to changes in pH. *Biochemistry* **1999**, *38*, 5296-5301.

[107] Griesbeck, O.; Baird, G. S.; Campbell, R. E.; Zacharias, D. A.; Tsien, R. Y. Reducing the environmental sensitivity of yellow fluorescent protein - Mechanism and applications. *J. Biol. Chem.* **2001**, *276*, 29188-29194.

[108] Nagai, T.; Ibata, K.; Park, E. S.; Kubota, M.; Mikoshiba, K.; Miyawaki, A. A variant of yellow fluorescent protein with fast and efficient maturation for cell-biological applications. *Nat. Biotechnol.* **2002**, *20*, 87-90.

[109] Rekas, A.; Alattia, J. R.; Nagai, T.; Miyawaki, A.; Ikura, M. Crystal structure of Venus, a yellow fluorescent protein with improved maturation and reduced environmental sensitivity. *J. Biol. Chem.* **2002**, *277*, 50573-50578.

[110] Wachter, R. M.; Elsliger, M. A.; Kallio, K.; Hanson, G. T.; Remington, S. J. Structural basis of spectral shifts in the yellow-emission variants of green fluorescent protein. *Struct. Fold. Des.* **1998**, *6*, 1267-1277.

[111] Wachter, R. M.; Remington, S. J. Sensitivity of the yellow variant of green fluorescent protein to halides and nitrate. *Curr. Biol.* **1999**, *9*, R628-R629.

[112] Wachter, R. M.; Yarbrough, D.; Kallio, K.; Remington, S. J. Crystallographic and energetic analysis of binding of selected anions to the yellow variants of green fluorescent protein. *J. Mol. Biol.* **2000**, *301*, 157-171.

[113] Baird, G. S.; Zacharias, D. A.; Tsien, R. Y. Biochemistry, mutagenesis, and oligomerization of DsRed, a red fluorescent protein from coral. *Proc. Natl. Acad. Sci. U. S. A.* **2000**, *97*, 11984-11989.

[114] Verkhusha, V. V.; Kuznetsova, I. M.; Stepanenko, O. V.; Zaraisky, A. G.; Shavlovsky, M. M.; Turoverov, K. K.; Uversky, V. N. High stability of Discosoma DsRed as compared to Aequorea EGFP. *Biochemistry* **2003**, *42*, 7879-7884.

[115] Wall, M. A.; Socolich, M.; Ranganathan, R. The structural basis for red fluorescence in the tetrameric GFP homolog DsRed. *Nat. Struct. Biol.* **2000**, *7*, 1133-1138.

[116] Yarbrough, D.; Wachter, R. M.; Kallio, K.; Matz, M. V.; Remington, S. J. Refined crystal structure of DsRed, a red fluorescent protein from coral, at 2.0-angstrom resolution. *Proc. Natl. Acad. Sci. U. S. A.* **2001**, *98*, 462-467.

[117] Matz, M. V.; Fradkov, A. F.; Labas, Y. A.; Savitsky, A. P.; Zaraisky, A. G.; Markelov, M. L.; Lukyanov, S. A. Fluorescent proteins from nonbioluminescent Anthozoa species. *Nat. Biotechnol.* **1999**, *17*, 969-973.

[118] Stiel, A. C.; Trowitzsch, S.; Weber, G.; Andresen, M.; Eggeling, C.; Hell, S. W.; Jakobs, S.; Wahl, M. C. 1.8 angstrom bright-state structure of the reversibly switchable fluorescent protein Dronpa guides the generation of fast switching variants. *Biochem. J.* **2007**, *402*, 35-42.

[119] Andresen, M.; Stiel, A. C.; Folling, J.; Wenzel, D.; Schonle, A.; Egner, A.; Eggeling, C.; Hell, S. W.; Jakobs, S. Photoswitchable fluorescent proteins enable monochromatic multilabel imaging and dual color fluorescence nanoscopy. *Nat. Biotechnol.* **2008**, *26*, 1035-1040.

[120] Andresen, M.; Stiel, A. C.; Trowitzsch, S.; Weber, G.; Eggeling, C.; Wahl, M. C.; Hell, S. W.; Jakobs, S. Structural basis for reversible photoswitching in Dronpa. *Proc. Natl. Acad. Sci. U. S. A.* **2007**, *104*, 13005-13009.

[121] Subach, F. V.; Zhang, L. J.; Gadella, T. W. J.; Gurskaya, N. G.; Lukyanov, K. A.; Verkhusha, V. V. Red fluorescent protein with reversibly photoswitchable absorbance for photochromic FRET. *Chem. Biol.* **2010**, *17*, 745-755.

[122] Brakemann, T.; Weber, G.; Andresen, M.; Groenhof, G.; Stiel, A. C.; Trowitzsch, S.; Eggeling, C.; Grubmuller, H.; Hell, S. W.; Wahl, M. C.; Jakobs, S. Molecular basis of the light-driven switching of the photochromic fluorescent protein Padron. *J. Biol. Chem.* **2010**, *285*, 14603-14609.

[123] Habuchi, S.; Ando, R.; Dedecker, P.; Verheijen, W.; Mizuno, H.; Miyawaki, A.; Hofkens, J. Reversible single-molecule photoswitching in the GFP-like fluorescent protein Dronpa. *Proc. Natl. Acad. Sci. U. S. A.* **2005**, *102*, 9511-9516.

[124] Habuchi, S.; Dedecker, P.; Hotta, J. I.; Flors, C.; Ando, R.; Mizuno, H.; Miyawaki, A.; Hofkens, J. Photo-induced protonation/deprotonation in the GFP-like fluorescent protein Dronpa: mechanism responsible for the reversible photoswitching. *Photochem. Photobiol. Sci.* **2006**, *5*, 567-576.

[125] Henderson, J. N.; Ai, H. W.; Campbell, R. E.; Remington, S. J. Structural basis for reversible photobleaching of a green fluorescent protein homologue. *Proc. Natl. Acad. Sci. U. S. A.* **2007**, *104*, 6672-6677.

[126] Pletnev, S.; Subach, F. V.; Dauter, Z.; Wlodawer, A.; Verkhusha, V. V. A structural basis for reversible photoswitching of absorbance spectra in red fluorescent protein rsTagRFP. *J. Mol. Biol.* **2012**, *417*, 144-151.

[127] Wilmann, P. G.; Turcic, K.; Battad, J. M.; Wilce, M. C. J.; Devenish, R. J.; Prescott, M.; Rossjohn, J. The 1.7 angstrom crystal structure of Dronpa: A photoswitchable green fluorescent protein. *J. Mol. Biol.* **2006**, *364*, 213-224.

[128] Dong, J.; Solntsev, K. M.; Tolbert, L. M. Solvatochromism of the green fluorescence protein chromophore and its derivatives. *J. Am. Chem. Soc.* **2006**, *128*, 12038-12039.

[129] He, X.; Bell, A. F.; Tonge, P. J. Isotopic labeling and normal-mode analysis of a model green fluorescent protein chromophore. *J. Phys. Chem. B* **2002**, *106*, 6056-6066.

[130] He, X.; Bell, A. F.; Tonge, P. J. Ground state isomerization of a model green fluorescent protein chromophore. *FEBS Lett.* **2003**, *549*, 35-38.

[131] Leiderman, P.; Genosar, L.; Huppert, D.; Shu, X.; Remington, S. J.; Solntsev, K. M.; Tolbert, L. M. Ultrafast excited-state dynamics in the green fluorescent protein variant S65T/H148D. 3. Short- and long-time dynamics of the excited-state proton transfer. *Biochemistry* **2007**, *46*, 12026-12036.

[132] Leiderman, P.; Huppert, D.; Remington, S. J.; Tolbert, L. M.; Solntsev, K. M. The effect of pressure on the excited-state proton transfer in the wild-type green fluorescent protein. *Chem. Phys. Lett.* **2008**, *455*, 303-306.

[133] Olsen, S.; Smith, S. C. Bond selection in the photoisomerization reaction of anionic green fluorescent protein and kindling fluorescent protein chromophore models. *J. Am. Chem. Soc.* **2008**, *130*, 8677-8689.

[134] Remington, S. J. Fluorescent proteins: maturation, photochemistry and photophysics. *Curr. Opin. Struct. Biol.* **2006**, *16*, 714-721.

[135] Stavrov, S. S.; Solntsev, K. M.; Tolbert, L. M.; Huppert, D. Probing the decay coordinate of the green fluorescent protein: Arrest of cis-trans isomerization by the protein significantly narrows the fluorescence spectra. *J. Am. Chem. Soc.* **2006**, *128*, 1540-1546.

[136] Tolbert, L. M.; Solntsev, K. M. Excited-state proton transfer: From constrained systems to "super" photoacids to superfast proton transfer. *Accounts Chem. Res.* **2002**, *35*, 19-27.

[137] Usman, A.; Mohammed, O. F.; Nibbering, E. T. J.; Dong, J.; Solntsev, K. M.; Tolbert, L. M. Excited-state structure determination of the green fluorescent protein chromophore. *J. Am. Chem. Soc.* **2005**, *127*, 11214-11215.

[138] Chattoraj, M.; King, B. A.; Bublitz, G. U.; Boxer, S. G. Ultra-fast excited state dynamics in green fluorescent protein: Multiple states and proton transfer. *Proc. Natl. Acad. Sci. U. S. A.* **1996**, *93*, 8362-8367.

[139] Brejc, K.; Sixma, T. K.; Kitts, P. A.; Kain, S. R.; Tsien, R. Y.; Ormo, M.; Remington, S. J. Structural basis for dual excitation and photoisomerization of the Aequorea victoria green fluorescent protein. *Proc. Natl. Acad. Sci. U. S. A.* **1997**, *94*, 2306-2311.

[140] Dickson, R. M.; Cubitt, A. B.; Tsien, R. Y.; Moerner, W. E. On/off blinking and switching behaviour of single molecules of green fluorescent protein. *Nature* **1997**, *388*, 355-358.

[141] Grotjohann, T.; Testa, I.; Leutenegger, M.; Bock, H.; Urban, N. T.; Lavoie-Cardinal, F.; Willig, K. I.; Eggeling, C.; Jakobs, S.; Hell, S. W. Diffraction-unlimited all-optical imaging and writing with a photochromic GFP. *Nature* **2011**, *478*, 204-208.

[142] Mudalige, K.; Habuchi, S.; Goodwin, P. M.; Pai, R. K.; De Schryver, F.; Cotlet, M. Photophysics of the red chromophore of HcRed: Evidence for cis-trans isomerization and protonation-state changes. *J. Phys. Chem. B* **2010**, *114*, 4678-4685.

[143] Hess, S. T.; Heikal, A. A.; Webb, W. W. Fluorescence photoconversion kinetics in novel green fluorescent protein pH sensors (pHluorins). *J. Phys. Chem. B* **2004**, *108*, 10138-10148.

[144] Weber, W.; Helms, V.; McCammon, J. A.; Langhoff, P. W. Shedding light on the dark and weakly fluorescent states of green fluorescent proteins. *Proc. Natl. Acad. Sci. U. S. A.* **1999**, *96*, 6177-6182.

[145] Drobizhev, M.; Makarov, N. S.; Tillo, S. E.; Hughes, T. E.; Rebane, A. Two-photon absorption properties of fluorescent proteins. *Nat. Methods* **2011**, *8*, 393-399.

[146] Xu, C.; Zipfel, W.; Shear, J. B.; Williams, R. M.; Webb, W. W. Multiphoton fluorescence excitation: New spectral windows for biological nonlinear microscopy. *Proc. Natl. Acad. Sci. U. S. A.* **1996**, *93*, 10763-10768.

[147] Llopis, J.; McCaffery, J. M.; Miyawaki, A.; Farquhar, M. G.; Tsien, R. Y. Measurement of cytosolic, mitochondrial, and Golgi pH in single living cells with green fluorescent proteins. *Proc. Natl. Acad. Sci. U. S. A.* **1998**, *95*, 6803-6808.

[148] Shaner, N. C.; Steinbach, P. A.; Tsien, R. Y. A guide to choosing fluorescent proteins. *Nat. Methods* **2005**, *2*, 905-909.

[149] Dedecker, P.; Mo, G. C. H.; Dertinger, T.; Zhang, J. Widely accessible method for superresolution fluorescence imaging of living systems. *Proc. Natl. Acad. Sci. U. S. A.* **2012**, *109*, 10909-10914.

[150] Kneen, M.; Farinas, J.; Li, Y. X.; Verkman, A. S. Green fluorescent protein as a noninvasive intracellular pH indicator. *Biophys. J.* **1998**, *74*, 1591-1599.

[151] Baird, G. S.; Zacharias, D. A.; Tsien, R. Y. Circular permutation and receptor insertion within green fluorescent proteins. *Proc. Natl. Acad. Sci. U. S. A.* **1999**, *96*, 11241-11246.

[152] Nagai, T.; Sawano, A.; Park, E. S.; Miyawaki, A. Circularly permuted green fluorescent proteins engineered to sense Ca2+. *Proc. Natl. Acad. Sci. U. S. A.* **2001**, *98*, 3197-3202.

[153] Nakai, J.; Ohkura, M.; Imoto, K. A high signal-to-noise Ca2+ probe composed of a single green fluorescent protein. *Nat. Biotechnol.* **2001**, *19*, 137-141.

[154] Ataka, K.; Pieribone, V. A. A genetically targetable fluorescent probe of channel gating with rapid kinetics. *Biophys. J.* **2002**, *82*, 509-516.

[155] Siegel, M. S.; Isacoff, E. Y. A genetically encoded optical probe of membrane voltage. *Neuron* **1997**, *19*, 735-741.

[156] Kohl, T.; Heinze, K. G.; Kuhlemann, R.; Koltermann, A.; Schwille, P. A protease assay for two-photon crosscorrelation and FRET analysis based solely on fluorescent proteins. *Proc. Natl. Acad. Sci. U. S. A.* **2002**, *99*, 12161-12166.

[157] Mitra, R. D.; Silva, C. M.; Youvan, D. C. Fluorescence resonance energy transfer between blue-emitting and red-shifted excitation derivatives of the green fluorescent protein. *Gene* **1996**, *173*, 13-17.

[158] Takemoto, K.; Nagai, T.; Miyawaki, A.; Miura, M. Spatio-temporal activation of caspase revealed by indicator that is insensitive to environmental effects. *J. Cell Biol.* **2003**, *160*, 235-243.

[159] Miyawaki, A.; Griesbeck, O.; Heim, R.; Tsien, R. Y. Dynamic and quantitative Ca2+ measurements using improved cameleons. *Proc. Natl. Acad. Sci. U. S. A.* **1999**, *96*, 2135-2140.

[160] Miyawaki, A.; Llopis, J.; Heim, R.; McCaffery, J. M.; Adams, J. A.; Ikura, M.; Tsien, R. Y. Fluorescent indicators for Ca2+ based on green fluorescent proteins and calmodulin. *Nature* **1997**, *388*, 882-887.

[161] Liu, P.; Sudhaharan, T.; Koh, R. M. L.; Hwang, L. C.; Ahmed, S.; Maruyama, I. N.; Wohland, T. Investigation of the dimerization of proteins from the epidermal growth factor receptor family by single wavelength fluorescence cross-correlation spectroscopy. *Biophys. J.* **2007**, *93*, 684-698.

[162] Slaughter, B. D.; Schwartz, J. W.; Li, R. Mapping dynamic protein interactions in MAP kinase signaling using live-cell fluorescence fluctuation spectroscopy and imaging. *Proc. Natl. Acad. Sci. U. S. A.* **2007**, *104*, 20320-20325.

[163] Fan, J.-Y.; Cui, Z.-Q.; Wei, H.-P.; Zhang, Z.-P.; Zhou, Y.-F.; Wang, Y.-P.; Zhang, X.-E. Split mCherry as a new red bimolecular fluorescence complementation system for visualizing protein–protein interactions in living cells. *Biochemical and Biophysical Research Communications* **2008**, *367*, 47-53.

[164] Ogston, A. G. The spaces in a uniform random suspension of fibres. *Transactions of the Faraday Society* **1958**, *54*, 1754-1757.

[165] Dickson, R. M.; Norris, D. J.; Tzeng, Y. L.; Moerner, W. E. Three-dimensional imaging of single molecules solvated in pores of poly(acrylamide) gels. *Science* **1996**, *274*, 966-969.

[166] Green, M. R. *Molecular cloning : a laboratory manual*; 4th ed. ed.; Cold Spring Harbor, N.Y.: Cold Spring Harbor Laboratory Press, 2012.

[167] Shaw, B. F.; Durazo, A.; Nersissian, A. M.; Whitelegge, J. P.; Faull, K. F.; Valentine, J. S. Local unfolding in a destabilized, pathogenic variant of superoxide dismutase 1 observed with H/D exchange and mass spectrometry. *J. Biol. Chem.* **2006**, *281*, 18167-18176.

[168] Glasoe, P. K.; Long, F. A. Use of glass electrodes to measure acidities in deuterium oxide. *J. Phys. Chem.* **1960**, *64*, 188-190.

[169] Mikkelsen, K.; Nielsen, S. O. Acidity measurements with the glass electrode in H2O-D2O mixtures. *J. Phys. Chem.* **1960**, *64*, 632-637.

[170] Williams, A. T. R.; Winfield, S. A.; Miller, J. N. Relative fluorescence quantum yields using a computer-controlled luminescence spectrometer. *Analyst* **1983**, *108*, 1067-1071.

[171] Gasteiger, E.; Hoogland, C.; Gattiker, A.; Duvaud, S. e.; Wilkins, M. R.; Appel, R. D.; Bairoch, A. In *The Proteomics Protocols Handbook*; Walker, J. M., Ed. 2005, p 571-607.

[172] Rizzuto, R.; Brini, M.; DeGiorgi, F.; Rossi, R.; Heim, R.; Tsien, R. Y.; Pozzan, T. Double labelling of subcellular structures with organelle-targeted GFP mutants in vivo. *Curr. Biol.* **1996**, *6*, 183-188.

[173] Simkovitch, R.; Huppert, A.; Huppert, D.; Remington, S. J.; Miller, Y. Proton transfer in Wild-Type GFP and S205V mutant is reduced by conformational changes of residues in the proton wire. *J. Phys. Chem. B* **2013**, *117*, 11921-11931.

[174] Kummer, A. D.; Wiehler, J.; Rehaber, H.; Kompa, C.; Steipe, B.; Michel-Beyerle, M. E. Effects of threonine 203 replacements on excited-state dynamics and fluorescence properties of the green fluorescent protein (GFP). *J. Phys. Chem. B* **2000**, *104*, 4791-4798.

[175] Agmon, N. Proton pathways in green fluorescence protein. *Biophys. J.* **2005**, *88*, 2452-2461.

[176] Agmon, N. Kinetics of switchable proton escape from a proton-wire within green fluorescence protein. *J. Phys. Chem. B* **2007**, *111*, 7870-7878.

[177] Wachter, R. M.; King, B. A.; Heim, R.; Kallio, K.; Tsien, R. Y.; Boxer, S. G.; Remington, S. J. Crystal structure and photodynamic behavior of the blue emission variant Y66H/Y145F of green fluorescent protein. *Biochemistry* **1997**, *36*, 9759-9765.

[178] Spencer, R. D.; Weber, G. Measurements of subnanosecond fluorescence lifetimes with a cross-correlation phase fluorometer. *Ann.NY Acad.Sci.* **1969**, *158*, 361-&.

[179] Quercioli, V.; Bosisio, C.; Daglio, S. C.; Rocca, F.; D'Alfonso, L.; Collini, M.; Baldini, G.; Chirico, G.; Bettati, S.; Raboni, S.; Campanini, B. Photoinduced millisecond switching kinetics in the GFPMut2 E222Q mutant. *J. Phys. Chem. B* **2010**, *114*, 4664-4677.

[180] Gurskaya, N. G.; Fradkov, A. F.; Pounkova, N. I.; Staroverov, D. B.; Bulina, M. E.; Yanushevich, Y. G.; Labas, Y. A.; Lukyanov, S.; Lukyanov, K. A. Colourless green fluorescent protein homologue from the non-fluorescent hydromedusa Aequorea coerulescens and its fluorescent mutants. *Biochem. J.* **2003**, *373*, 403-408.

[181] Pletneva, N. V.; Pletnev, V. Z.; Lukyanov, K. A.; Gurskaya, N. G.; Goryacheva, E. A.; Martynov, V. I.; Wlodawer, A.; Dauter, Z.; Pletnev, S. Structural evidence for a dehydrated intermediate in green fluorescent protein chromophore biosynthesis. *J. Biol. Chem.* **2010**, *285*, 15978-15984.

[182] Cormack, B. P.; Valdivia, R. H.; Falkow, S. FACS-optimized mutants of the green fluorescent protein (GFP). *Gene* **1996**, *173*, 33-38.

[183] Dayel, M. J.; Hom, E. F. Y.; Verkman, A. S. Diffusion of green fluorescent protein in the aqueous-phase lumen of endoplasmic reticulum. *Biophys. J.* **1999**, *76*, 2843-2851.

[184] Swaminathan, R.; Hoang, C. P.; Verkman, A. S. Photobleaching recovery and anisotropy decay of green fluorescent protein GFP-S65T in solution and cells: Cytoplasmic viscosity probed by green fluorescent protein translational and rotational diffusion. *Biophys. J.* **1997**, *72*, 1900-1907.

[185] Widengren, J.; Mets, U.; Rigler, R. Photodynamic properties of green fluorescent proteins investigated by fluorescence correlation spectroscopy. *Chem. Phys.* **1999**, *250*, 171-186.

[186] Liu, Y. X.; Kim, H. R.; Heikal, A. A. Structural basis of fluorescence fluctuation dynamics of green fluorescent proteins in acidic environments. *J. Phys. Chem. B* **2006**, *110*, 24138-24146.

[187] Rizzo, M. A.; Piston, D. W. In *Live Cell Imaging: A Laboratory Manual*; 2nd ed.; Goldman, R. D., Spector, D. L., Eds.; Cold Spring Harbor Laboratory Press: Cold Spring Harbor, New York, 2005, p 3-23.

[188] David, C. C.; Dedecker, P.; De Cremer, G.; Verstraeten, N.; Kint, C.; Michiels, J.; Hofkens, J. Spectroscopic characterization of Venus at the single molecule level. *Photochem. Photobiol. Sci.* **2012**, *11*, 358-363.

[189] Sarkar, P.; Koushik, S. V.; Vogel, S. S.; Gryczynski, I.; Gryczynski, Z. Photophysical properties of Cerulean and Venus fluorescent proteins. *J. Biomed. Opt.* **2009**, *14*, 9.

[190] Verkhusha, V. V.; Lukyanov, K. A. The molecular properties and applications of Anthozoa fluorescent proteins and chromoproteins. *Nat. Biotechnol.* **2004**, *22*, 289-296.

[191] Royant, A.; Noirclerc-Savoye, M. Stabilizing role of glutamic acid 222 in the structure of Enhanced Green Fluorescent Protein. *J. Struct. Biol.* **2011**, *174*, 385-390.

[192] Jung, G.; Wiehler, J.; Zumbusch, A. The photophysics of green fluorescent protein: Influence of the key amino acids at positions 65, 203, and 222. *Biophys. J.* **2005**, *88*, 1932-1947.

[193] Stoner-Ma, D.; Jaye, A. A.; Ronayne, K. L.; Nappa, J.; Meech, S. R.; Tonge, P. J. An alternate proton acceptor for excited-state proton transfer in green fluorescent protein: Rewiring GFP. *J. Am. Chem. Soc.* **2008**, *130*, 1227-1235.

[194] Dean, K. M.; Lubbeck, J. L.; Binder, J. K.; Schwall, L. R.; Jimenez, R.; Palmer, A. E. Analysis of red-fluorescent proteins provides insight into dark-state conversion and photodegradation. *Biophys. J.* **2011**, *101*, 961-969.

[195] Hendrix, J.; Flors, C.; Dedecker, P.; Hofkens, J.; Engelborghs, Y. Dark states in monomeric red fluorescent proteins studied by fluorescence correlation and single molecule spectroscopy. *Biophys. J.* **2008**, *94*, 4103-4113.

[196] Ringemann, C.; Schonle, A.; Giske, A.; von Middendorff, C.; Hell, S. W.; Eggeling, C. Enhancing fluorescence brightness: Effect of reverse intersystem crossing studied by fluorescence fluctuation spectroscopy. *ChemPhysChem* **2008**, *9*, 612-624.

[197] Schwille, P.; Kummer, S.; Heikal, A. A.; Moerner, W. E.; Webb, W. W. Fluorescence correlation spectroscopy reveals fast optical excitation-driven intramolecular dynamics of yellow fluorescent proteins. *Proc. Natl. Acad. Sci. U. S. A.* **2000**, *97*, 151-156.

[198] Habuchi, S.; Cotlet, M.; Gensch, T.; Bednarz, T.; Haber-Pohlmeier, S.; Rozenski, J.; Dirix, G.; Michiels, J.; Vanderleyden, J.; Heberle, J.; De Schryver, F. C.; Hofkens, J. Evidence for the isomerization and decarboxylation in the photoconversion of the red fluorescent protein DsRed. *J. Am. Chem. Soc.* **2005**, *127*, 8977-8984.

[199] Lossau, H.; Kummer, A.; Heinecke, R.; Pöllinger-Dammer, F.; Kompa, C.; Bieser, G.; Jonsson, T.; Silva, C. M.; Yang, M. M.; Youvan, D. C.; Michel-Beyerle, M. E. Time-resolved spectroscopy of wild-type and mutant Green Fluorescent Proteins reveals excited state deprotonation consistent with fluorophore-protein interactions. *Chem. Phys.* **1996**, *213*, 1-16.

[200] Sample, V.; Newman, R. H.; Zhang, J. The structure and function of fluorescent proteins. *Chem. Soc. Rev.* **2009**, *38*, 2852-2864.

[201] Kao, Y.-T.; Zhu, X.; Min, W. Protein-flexibility mediated coupling between photoswitching kinetics and surrounding viscosity of a photochromic fluorescent protein. *Proceedings of the National Academy of Sciences* **2012**, *109*, 3220-3225.

[202] Ando, R.; Flors, C.; Mizuno, H.; Hofkens, J.; Miyawaki, A. Highlighted generation of fluorescence signals using simultaneous two-color irradiation on Dronpa mutants. *Biophys. J.* **2007**, *92*, L97-L99.

[203] Patterson, G.; Day, R. N.; Piston, D. Fluorescent protein spectra. *J. Cell Sci*. **2001**, *114*, 837-838.

[204] Zhang, J.; Campbell, R. E.; Ting, A. Y.; Tsien, R. Y. Creating new fluorescent probes for cell biology. *Nat. Rev. Mol. Cell Biol.* **2002**, *3*, 906-918.

[205] Miyawaki, A. Fluorescence imaging of physiological activity in complex systems using GFP-based probes. *Curr. Opin. Neurobiol.* **2003**, *13*, 591-596.

[206] Sinnecker, D.; Voigt, P.; Hellwig, N.; Schaefer, M. Reversible photobleaching of enhanced green fluorescent proteins. *Biochemistry* **2005**, *44*, 7085-7094.

[207] Richards, C. I.; Hsiang, J. C.; Khalil, A. M.; Hull, N. P.; Dickson, R. M. FRET-enabled optical modulation for high sensitivity fluorescence imaging. *J. Am. Chem. Soc.* **2010**, *132*, 6318-6323.

[208] Palmer, A. E.; Tsien, R. Y. Measuring calcium signaling using genetically targetable fluorescent indicators. *Nat. Protoc.* **2006**, *1*, 1057-1065.